

## **INFORMATION TO USERS**

**This manuscript has been reproduced from the microfilm master. UMI films the text directly from the original or copy submitted. Thus, some thesis and dissertation copies are in typewriter face, while others may be from any type of computer printer.**

**The quality of this reproduction is dependent upon the quality of the copy submitted. Broken or indistinct print, colored or poor quality illustrations and photographs, print bleedthrough, substandard margins, and improper alignment can adversely affect reproduction.**

**In the unlikely event that the author did not send UMI a complete manuscript and there are missing pages, these will be noted. Also, if unauthorized copyright material had to be removed, a note will indicate the deletion.**

**Oversize materials (e.g., maps, drawings, charts) are reproduced by sectioning the original, beginning at the upper left-hand corner and continuing from left to right in equal sections with small overlaps.**

**ProQuest Information and Learning  
300 North Zeeb Road, Ann Arbor, MI 48106-1346 USA  
800-521-0600**

**UMI<sup>®</sup>**





# **Theoretical Analysis and Simulation of Immobilized Enzyme Reactors**

BY

*Ali Ebrahim AL-Muftah*

A Thesis Presented to the

DEANSHIP OF GRADUATE STUDIES

**KING FAHD UNIVERSITY OF PETROLEUM & MINERALS**

DHAHRAN, SAUDI ARABIA

In Partial Fulfillment of the  
Requirements for the Degree of

**MASTER OF SCIENCE**

In

**CHEMICAL ENGINEERING**

March, 2003

**UMI Number: 1413040**

**UMI<sup>®</sup>**

---

**UMI Microform 1413040**

**Copyright 2003 by ProQuest Information and Learning Company.  
All rights reserved. This microform edition is protected against  
unauthorized copying under Title 17, United States Code.**

---

**ProQuest Information and Learning Company  
300 North Zeeb Road  
P.O. Box 1346  
Ann Arbor, MI 48106-1346**

King Fahd University of Petroleum & Minerals  
DHAHRAN 31261, SAUDI ARABIA

DEANSHIP OF GRADUATE STUDIES

This Thesis, written by **Ali Ebrahim AL-MUFTAH** under the direction of his thesis advisor and approved by his thesis committee, has been presented to and accepted by the Dean of Graduate Studies, in partial fulfillment of the requirements for the degree of **MASTER OF SCIENCE IN CHEMICAL ENGINEERING**

Thesis committee

*Ibrahim Abu-Reesh*

Dr. Ibrahim M. Abu-Reesh  
(Thesis Advisor)

*Mohammed B. Amin*

Prof. Mohammed B. Amin  
(Department Chairman)

*Abdullah A. Shaikh*

Prof. Abdullah A. Shaikh  
(Member)

*Osama Ahmed Jannadi*

Prof. Osama Ahmed Jannadi  
(Dean Of Graduate Studies)

*Kevin F. Loughlin*

Dr. Kevin F. Loughlin  
(Member)

5-3-2003

Date



## **DEDICATION**

*This work is dedicated to my father,*

*To whom I love with all strength of love that she taught me*

*The love that sustains in the storms of life and protect me*

*To whom I see in every ray of light in a glorious sunrise*

*To my mother for whom it is worth living this life.*

# **ACKNOWLEDGMENT**

Thanks God. It is my pleasure to take this opportunity to express my deepest indebtedness to Dr. I. M. Abu-Reesh, my thesis advisor, for suggesting this thesis topic to me, for his encouragement, and for his infinite patience during the past two semesters in fruitful discussions, guidance and valuable suggestions. I wish also to acknowledge my gratitude to Prof. Abdulla A. Shaikh, chairman of Chemical Engineering department and a member of my thesis committee, for his incessant encouragement of my efforts during my study; your are the necessary condition for my presence in KFUPM. I wish to acknowledge my gratitude to my graduate advisor and member of my thesis committee, Dr. Keven F. Loughlin for his encouragements to take four courses per semester. Your are the person who reshaped my thinking toward mathematical modeling and numerical simulation and we enjoyed your course. I am happy to convey my deep sense of gratitude to the person whose profound influence initiated, deeply changed, and permanently shaped my thinking in the mathematical modeling in chemical engineering and understanding of transport phenomena courses, to my extraordinary teacher Prof. Der-Tau Chin, Clarkson University, USA. I am deeply indebted to current department chairman Dr. Mohammed Amin and his entire department for the warm congenial atmosphere. Moreover, I would like to acknowledge Prof. Raymond Adomaitis, University of Maryland, USA for his assistance and correspondences that update my numerical background and for provision of the latest methods and improvements that have been developed.

These acknowledgments are surely incomplete without declaring my gratitude and appreciation to Mr. Faisal Al-Mahroos, Manager Petroleum Engineering, BAPCO. I would also like to thank Mr. Isa Janahi, Head Production Engineering, for his assistance, appreciation and guidance during this thesis. I would also like to offer my sincere thanks to Mr. Hisham Zubari, Head Reservoir Engineer, for his help and cooperation. Finally, I am thankful to all Petroleum Engineering engineers and staffs for their cooperation and encouragements.

(Ali Ebrahim Al-Muftah)

# **CONTENTS**

<b>ACKNOWLEDGMENT .....</b>	<b>iv</b>
<b>CONTENTS.....</b>	<b>v</b>
<b>LIST OF TABLES .....</b>	<b>viii</b>
<b>LIST OF FIGURES.....</b>	<b>ix</b>
<b>1 Introduction.....</b>	<b>1</b>
1.1 Statement of The Problem.....	1
1.2 Motivation and Goals of This Thesis.....	2
1.3 Methodology.....	3
<b>2 Literature Review.....</b>	<b>5</b>
2.1 Mass Transfer Limitations In Immobilized Enzyme Reactors.....	5
2.2 Application of Immobilized Enzyme Reactor.....	16
2.2.1 Isomerization of Glucose to Fructose.....	16
2.2.2 Lactose hydrolysis.....	18
2.2.2.1 Introduction.....	18
2.2.2.2 Application of Lactose Hydrolysis.....	20
2.2.2.3 Kinetic of Lactose Hydrolysis.....	21
<b>3 Mathematical Analysis .....</b>	<b>23</b>
3.1 Internal and External Mass Transfer – Reaction Model.....	23
3.1.1 Assumptions.....	23
3.1.2 Mass Balance on the Reactor.....	26
3.1.3 Kinetic Equation of Lactose Hydrolysis.....	27
3.1.4 Governing Equations in Dimensionless Form.....	29
3.2 Effects of External Mass Transfer Limitation.....	33



3.2.1	Assumptions .....	33
3.2.2	Dispersed Plug Flow Reactor Model.....	33
3.2.3	Governing Equations in Dimensionless Form .....	35
3.2.3.1	Plug Flow Reactor ( $Pe \rightarrow \infty$ ) .....	37
3.2.3.2	Continuous Stirred Tank Reactor ( $Pe \rightarrow 0$ ).....	37
3.2.3.3	Mass transfer limitations ( $S_i \approx 0$ ) .....	38
3.3	CSTR Model .....	39
3.3.1	Assumptions .....	39
3.3.2	CSTR Mathematical Model .....	39
3.3.3	Normalized Mathematical Model .....	41
3.4	Criteria for Reactor Performance.....	43
3.4.1	Average Concentrations and Average Reaction Rate.....	43
3.4.2	Effectiveness Factor.....	43
3.4.3	Fractional Conversion and Yield .....	45
<b>4</b>	<b>Numerical Simulation .....</b>	<b>46</b>
4.1	Introduction.....	46
4.2	The Spectral Methods .....	48
4.2.1	Numerical Algorithms .....	51
4.2.2	Eigenfunction Expansion.....	52
4.2.3	Galerkin's Method.....	53
4.2.4	Orthogonal Collocation Method .....	53
4.2.5	Orthogonal Collocation on Finite Element (OCFE) .....	55
4.2.6	High Degree-Orthogonal and Special Polynomials.....	56
4.3	Galerkin Numerical Solution .....	59
4.3.1	Expansion of Solution.....	59
4.3.2	Quadrature Projection Methods.....	60
4.3.3	Trial Functions.....	63
4.3.4	Discretization of the PDEs.....	64
4.4	OCFE Numerical Simulation.....	67
4.4.1	Steady State Solution.....	68
4.4.2	Unsteady State Solution.....	73
4.5	Numerical Solution of External Mass Transfer Model .....	76

<b>5 Results and Discussions .....</b>	<b>79</b>
5.1 Effects of kinetic parameters with intraparticle diffusion.....	81
5.1.1 Effect of Michaelis Modulus, $\theta$ .....	81
5.1.2 Effect of product inhibition modulus, $\gamma$ .....	86
5.2 Effect of Transport Parameters .....	89
5.2.1 Effects of Stanton number and Thiele modulus.....	89
5.2.2 Effect of $St$ and $\theta$ .....	93
5.2.3 Effects of $St$ and $\gamma$ .....	97
5.3 Effects of Biot number, $Bi$ .....	101
5.3.1 Effects of Biot number and Thiele modulus.....	101
5.3.2 Effects of Biot, Michaelis modulus and $St$ .....	105
5.3.3 Effects of Biot number, $St$ and product inhibition .....	111
5.4 Effect of Reactor Hydrodynamics .....	120
5.4.1 Effects of $Pe$ , $\phi$ and $St$ .....	120
5.4.2 Effects of $Pe$ , $\theta$ , $\gamma$ and $St$ .....	124
5.5 Unsteady State Behavior.....	128
5.5.1 Unsteady State Effects of Michealis Modulus, $\theta$ .....	128
5.5.2 Unsteady State Effects of Product Inhibition, $\gamma$ .....	131
5.5.3 Unsteady State Effect of $St$ and $\theta$ .....	133
5.5.4 Unsteady State Effect of $St$ and $\gamma$ .....	137
5.5.5 Unsteady State Effect of Biot number .....	142
5.5.6 Unsteady State Effect of Thiele Modulus.....	144
5.5.7 Unsteady State Effect of $Pe$ .....	146
<b>6 Conclusions and Recommendations.....</b>	<b>151</b>
6.1 Conclusions.....	151
6.2 Recommendations.....	153
<b>NOMENCLATURE.....</b>	<b>154</b>
<b>REFERENCES.....</b>	<b>158</b>
<b>VITA.....</b>	<b>167</b>

## **LIST OF TABLES**

---

Table 3.1: Dimensionless parameters .....	30
Table 5.1: Calculated $\beta_{x_0}$ from different simulation results .....	114

## **LIST OF FIGURES**

---

Figure 2.1:	Schematic diagram of (a) Encapsulated enzyme particle (b) Substrate profile inside an encapsulated enzyme particle.....	10
Figure 2.2:	Molecular Formula of (a) D-glucose (b) D-fructose .....	17
Figure 2.3:	Lactose, a 1,4'- $\beta$ -glycoside.....	19
Figure 2.4:	Galactose chemical formula – Hworth formula .....	19
Figure 3.1:	Packed Bed immobilized enzyme Reactor .....	25
Figure 4.1:	OCFE Numerical Scheme for discretization in bulk phase and spherical particle for element $m$ .....	72
Figure 5.1:	Effects of product inhibition modulus, $\gamma$ , on substrate conversion for varying Thiele and Michaelis modulus with $Pe = 2.0$ , $Bi = 0.1$ and $St = 1.0$ .....	84
Figure 5.2:	Effects of Michaelis modulus on substrate conversion as a function of Thiele modulus for $\gamma = 0, 1, 10$ ; $Pe = 2.0$ , $Bi = 0.1$ and $St = 1.0$ .....	84
Figure 5.3:	Effects of product inhibition $\gamma$ on internal effectiveness factor for varying Michaelis and Thiele modulus for $\gamma = 0, 1, 10$ ; $Pe = 2.0$ , $Bi = 0.1$ and $St = 1.0$ .....	85
Figure 5.4:	Effects of Michaelis modulus on internal effectiveness factor as a function of Thiele modulus for $\gamma = 0, 1, 10$ ; $Pe = 2.0$ , $Bi = 0.1$ and $St = 1.0$ .....	85
Figure 5.5:	Effects of product inhibition on reactor conversion as a function of Thiele modulus for $\theta = 0.1, 1, 10$ ; $Pe = 2.0$ , $Bi = 0.1$ and $St = 1.0$ .....	88
Figure 5.6:	Effects of product inhibition on internal effectiveness factor as a function of Thiele modulus for $\theta = 0.1, 1, 10$ ; $Pe = 2.0$ , $Bi = 0.1$ and $St = 1.0$ .....	88

Figure 5.7:	Effects of product inhibition on reactor conversion for varying Stanton number and Thiele modulus with $\theta = 1, \gamma = 1; Pe = 2.0$ and $Bi = 0.1$ .....	91
Figure 5.8:	Effects of Thiele modulus on reactor conversion as a function of Stanton number with $\theta = 1, \gamma = 1; Pe = 2.0$ and $Bi = 0.1$ .....	91
Figure 5.9:	Dependence of effectiveness factor on Thiele modulus with $0.1 < St < 10$ for $\theta = 1, \gamma = 1; Pe = 2.0$ and $Bi = 0.1$ .....	92
Figure 5.10:	Effects of Michaelis modulus on reactor conversion as a function of Stanton number for $\phi = 0.1, 1, 10, \gamma = 1; Pe = 2.0$ and $Bi = 0.1$ .....	95
Figure 5.11:	Effects of Stanton number on internal effectiveness factor as a function of Michaelis modulus for $\phi = 0.1, 1, 10, \gamma = 1; Pe = 2.0$ and $Bi = 0.1$ .....	95
Figure 5.12:	Effects of Michaelis modulus on internal effectiveness factor as a function of Stanton number for $\phi = 0.1, 1, 10, \gamma = 1; Pe = 2.0$ and $Bi = 0.1$ .....	96
Figure 5.13:	Effects of product inhibition modulus on reactor conversion as a function of Stanton number for $\phi = 0.1, 1, 10, \theta = 1; Pe = 2.0$ and $Bi = 0.1$ .....	99
Figure 5.14:	Effects of product inhibition modulus on internal effectiveness factor as a function of Stanton number for $\phi = 0.1, 1, 10, \theta = 1; Pe = 2.0$ and $Bi = 0.1$ .....	99
Figure 5.15:	Effects of Stanton number on internal effectiveness factor as a function of product inhibition modulus for $\phi = 0.1, 1, 10, \theta = 1; Pe = 2.0$ and $Bi = 0.1$ .....	100
Figure 5.16:	Effect of $St$ on internal effectiveness factor for different $\theta$ and $\gamma$ at $\phi = 2$ and $Bi = 0.1$ .....	100
Figure 5.17:	Effects of Biot number on reactor conversion as a function of Thiele modulus with $\theta = 1, \gamma = 1; Pe = 2.0$ and $St = 1.0$ .....	103
Figure 5.18:	Effects of Thiele modulus on reactor conversion as a function of Biot number with $\theta = 1, \gamma = 1; Pe = 2.0$ and $St = 1.0$ .....	103

Figure 5.19: Effects of Biot number on internal effectiveness factor as a function of Thiele modulus with $\theta = 1, \gamma = 1; Pe = 2.0$ and $St = 1.0$ .....	104
Figure 5.20: Effects of Thiele modulus on internal effectiveness factor as a function of Biot number with $\theta = 1, \gamma = 1; Pe = 2.0$ and $St = 1.0$ .....	104
Figure 5.21: Effects of Michaelis modulus on reactor conversion for varying Biot number and Stanton number with $\gamma = 1, \phi = 2.0$ and $Pe = 2.0$ .....	107
Figure 5.22: Effects of $St$ number on reactor conversion as a function of Biot number with $\theta = 0.1, 1, 10, \gamma = 1, \phi = 2.0$ and $Pe = 2.0$ .....	107
Figure 5.23: Effects of $\theta$ on internal effectiveness factor for varying Biot number and Stanton number with $\theta = 0.1, 1, 10, \gamma = 1, \phi = 2.0$ and $Pe = 2.0$ .....	108
Figure 5.24: Effects of Biot number on internal effectiveness factor as a function of Stanton number with $\gamma = 1, \phi = 2.0$ and $Pe = 2.0$ for (a) $\theta = 0.1, 1, 10$ (b) $\theta = 0.5, 2, 4$ .....	109
Figure 5.25: Effects of Stanton number on internal effectiveness factor as a function of Biot number for $\theta = 0.1, 1, 10, \gamma = 1, \phi = 2.0$ and $Pe = 2.0$ .....	110
Figure 5.26: Effects of product inhibition on reactor conversion for varying Biot and Stanton number with $\gamma = 0, 1, 10, \theta = 1, \phi = 2.0$ and $Pe = 2.0$ .....	115
Figure 5.27: Effects of $St$ number on reactor conversion as a function of Biot number with $\gamma = 0, 1, 10, \theta = 1, \phi = 2.0$ and $Pe = 2.0$ .....	115
Figure 5.28: Effects of product inhibition on internal effectiveness factor for varying Biot and Stanton number with $\theta = 1, \phi = 2.0$ and $Pe = 2.0$ .....	116
Figure 5.29: Effects of product inhibition on internal effectiveness factor for varying Biot and Stanton number with $\theta = 1, Pe = 2.0$ for (a) $\phi = 0.5$ (b) $\phi = 4.0$ .....	117
Figure 5.30: Effects of product inhibition on internal effectiveness factor as a function of Biot number and Stanton number with $\theta = 1, Pe = 2.0, \phi = 2.0$ for (a) $\theta =$	

0.1 (b) $\theta = 5.0$ .....	118
Figure 5.31: Effects of product inhibition on internal effectiveness factor with $Pe = 2.0$ ; (a) varying $Bi$ and $St$ at $\phi = 2.0$ , $\theta = 0.5$ ; (b) varying $St$ and $\phi$ at $\theta = 5.0$ , $Bi = 0.1$ .....	119
Figure 5.32: Effects of Peclet number on reactor conversion for varying Thiele modulus and Stanton number with $\gamma = 1$ , $\theta = 1$ and $Bi = 0.1$ .....	122
Figure 5.33: Effects of Stanton number on reactor conversion as a function of Thiele modulus for $Pe = 0.001, 5, 10^4$ ; $\gamma = 1$ , $\theta = 1$ and $Bi = 0.1$ .....	122
Figure 5.34: Effects of Thiele modulus on reactor conversion as a function of Stanton number for $Pe = 0.001, 5, 10^4$ ; $\gamma = 1$ , $\theta = 1$ and $Bi = 0.1$ .....	123
Figure 5.35: Effects of Peclet number on reactor conversion as a function of Stanton number with $\theta = 1$ , $\gamma = 1$ , $\phi = 2$ and $Bi = 0.1$ .....	123
Figure 5.36: Effects of Michaelis modulus on internal effectiveness factor as a function of Stanton number for $Pe = 0.001, 5, 10^4$ ; $\gamma = 1$ , $\phi = 2$ and $Bi = 0.1$ .....	126
Figure 5.37: Effects of $St$ number on internal effectiveness factor as a function of Michaelis modulus for $Pe = 0.001, 5, 10^4$ ; $\theta = 1$ , $\phi = 2$ and $Bi = 0.1$ .....	126
Figure 5.38: Effects of product inhibition on internal effectiveness factor as a function of $St$ for $Pe = 0.001, 5, 10^4$ ; $\gamma = 1$ , $\phi = 2$ and $Bi = 0.1$ .....	127
Figure 5.39: Effects of Michaelis modulus on unsteady state reactor conversion with $\gamma = 1$ , $\phi = 2.0$ , $Bi = 0.1$ , $St = 1.0$ .....	130
Figure 5.40: Effects of Michaelis modulus on unsteady state effectiveness factor with $\gamma = 1$ , $\phi = 2.0$ , $Bi = 0.1$ , $St = 1.0$ .....	130
Figure 5.41: Effects of product inhibition modulus on unsteady state conversion with $\theta = 1$ , $\phi = 2.0$ , $Bi = 0.1$ , $St = 1.0$ .....	132

Figure 5.42: Effects of product inhibition modulus on unsteady state effectiveness factor with $\theta = 1$ , $\phi = 2.0$ , $Bi = 0.1$ , $St = 1.0$ .....	132
Figure 5.43: Effects of Stanton number on unsteady state conversion with $\theta = 0.1, 1, 10$ , $\gamma = 1.0$ , $\phi = 2.0$ , $Bi = 0.1$ .....	135
Figure 5.44: Effects of Stanton number on unsteady state effectiveness factor at $\theta = 0.1$ , $\gamma = 1.0$ , $\phi = 2.0$ , $Bi = 0.1$ .....	135
Figure 5.45: Effects of Stanton number on unsteady state effectiveness factor at $\theta = 1.0$ , $\gamma = 1.0$ , $\phi = 2.0$ , $Bi = 0.1$ .....	136
Figure 5.46: Effects of Stanton number on unsteady state effectiveness factor at $\theta = 10.0$ , $\gamma = 1.0$ , $\phi = 2.0$ , $Bi = 0.1$ .....	136
Figure 5.47: Effects of Stanton number on unsteady substrate conversion at $\gamma = 0.1, 1, 10$ , $\theta = 1.0$ , $\phi = 2.0$ , $Bi = 0.1$ .....	140
Figure 5.48: Unsteady state effectiveness factor as a function of Stanton number for different product inhibition $\gamma = 0, 1, 10$ , $\theta = 1$ , $\phi = 2.0$ , $Bi = 0.1$ .....	140
Figure 5.49: Effects of Stanton number on unsteady state effectiveness factor at $\gamma = 0$ , $\theta = 1.0$ , $\phi = 2.0$ , $Bi = 0.1$ .....	141
Figure 5.50: Effects of Stanton number on unsteady state effectiveness factor at $\gamma = 10$ , $\theta = 1.0$ , $\phi = 2.0$ , $Bi = 0.1$ .....	141
Figure 5.51: Effects of Biot number on unsteady state reactor conversion at $\theta = 1$ , $\gamma = 1.0$ , $\phi = 2.0$ , $St = 1.0$ .....	143
Figure 5.52: Effects of Biot number on unsteady state effectiveness factor at $\theta = 1$ , $\gamma = 1.0$ , $\phi = 2.0$ , $St = 1.0$ .....	143
Figure 5.53: Effects of Thiele modulus on unsteady state conversion at $\theta = 1$ , $\gamma = 1.0$ , $Bi = 0.1$ , $St = 1.0$ .....	145



Figure 5.54: Effects of Thiele modulus on unsteady state effectiveness factor at $\theta = 1$ , $\gamma = 1.0$ , $Bi = 0.1$ , $St = 1.0$ .....	145
Figure 5.55: Effects of Peclet number on unsteady state conversion at $\theta = 1$ , $\gamma = 1.0$ , $Bi = 0.1$ , $\phi = 2.0$ , $St = 1.0$ .....	148
Figure 5.56: Effects of Peclet number on unsteady state effectiveness factor at $\theta = 1$ , $\gamma = 1.0$ , $Bi = 0.1$ , $\phi = 2.0$ , $St = 1.0$ .....	148
Figure 5.57: Effects of Peclet number on unsteady substrate conversion for $St = 0.1, 1, 10$ ; $\gamma = 1$ , $\theta = 1.0$ , $\phi = 2.0$ , $Bi = 0.1$ .....	149
Figure 5.58: Effects of Stanton number on unsteady state effectiveness factor at $\theta = 1.0$ , $\gamma = 1.0$ , $\phi = 2.0$ , $Bi = 0.1$ , $Pe = 0.01$ .....	149
Figure 5.59: Effects of Stanton number on unsteady state effectiveness factor at $\theta = 1.0$ , $\gamma = 1.0$ , $\phi = 2.0$ , $Bi = 0.1$ , $Pe = 100$ .....	150

## **ABSTRACT**

**FULL NAME OF STUDENT:** ALI EBRAHIM AL-MUFTAH  
**TITLE OF STUDY:** THEORETICAL ANALYSIS AND SIMULATION  
OF IMMOBILIZED ENZYME REACTORS  
**MAJOR FIELD:** CHEMICAL ENGINEERING  
**DATE OF DEGREE:** MARCH 2003

A general mathematical model has been developed for predicting the performance and simulation of a packed bed immobilized enzyme reactor performing lactose hydrolysis, which follows Michaelis – Menten kinetics with competitive product (galactose) inhibition. The performance characteristics of a packed bed immobilized enzyme reactor have been analyzed taking into account the effects of various diffusional phenomena like axial dispersion, internal, external and simultaneous effects of internal and external mass transfer limitations. The model design equations are then solved by the method of weighted residuals such as Galerkin's method and orthogonal collocation on finite elements.

The effects of intraparticle diffusion resistances, external mass transfer and axial dispersion have been studied and their effects were shown to reduce both internal effectiveness factor and time required to reach final steady – state. The effects of product

inhibition have been investigated at different operating conditions correlated at different regimes using dimensionless  $\beta_{x_0}$  ( $St$ ,  $Bi$ ,  $\theta$ ,  $\phi$ ). Product inhibition was shown to reduce substrate conversion, and to decrease effectiveness factor when  $\beta_s > \beta_{x_0}$ , however it increases internal effectiveness factor when  $\beta_s < \beta_{x_0}$ . The effectiveness factor is found to be independent of product inhibition at cross – over point at which  $\beta_{x_0}$  is defined. Effects of  $St$  and  $Pe$  have been investigated at different kinetic regimes and the results show their effects have a strong dependence on kinetic parameters  $\theta$   $\gamma$  (i.e  $K_m / K_p$ ) and  $\beta_{x_0}$ .

**Master of Science Degree**

**King Fahd University of Petroleum & Minerals**

**Dhahran, Saudi Arabia**

**March 2003**

## ملخص بحث

درجة الماجستير في العلوم

الاسم: علي إبراهيم آل مفتاح

عنوان الرسالة: التحليل النظري و المحاكاة للمفاعلات الإنزيمية المثبتة

التخصص: الهندسة الكيميائية

تاريخ التخرج: مارس 2003

لقد تم تطوير نموذجاً رياضياً عاماً لحساب أداء و محاكاة المفاعلات الإنزيمية ذات الطبقة الثابتة ( Packed bed ) والتي يتم فيها تفاعل تحلل اللاكتوز وهذا التفاعل يخضع لمعادلة Michaelis – Menten لميكانيكية التفاعل مع وجود تثبيط من قبل السكر الناتج من التفاعل ( Galactose ) . لقد تم تحليل صفات وأداء المفاعلات الإنزيمية مع الأخذ في الاعتبار عدة عوامل منها ظواهر الانتقال ، التشتت المحوري ( Axial dispersion ) ووجود المؤثرات الداخلية والخارجية لانتقال المادة أو كلاهما معا. ولقد تم حل المعادلات التفاضلية الجزئية الناتجة عن وصف المفاعل بطريقتي Galerkin والدوال المتعامدة ( Orthogonal collation on finite elements ) .

في هذا البحث تم دراسة تأثير مقاومة انتقال المادة الداخلية ، والخارجية و التشتت في المفاعلات الإنزيمية الحفازة وتأثيرها في تقليل معامل الأداء ( effectiveness factor ) ، وزمن الوصول إلى حالة الاستقرار . ولقد تم دراسة تأثير التثبيط بفعل المنتج عند ظروف تشغيل مختلفة معتمدة على  $\beta_{x0}$  ووجد أن التثبيط بفعل المنتج يعمل على خفض تحويل اللاكتوز ( Conversion ) وخفض معامل الأداء عندما تكون  $\beta_s$  أكبر من  $\beta_{x0}$  بينما تزيد من معامل الأداء عندما تكون  $\beta_s$  أصغر من  $\beta_{x0}$ . هذا وقد وجد أن معامل الأداء لا يعتمد على مقدار التثبيط بواسطة المنتج عند نقطة التقاء منحنيات مختلفة لمعامل التثبيط وهذه النقطة عرفت بواسطة  $\beta_{x0}$  . ولقد تم دراسة تأثير كل من رقم Stanton ورقم Paclet عند ظروف تفاعل حركية مختلفة وأشارت النتائج على وجود علاقة قوية مع معاملات ميكانيكية التفاعل  $(\theta\gamma = K_m / K_p)$  و المعامل  $\beta_{x0}$ .

درجة الماجستير في العلوم

جامعة الملك فهد للبترول والمعادن

الظهران ، المملكة العربية السعودية

مارس 2003 م

# **1**

---

## **INTRODUCTION**

### **1.1 Statement of The Problem**

Since the effects of various phenomena such as axial dispersion, internal, external and simultaneous internal and external mass transfer with reversible Michaelis – Menten kinetics are strongly coupled, this makes prediction of reactor performance difficult. Little is published about performance of immobilized enzyme reactor performing reversible enzyme reaction coupled with internal and external mass transfer in an immobilized enzyme reactor. Most of the published work assumed either first order or Michaelis – Menten kinetics with external or internal mass transfer limitations. Little effort was put into generalizing a model that combines all enzymatic reactions with axial dispersion (fluid hydrodynamic in the reactor) and mass transport phenomena in various combinations in an immobilized enzyme on a porous spherical particles.

The proposed model, in this work, is formulated to examine extreme cases considered in the literature. Hydrodynamics of immobilized enzyme reactor (IMER) can be described

by dispersed plug flow model characterized by a Peclet number. The value of  $Pe$  number is a measure of the degree of dispersion. High values of  $Pe$  number ( $Pe \rightarrow \infty$ ) correspond to a slightly dispersed reactor, approaching plug flow and when ( $Pe \rightarrow 0$ ) the reactor operates as a highly dispersed reactor, approaching CSTR. Thus a finite  $Pe$  number can represent real reactor. Little work has been conducted to study the performance of IME reactor performing reversible enzyme reaction, competitive product inhibition reaction. Most work is limited to special cases such as CSTR.

## **1.2 Motivation and Goals of This Thesis**

Therefore, the objective of this thesis is to study the performance of a packed bed immobilized enzyme reactor performing reversible Michaelis – Menten kinetics at various operational conditions. The effects of various phenomena such as external, internal mass transfer limitations in an enzyme immobilized on a porous spherical particles and axial dispersion are studied. The performance of packed bed immobilized enzyme reactor is tested over a wide range of operating conditions in terms of effectiveness factor and substrate conversion as a function of Thiele Modulus, Peclet number, Damkholer number, Biot number and product inhibition and Michaelis modulus.

The reactor performance is reduced to a function of the following phenomena that can be represented by dimensionless parameters

- (1) Effect of external mass transfer limitation characterized by Damkholer number.

- (2) Effect of internal mass transfer limitations on an immobilized enzyme on a porous spherical particles support, characterized by Thiele modulus.
- (3) Effect of axial dispersion, represented by Peclet number.
- (4) Simultaneous external and internal diffusional limitations described by studying the effect of Biot number
- (5) The enzyme that catalyzes a specific reaction according to reversible Michaelis – Menten kinetics is immobilized on porous spherical particles. Michaelis modulus, product inhibition modulus and dimensionless equilibrium modulus are kinetics parameters used to describe IME reactions.
- (6) Study unsteady state behavior.

### **1.3 Methodology**

In this thesis, it is proposed to present a general mathematical model that represents a packed bed immobilized enzyme catalyzed reactor. This is done, by setting up the differential material balance considering external and internal diffusional limitations on the enzymatic reaction. The resulting governing equations are then normalized to specified dimensionless parameters that describe system behavior and characterize its nature.

A simplified assumption is then incorporated to predict special cases such as study of the effects of external mass transfer with enzymatic reaction. Specialized cases for a specific type of immobilized enzyme reactors such as CSTR or plug flow reactor are studied. On

the other hand, some special cases constraining control rate either mass transfer limitation or reaction rate control are also developed.

Chapter 2 reviews the modeling of immobilized enzyme reactor encountered in the literature and related assumptions. In this chapter a more detailed review is classified according to the reactor hydrodynamic type, isothermal / nonisothermal and effects of mass transfer diffusional limitations.

Chapter 3 gives a details of the proposed mathematical model of an immobilized enzyme reactor. This general model is set up with its dimensionless parameters that describe the reactor behavior. A CSTR immobilized enzyme reactor and external mass transfer model are two special cases studied with simplified assumptions.

Numerical simulations of the nonlinear and non-homogeneous partial differential equations proposed in chapter 3 are solved using fast and efficient solutions. Much more emphasis is put on toward spectral method of solution such as collocation method and Galerkin's method. The first method is used extensively in this work because it approximates the Galerkin's solution. However, Galerkin's method is used to propose a more analytical approach to solve the immobilized enzyme catalyzed reactor system. All this numerical solutions are discussed in chapter 4. Chapter 5 discusses the simulation results which include effects of kinetic and transport parameters on both substrate conversion and internal effectiveness factor. In this chapter, both steady and unsteady state behaviors have been discussed. Finally, chapter 6 concludes the main findings from this theoretical study with recommendation to be taken in future study.



# **2**

---

## **LITERATURE REVIEW**

### **2.1 Mass Transfer Limitations In Immobilized Enzyme Reactors**

Enzyme immobilization offers a number of advantages over enzymes in suspension. Immobilization permits the reuse of the enzyme and may provide a better environment for catalyst activity and also it reduces the cost of downstream processing in addition to good product quality. These factors make it widely used in industry where many enzyme – catalyzed reactions are of industrial interest.

Continuous processes with immobilized enzymes can be carried out in different types of reactor. Lortie and Pelletier (1992) have shown that plug-flow reactor model with external mass transfer resistance can represent adequately a fixed bed immobilized enzyme reactor for moderate or low dispersion. However, dispersed plug flow reactor model is superior in predicting the performance of packed bed reactor for isomerization of glucose to fructose (Ching and Ho, 1984). Furthermore, a comprehensive model for a

general rate expression such as reversible Michaelis – Menten kinetics was developed by Abu-Reesh (1997) neglecting internal mass transfer resistance. A fluidized bed reactor model taking into account the reversibility of the reaction, inhibition by substrate and products or diffusional limitations was developed (Bodalo *et al.*, 1995; Kissler *et al.*, 1990).

In a continuous stirred-tank reactor (CSTR), the average reaction rate is lower than it would be in a plug flow or packed bed reactor. Moreover, ease of replacement of immobilized enzyme catalyst and easier control of temperature and pH are plusses for a CSTR. Furthermore, CSTR performance is superior to that of a packed bed, when the immobilized enzymes are kept suspended at fairly high agitation rates. Bodalo *et al.* (1993) put forward a general mathematical unsteady state model for the analysis and simulation of such a CSTR.

One way of immobilizing an enzyme is by encapsulation of enzyme in a Hollow fiber bioreactor (HFBR) by placing the enzyme solution within the fiber lumen. The enzyme solution saturates the porous sponge section of the fiber wall and substrate passes through the fiber lumen (the reactant which is fed through the inner tube). The enzyme is immobilized in the spongy matrix and cannot pass through the matrix of membrane skin. This method of immobilization has several advantages such as the enzyme is prevented from leaving the spongy matrix due to the sponge-gas interface at the shell-side fiber boundary. Also, it serves to minimize mass transfer diffusional resistances, thereby making it a very attractive method for enzyme immobilization where, the substrate and enzyme are physically separated. Another very important practical advantage of this type

of enzyme immobilization is the fact that the enzyme is only immobilized with respect to the solution flowing in the fiber lumen. Furthermore, by the simple expedient of flushing solution through the annular sponge, it is possible to remove and replace the enzyme (or introduce another enzyme) as desired. So, it is well suited for the conduct of multi-enzyme conversions and to the use of highly labile enzymes, which cannot tolerate chemical immobilization.

Many models are available for the theoretical description of HFBR (Belfort, 1989; Kelsey *et al.*, 1990; Kleinstreuer and Agramel, 1987). Waterland *et al.* (1974) have solved both linear and nonlinear reaction kinetics in membrane reactors. The behaviors of HFBR are studied in terms of bulk concentration and dimensionless axial coordinate as a function of Thiele modulus, radial profile and Michaelis – Menten modulus. Also, an exact analytical solution for substrate concentration profile throughout an idealized fiber, which incorporates the membrane and hydrodynamic mass transfer resistances, are obtained for first order enzyme reaction and numerical finite difference solution for nonlinear Michaelis-Menten reaction kinetics. Furthermore, numerical finite difference solution are employed for nonlinear kinetics.

However, the coupled set of model equations describing the behavior of this reactor represents an extended Greatz problem in the fiber lumen, with diffusion through the thin membrane skin and reaction in the micro-porous spongy matrix. Kim and Cooney (1976) and Jayaraman (1992) have obtained compact solution to the first order reaction kinetics in HFBR. Jayaraman and Kulkarni (1997) have solved nonlinear reaction kinetics, by developing a general iterative algorithm based on evaluation of effectiveness factor. They

have a good agreement between their results and that of finite difference method.

Willaert *et al.* (1999) studied diffusional mass transfer limitations in hollow fiber bioreactors. Theoretical analysis was used for steady-state diffusion and reaction model. Analytical expressions were derived for zero- and first – order kinetics including the effects of Thiele modulus on effectiveness factor for first order kinetics. Moreover, the influences of effective diffusivity ratio, and the thickness of membrane on the reactor performance were studied. Deviation from Newtonian fluid behavior was considered in the analysis for designing HFBR, where the first order and Michaelis – Menten kinetics was assumed in the analysis (Jayaraman, 1994).

Paunovic *et al.* (1993) developed a one-dimensional mathematical model of isothermal anaerobic biodegradation in HFBR with Monod type of growth in recycle reactor. Kumar and Modak (1997) studied the effect of various operating conditions, such as substrate feed rate, length of bioreactor and diffusivity of substrate, on the reactor performance. Diffusion is assumed to be the dominant process in the radial direction while axial convection dominates in the lumen of the bioreactor. The diffusion reaction and convection control regimes are identified based on Peclet number and Thiele modulus. Moving boundary of biofilm was considered in their analysis.

Among these reactors, packed bed enzyme-catalyzed reactors have promising applications in many biochemical processes (Abu-Reesh, 1997; Hassan *et al.*, 1996 & 1995) and biological processes (Hassan and Beg, 1987) having advantages of longer solid retention times and ease of operation and relatively high conversion rates.

**In spite of the well-established industrial application of packed bed immobilized enzyme reactors, little effort has been made toward mathematical modeling of such reactor with kinetics other than Micaelis – Menten equation. In most of the cases, enzyme immobilization is accompanied by mass transfer limitation. Different factors have to be taken into consideration in modeling of immobilized enzyme reactors shown in Figure 2.1:**

- (1) Mode of operation, whether the steady state or transient.**
- (2) Mass transfer limitations (external, internal and simultaneous transfer).**
- (3) Resistance of the membrane to any transport processes.**
- (4) The kinetics of enzyme catalyzed reaction.**
- (5) The axial dispersion effects.**
- (6) Types of reactors: Packed Bed, CSTR, Hollow Fiber Bioreactor (HFBR) or Fluidized Bed Reactor (FBR).**
- (7) The stability of enzyme and effect of temperature on the enzyme activity.**
- (8) Heat transfer effects.**

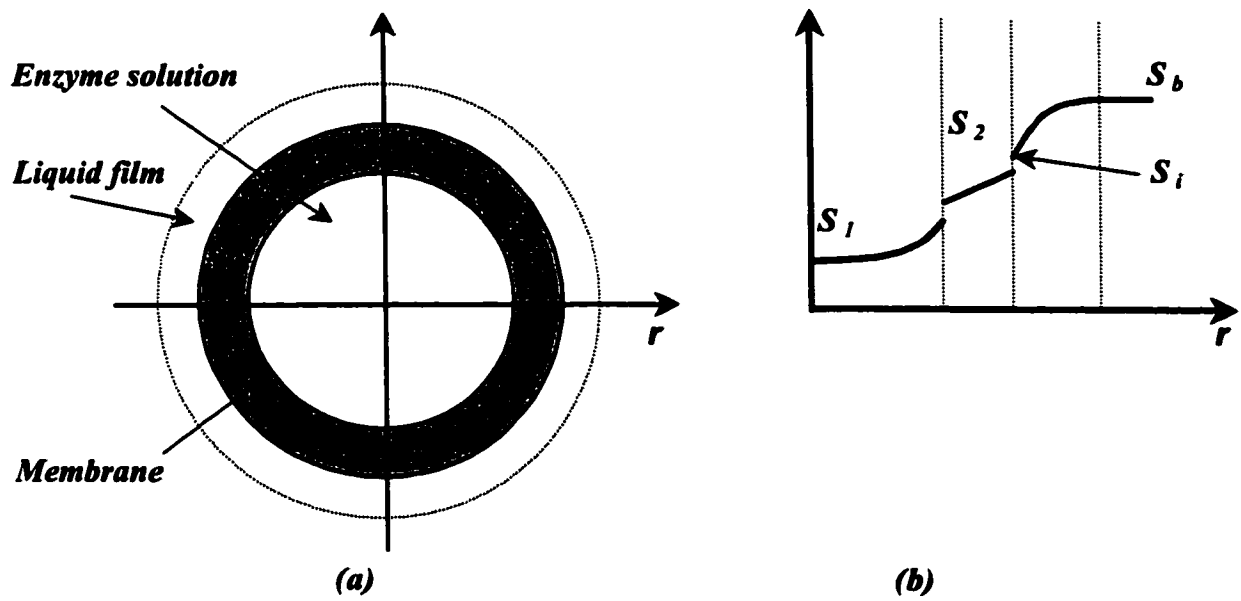


**Figure 2.1: Schematic diagram of (a) Encapsulated enzyme particle (b) Substrate profile inside an encapsulated enzyme particle**

Quantitative knowledge of the effect of these factors on the reactor performance and simulation is required for efficient design of immobilized enzyme reactor. Several isothermal steady state models have been considered using one or more of these phenomena in various combinations.

External mass transfer limitation is shown to have significant effect on the performance of immobilized enzyme reactor (Vasic-Racki *et al.*, 1991) using reversible enzyme reactions (Park *et al.*, 1984). Analytical solution was given by Carrara and Rubiolo (1997) and tested with experimental setup, for evaluation of mass transfer coefficient and conversion. However, Kobayashi and Moo-Young (1971) were the first to apply the dispersion model to immobilized enzyme reactor. Dispersed plug flow reactor model (taking into account the effect of axial dispersion on flow reactor) is shown to be superior in predicting the performance of packed bed reactor for isomerization of glucose to fructose described by Michaelis – Menten (Ching and Ho, 1984; Ching and Chu, 1988). Furthermore, dynamic behavior of plug flow reactor was studied and the kinetics parameters were estimated by fitting the experimental data to satisfy the dynamic response RTD curve. Michaelis – Menten kinetics is considered in experimental validation of PFR (Lortie and Thomas, 1986 and Lortie, 1994) and in spiral reactor (Bakken *et al.*, 1989).

Abu-Reesh (1997) developed a general dimensionless model for predicting the steady state performance of immobilized dispersed plug-flow reactor performing reversible

Michaelis – Menten kinetics. The effects of dimensionless parameters of Damkohler number ( $Da$ ), Stanton number ( $St$ ), Peclet number ( $Pe$ ), the equilibrium constant and input substrate concentration were studied parametrically. Abu-Reesh (1997) found that conversion is almost complete for high  $Da$  and  $St$  number especially in plug flow reactor which gives higher conversion compared to other reactor models. Furthermore, it is found that substrate conversion increases with increasing substrate external diffusion (i.e., decreasing diffusion resistance) and residence time. Moreover, the higher the  $St$  number, the higher the maximum conversion that can be achieved. The effect of the equilibrium constant on reactor performance was also studied. Recently, Carrara *et al.* (2001) studied the behavior of fixed bed reactor considering steady – state conditions and external mass transfer resistance in the fluid around spherical catalyst particles. Their results showed the importance of hydrodynamic and kinetic reaction parameters for error reduction in the prediction of experimental behavior.

When enzyme is attached to a porous carrier matrix the internal mass-transfer limitations have a great influence on the intrinsic kinetics. It is necessary to develop comprehensive models that quantitatively account for the internal diffusional effects in addition to external one. The internal diffusional limitations with external diffusional effects can be quantified through the use of an effectiveness factor,  $\eta$ , or apparent kinetic parameters using the idealized plug flow reactor assuming Michaelis – Menten kinetics (Jung and Bauer, 1992; Marrazo and McCoy; 1981; Shiraishi *et al.*; 1996a, 1996b, 1995; Shiraishi and Fujiwara, 1996; Miyakawa *et al.*; 1999a, 1999b). Isothermal, steady state and omission of the axial dispersion term were assumed in these analyses. The Biot number,



effectiveness factor and Thiele modulus were studied numerically using Taylor expansion and orthogonal collocation methods. Theoretical analysis was incorporated with experimental data to correlate mass transfer coefficient (Shiraishi *et al.*, 1996b).

Many researchers considered coupled internal and external diffusional limitation (Bodalo *et al.*, 1986; Bodalo *et al.*, 1991; Baratti *et al.*, 1994; Do *et al.*, 1982; Clark & Bailey, 1983; Dennis *et al.*, 1984; Clark & Bailey, 1984; Clark *et al.*, 1985; Shyan *et al.*, 1975). Coupled internal and external diffusional limitation were considered in development of a general CSTR model in which the effect of membrane diffusional resistance and Biot number were taken into account for prediction the effectiveness factor of an encapsulated enzyme particle (Lin, 1979). Also, analytical solution of effectiveness factor was developed for Michaelis – Menten kinetics. Bodalo *et al.* (1995) and Manjon *et al.* (1987) considered the external and internal diffusional limitations and their model was solved numerically for reversible Michaelis – Menten kinetics with competitive product inhibition in a fluidized bed reactor (FBR). They found a good agreement between the model predictions experimental data obtained from operating a FBR containing  $\beta$ -galactosidase covalently immobilized in Chromosorb-W. In the last few years, considerable progress has been made in enzyme reactor engineering. Most of the studies published on enzyme reactor modeling have been confined to steady-state isothermal reactor operation. Although many practical systems of interest would fall into this category, it is useful to examine their transient behavior with thermal deactivation of enzyme. Recently, Xiu *et al.* (2001) developed a model for immobilized enzyme

catalyzed kinetic resolution of racemate in a fixed – bed reactor. They studied the effects of mass transfer limitations, competitive substrate inhibition and deactivation of immobilized enzyme.

Unsteady state isothermal models in which coupled internal, external and axial dispersion is considered in this research. It is useful to examine reactor transient behavior for several reasons:

1. For understanding the start-up and shutdown performance of a reactor
2. To study the reactor dynamics and control characteristics under various operating conditions and disturbances
3. To estimate the time required to reach a new steady state when a definite disturbance is introduced into a reactor system at steady state
4. To explore possibilities of multiple steady states of a given reactor scheme
5. To analyze the regulation and control of reactors by injected activators, inhibitors, or co substrates;

Hassan and Beg (1987) studied the performance and simulation of a packed bed biological reactor assuming that the diffusional limitations is the biofilm with Michaelis – Menten kinetic. They studied the effects of Peclet number, product inhibition of an inert, Biot number, Biofilm thickness and surface area on the exit concentration. Bodalo *et al.* (1993) developed a mathematical model applicable to the analysis and simulation of heterogeneous enzymatic reaction in a CSTR. The model describes the unsteady state

behavior for CSTR and the diffusion reaction equation in the spherical catalyst particles for reversible Michaelis – Menten kinetics. The dynamic behavior and the effect of effectiveness factor on the exit substrate concentration were studied. The method of finite difference was used to simulate the design equations and to estimate effectiveness factor, conversion and average reaction rate.

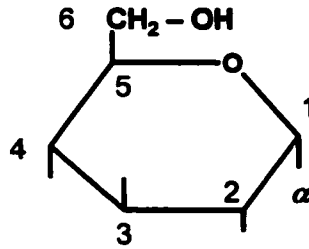
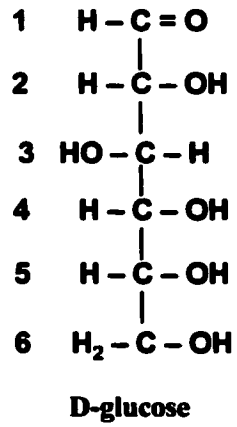
Nonisothermal model including coupled internal and external diffusional effects on the performance of packed bed reactors was considered by Lin (1991) and Hassan *et al.* (1996 and 1995). Lin (1991) developed nonisothermal model taking into consideration the effect of enzyme activity with temperature to predict the optimal feed temperature for immobilized enzyme packed bed reactor. Hassan *et al.* (1995) presented a transient model that considered axial dispersion of heat and mass, internal and external mass transport, assumed Michaelis – Menten kinetics for a bioreactor packed bed with spherical particles. Hassan *et al.* (1996) studied and analyzed the influence of the shape of enzyme microcapsule on the performance of the reactor.

## **2.2 Application of Immobilized Enzyme Reactor**

### **2.2.1 Isomerization of Glucose to Fructose**

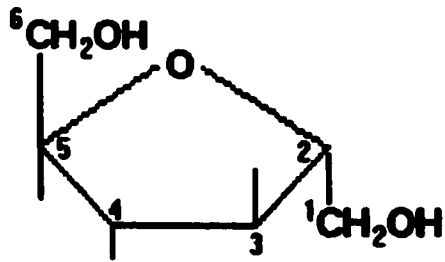
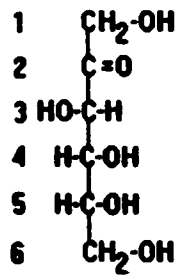
This reaction converts glucose which is not very sweet to fructose, the most sweet of the natural sugars. Syrups from this process compete with sucrose (cane sugar) in many food applications. Almost all manufacturers of soft drinks use high fructose syrups because they are less expensive than sucrose. This was devastating to world prices of cane sugar and crippled the economies of some countries. The forms of glucose and fructose are shown in Figure 2.2. The kinetics of this reaction follows reversible Michaelis – Menten.

The isomerization of glucose to fructose is part of the glycolysis cycle that converts glucose to pyruvate. The way this is done is to isomerize the aldehyde (hemiacetal) glucose to the ketone (as a hemiacetal) fructose, and make another phosphate ester. The isomerization takes advantage of the ease of breakage of a C-H bond which involves a carbon next to a carbonyl carbon. This is important in the next step which cleaves the bond between carbons three and four of fructose. It is noted that this bond involves the carbon next to the carbonyl carbon of fructose. This cleavage would not have been possible without the isomerization of glucose to fructose, because the carbonyl group of glucose is too far from carbons three and four to make that bond breakable.



$\alpha$  - D - glucose  
 if C<sub>1</sub> has OH up it will be  
 $\beta$  - D - glucose

(a)



(b)

**Figure 2.2: Molecular Formula of (a) D-glucose (b) D-fructose**

## **2.2.2 Lactose hydrolysis**

### **2.2.2.1 Introduction**

The main purpose of using immobilized enzymes here is to convert the disaccharide lactose via hydrolysis into its monosaccharide components, glucose and galactose. Lactose is a disaccharide that occurs naturally in both human and cow's milk. It is widely used in baking and in commercial infant-milk formulas. One large problem with lactose is that many people are lactose intolerant - meaning that their body is incapable of digesting lactose. So it must be hydrolyzed into its monosaccharide components, allowing digestion which is the purpose of new products today such as Lactaid<sup>®</sup>. Like cellobiose and maltose, lactose is a reducing sugar. It exhibits meta - rotation and is a 1,4'- $\beta$ -linked glycoside (Figure 2.3). Unlike cellobiose and maltose, however, lactose contains two different monosaccharide units. Acidic hydrolysis of lactose yields 1 equiv of D-glucose and 1 equiv of D-galactose, the two are joined by a beta-glycoside bond between C<sub>1</sub> of galactose and C<sub>4</sub> of glucose (Figure 2.4). In other words, 100 g of lactose will produce 50 g each of galactose and glucose. The hydrolytic conversion of lactose to glucose and galactose represents one way of adding value to whey and whey-derived products. For the enzymatic lactose hydrolysis various mesophilic  $\beta$ -glycosidases have been described, some of which have already made it to the market. The application of known glycosidases is however partly hampered because of the moderate thermal stability and narrow pH profile of enzyme activity as well as due to the significant inhibition by galactose.

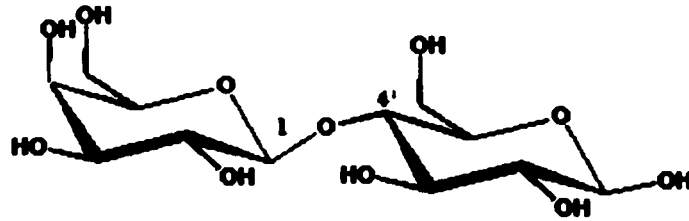


**Figure 2.3: Lactose, a 1,4'-β-glycoside**

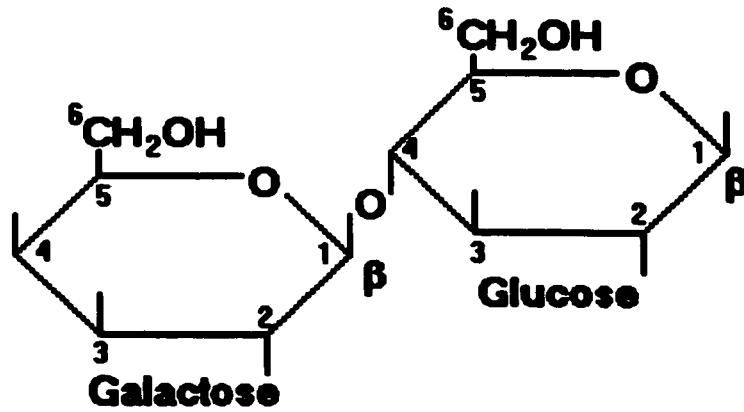


**Figure 2.4: Galactose chemical formula – Haworth formula**

### **2.2.2.2 Application of Lactose Hydrolysis**

Lactose is a disaccharide that occurs naturally in both human and cows milk which accounts for 40 % of milk solids. It is widely used in baking and commercial infant - milk formulas. The hydrolysis of lactose, the sugar of milk to glucose and galactose has received much attention in recent years (Santos *et al.*, 1998, Petzelbauer *et al.*, 1999 and Carrara and Rubiolo, 1995). It is used for production of low lactose milk for consumers that suffer from lactose deficiency (70 % of the world population is lactose deficient, Carrara and Rubiolo, 1995). The hydrolysis product is sweeter and more soluble and biodegradable than lactose and can be used in further biotechnological processes.

The amount of lactose produced annually from whey is about 3.3 million tons (Carrara and Rubiolo, 1995). It is produced as cheese whey, which is the liquid, separated after milk coagulation. It represents about 90 % of the milk volume. The disposal of whey is considered a serious pollution problem facing dairy industry because of its high pollutant content (COD of about 70.000 ppm). Acid hydrolysis of lactose is not favorable because of color formation and fouling of ion exchange resins used in processing. A better alternative is the use of enzymatic method. Enzymatic lactose hydrolysis is carried out by adding  $\beta$ -galactosidase commonly known as lactase to milk, skim milk or whey to hydrolyze lactose prior to pasteurization. Lactase is commercially available and used in large scale processes. One problem associated with the use of lactase is that complete hydrolysis is difficult to achieve because of product (galactose) inhibition and production



of isomer of lactose, allolactose. Several microbial sources of  $\beta$ -galactosidase and reactor types have been used for the purpose of economic production of low lactose milk. Lactose hydrolysis in plug flow reactor gives higher conversion compared to continuous stirred tank reactor although the latter has good mixing and lower construction cost.

### **2.2.2.3 Kinetic of Lactose Hydrolysis**

Kinetics of lactose hydrolysis has been studied extensively in the literature (Santos *et al.*, 1998; Petzelbauer *et al.*, 1999 and Carrara & Rubiolo, 1997). Michaelis - Menten model with competitive product inhibition by galactose is widely used to describe the hydrolysis (Santos *et al.*, 1998). Different types of bioreactor (Yang and Okos, 1989; and Bakken *et al.*, 1984) and biocatalyst (Santos *et al.*, 1998; Petzelbauer *et al.*, 1999; Papayannakos *et al.*, 1993; and Tomaska *et al.*, 1995) have been investigated for lactose hydrolysis.

The use of lactose – hydrolyzed whey in ice cream would help to minimize the potential problems of sandy texture caused by the formation of lactose crystals while contributing to the sweetness (Bury and Jelen, 2000). They studied the effect of lactose hydrolysis on freezing point and dipping characteristics of ice cream. Lactose hydrolysis decreased the freezing point from - 1.63 °C (0 % hydrolysis) to - 1.74 °C in a sample hydrolyzed to 83 %. Firmness decreased from 0.35 Joules ( 0 % hydrolysis) to 0.08 Joules in the sample hydrolyzed to 83 %. Lactose hydrolyzed samples melted at a faster rate than the control (0 % hydrolysis). One problem limited the application of lactase derived from mesophilic sources is the non-satisfactory long-term stability of enzyme activity (Carrara

and Rubiolo, 1995). Santos *et al.* (1998) reported that some lactases are quite stable for temperature up to 40 °C. Above this temperature the enzyme deactivation effect becomes important (Santos *et al.*, 1998). The use of thermostable lactases with an operational temperature above 60 °C solves many problems related to lactose hydrolysis such as (1) substrate solubility, (2) microbial contamination, (3) enzyme stability, (4) product inhibition, and (5) product distribution.

The optimal flow axial velocity of packed-bed plug flow reactor employed for lactose hydrolysis was studied (Figueroa *et al.*, 1997). Results showed the existence and uniqueness of an optimal constant velocity in the packed bed column.

# 3

---

## MATHEMATICAL ANALYSIS

### 3.1 Internal and External Mass Transfer – Reaction Model

Consider a packed bed immobilized enzyme reactor (shown in Figure 3.1) of length,  $L$ , fluid velocity,  $u$ , where  $C_{S0}$  and  $C_{P0}$  are the substrate and product inlet concentrations respectively.

#### 3.1.1 Assumptions

The mathematical model that describe the behavior of a packed bed immobilized enzyme reactor has been formulated using the following assumptions:

- (1) Isothermal packed bed immobilized enzyme reactor.
- (2) Neglect the resistance of the membrane to any transport process (neglect partitioning coefficients).
- (3) Enzyme activity is uniform throughout the particle.

- (4) The enzyme is immobilized evenly inside porous spherical particles, which are uniformly packed in the reactor.**
- (5) The convective velocity is uniform.**
- (6) The hydrodynamics of the bed fluid is described by the dispersed plug-flow model.**
- (7) Pressure drop across the reactor and radial concentration gradient in the bulk fluid phase are assumed to be negligible.**
- (8) Assume the enzyme deactivation is absent. This may occur due to one or more of several phenomena such as thermal shock, continuous exposure to substrate for long period of time, formation of inactive complexes with substrate and foreign material present in the solution.**
- (9) The enzyme can catalyze a specific reaction according to reversible Michaelis – Menten kinetics.**
- (10) The enzymatic reaction is monosubstrate and yields only one product.**
- (11) Ficks Law can model the substrate and product diffusion inside the catalytic particle. The effective diffusivity does not change throughout the particles and is independent of the concentration**

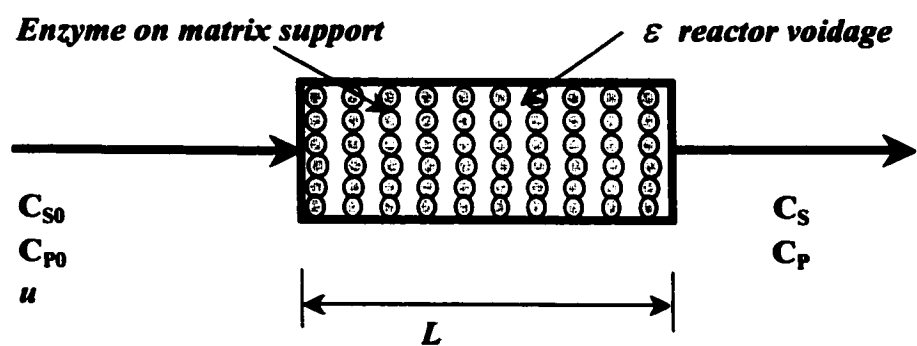


**Figure 3.1: Packed Bed immobilized enzyme Reactor**

### 3.1.2 Mass Balance on the Reactor

Under these assumptions, the differential mass balance in the liquid bulk phase for the substrate and the product can be written respectively as,

$$\varepsilon \frac{\partial C_{Sb}}{\partial t} = D_{S_z} \varepsilon \frac{\partial^2 C_{Sb}}{\partial z^2} - u \frac{\partial C_{Sb}}{\partial z} - (1 - \varepsilon) K_L a (C_{Sb} - C_S|_{r=R}) \quad (3.1)$$

$$\varepsilon \frac{\partial C_{Pb}}{\partial t} = D_{P_z} \varepsilon \frac{\partial^2 C_{Pb}}{\partial z^2} - u \frac{\partial C_{Pb}}{\partial z} - (1 - \varepsilon) K_L a (C_{Pb} - C_P|_{r=R}) \quad (3.2)$$

where,  $\varepsilon$  is the reactor voidage,  $D_{S_z}$ ,  $D_{P_z}$  are the effective substrate and product axial diffusivity (or axial dispersion coefficients) and  $K_L a$  is the overall mass transfer coefficient.

The initial condition for reactor start-up contains the immobilized enzyme particles suspended in a solution without substrate or product. At  $t = 0^+$  the substrate and product are continuously pumped into and out of the reactor at constant rate,

$$\text{at } t = 0^-, \quad C_{Sb} = 0$$

Equations (3.1) and (3.2) are subjected to the following boundary conditions requiring continuity of fluxes at both ends of the reactor (Danckwerts, 1953) for both substrate and product

$$\text{at } z = 0^+, \quad C_{Sb}|_{z=0^+} = C_{Sb}|_{z=0^-} + \frac{D_{S_z} \varepsilon}{u} \frac{\partial C_{Sb}}{\partial z} \Big|_{z=0^+} \quad (3.3a)$$

$$C_{Sb}|_{z=0^+} = C_{Sb}|_{z=0^-} + \frac{D_{S_z} \varepsilon}{u} \frac{\partial C_{Sb}}{\partial z} \Big|_{z=0^+} \quad (3.3b)$$

$$\text{at } z = L, \quad \left. \frac{\partial C_{Sb}}{\partial z} \right|_{z=L} = \left. \frac{\partial C_{Pb}}{\partial z} \right|_{z=L} = 0 \quad (3.4)$$

The substrate and product mass balance equations in immobilized enzyme particles on a porous spherical particle support is given as:

$$\frac{\partial C_S}{\partial t} = D_{Sp} \frac{1}{r^2} \frac{\partial}{\partial r} \left( r^2 \frac{\partial C_S}{\partial r} \right) - R_S \quad (3.5)$$

$$\frac{\partial C_P}{\partial t} = D_{Pp} \frac{1}{r^2} \frac{\partial}{\partial r} \left( r^2 \frac{\partial C_P}{\partial r} \right) + R_P \quad (3.6)$$

where,  $D_{Sp}$ ,  $D_{Pp}$  are the effective substrate and product inter-particle diffusivity.

### 3.1.3 Kinetic Equation of Lactose Hydrolysis

Consider the general mechanism of reversible Michaelis – Menten kinetics. The reversible equation is able to explain irreversible Michaelis – Menten when ( $K_e \rightarrow \infty$  and  $K_p \rightarrow \infty$ ) and competitive inhibition by a product when ( $K_e \rightarrow \infty$ ). For example, enzymatic lactose hydrolysis has been modeled in the literature using soluble  $\beta$ -galactosidase (Santos *et al.*, 1998). Michaelis – Menten model with competitive product inhibition by galactose is widely used to describe lactose hydrolysis. The hydrolysis rate is given by ( $K_e \rightarrow \infty$ ):

$$R_S = R_P = v_{\max} \frac{C_S - C_P / K_e}{K_m (1 + C_P / K_p) + C_S} \quad (3.7)$$

where,  $R(C_S, C_P)$  = Reaction rate, mole /l.h

$C_S$  = Substrate (lactose) concentration, mole/l.

$C_p$  = Product (galactose) concentration, mole/l.

$K_m$  = Apparent Michaelis – Menten constant, mole/l.

$K_p$  = Inhibition constant, mole/l.

$v_{max}$  = Apparent maximum reaction rate, mole/l.h.

The rate constants  $v_{max}$ ,  $K_m$ ,  $K_p$  depend on temperature according to Arrhenius relationship (Santos *et al.*, 1998),

$$v_{max} = E_0 \exp\left(11.30 - \frac{5870}{T}\right) \quad (\text{mol / l. h})$$

$$K_m = \exp\left(28.54 - \frac{10110}{T}\right) \quad (\text{mol / l})$$

$$K_p = \exp\left(24.58 - \frac{9001}{T}\right) \quad (\text{mol / l})$$

where  $E_0$  is the initial  $\beta$ -galactosidase (lactase) concentration (g/l).

The initial and boundary conditions are taken as,

$$\text{at } t = 0, \quad C_S = C_P = 0$$

$$\text{at } r = 0, \quad \left. \frac{\partial C_S}{\partial r} \right|_{r=0} = \left. \frac{\partial C_P}{\partial r} \right|_{r=0} = 0 \quad (3.8)$$

$$\text{at } r = R, \quad D_{Sp} \left. \frac{\partial C_S}{\partial r} \right|_{r=R} = K_{LS} (C_{Sb} - C_S|_{r=R}) \quad (3.9a)$$

$$D_{Pp} \left. \frac{\partial C_P}{\partial r} \right|_{r=R} = K_{LP} (C_{Pb} - C_P|_{r=R}) \quad (3.9b)$$



### 3.1.4 Governing Equations in Dimensionless Form

Equation (3.1) to (3.9) can be reduced to the corresponding dimensionless forms by introducing the following dimensionless parameters:

Substrate and product concentration variables

$$S = \frac{C_S}{C_{S0}} = \frac{C_S}{C_{Sb}|_{z=0^-}}, \quad S_b = \frac{C_{Sb}}{C_{S0}}, \quad P = \frac{C_P}{C_{S0}}, \quad P_b = \frac{C_{Pb}}{C_{S0}} \quad (3.10)$$

Dimensionless axial, radial coordinate variables and dimensionless residence time

$$\zeta = \frac{z}{L}, \quad \xi = \frac{r}{R}, \quad \tau = \frac{v_{\max} t}{C_{S0}} \quad (3.11)$$

The model can be described by the following dimensionless parameters

$$\theta = \frac{K_m}{C_{S0}} \quad \gamma = \frac{C_{S0}}{K_p} \quad K_E = 1/K_e$$

$$\phi^2 = \frac{v_{\max} R^2}{K_m D_{Sp}} \quad \alpha_p = \frac{D_{Sp}}{D_{Pp}}$$

$$Da' = \frac{L \varepsilon v_{\max}}{u C_{S0}} \quad \tilde{R}_s = \frac{K_m R_s}{v_{\max}}$$

$$Pe = \frac{L u}{D_{Ss} \varepsilon} \quad \alpha_z = \frac{D_{Ss}}{D_{Pz}} \quad St = (1 - \varepsilon) K_L a \frac{L}{u}$$

$$Bi_p = \frac{K_{Lp} R}{D_{Pp}} \quad Bi_s = \frac{K_{Ls} R}{D_{Sp}}$$

**Table 3.1: Dimensionless parameters**

**1. Kinetic parameters**

Michaelis modulus  $\theta = \frac{K_m}{C_{S0}}$

Product inhibition modulus  $\gamma = \frac{C_{S0}}{K_p}$

**2. Internal mass transfer parameters**

Dimensionless residence time,  $\beta_s$   $\beta_s = \frac{St}{Bi} \left( \frac{\epsilon}{1-\epsilon} \right) = \frac{L\epsilon}{u} \frac{D_{sp}}{R^2}$

Thiele modulus,  $\phi$   $\phi^2 = \frac{Da St}{\beta_s} = \frac{Da'}{\theta \beta_s} = \frac{v_{max} R^2}{K_m D_{sp}}$

Diffusivity ratio in the internal sites of the enzyme particles  $\alpha_p = \frac{D_{sp}}{D_{pp}}$

**3. External mass transfer parameters**

Stanton number,  $St$   $St = \beta_s Bi \left( \frac{1-\epsilon}{\epsilon} \right) = (1-\epsilon) K_L a \frac{L}{u}$

Damkohler number,  $Da$   $Da = \frac{Da'}{\theta St} = \frac{\phi^2}{Bi} \left( \frac{\epsilon}{1-\epsilon} \right) = \frac{\epsilon}{1-\epsilon} \frac{v_{max}}{K_m K_L a}$

Modified Damkohler number,  $Da'$   $Da' = \theta Da St = \frac{\theta \phi^2}{Bi} St = \frac{L\epsilon}{u} \frac{v_{max}}{C_{S0}}$

**4. Simultaneous internal and external mass transfer parameters**

Substrate , Product Biot mass number  $Bi_S = \frac{K_{LS} R}{D_{sp}}, Bi_P = \frac{K_{LP} R}{D_{pp}}$

**5. Axial dispersion on external fluid side**

Peclet number, Axial dispersion modulus  $Pe = \frac{L u}{D_{sz} \epsilon}$

Diffusivity ratio with respect to the axial position  $\alpha_z = \frac{D_{sz}}{D_{pz}}$

Consequently, equations (3.1) to (3.9) can be written in dimensionless form as follows,

$$Da' \frac{\partial S_b}{\partial \tau} = \frac{1}{Pe} \frac{\partial^2 S_b}{\partial \zeta^2} - \frac{\partial S_b}{\partial \zeta} - St(S_b - S|_{\zeta=1}) \quad (3.12a)$$

$$Da' \frac{\partial P_b}{\partial \tau} = \frac{1}{\alpha_z Pe} \frac{\partial^2 P_b}{\partial \zeta^2} - \frac{\partial P_b}{\partial \zeta} - St(P_b - P|_{\zeta=1}) \quad (3.12b)$$

with the following boundary conditions

$$\text{at } \zeta = 0^+, \quad S_b|_{\zeta=0^+} = 1 + \frac{1}{Pe} \frac{\partial S_b}{\partial \zeta} \Big|_{\zeta=0^+} \quad (3.13b)$$

$$P_b|_{\zeta=0^+} = P_b|_{\zeta=0^-} + \frac{1}{\alpha_z Pe} \frac{\partial P_b}{\partial \zeta} \Big|_{\zeta=0^+} \quad (3.13b)$$

$$\text{at } \zeta = 1, \quad \frac{\partial S_b}{\partial \zeta} \Big|_{\zeta=1} = \frac{\partial P_b}{\partial \zeta} \Big|_{\zeta=1} = 0 \quad (3.14)$$

Mass balance for the substrate in immobilized enzyme particles supported on porous spherical particles is given by,

$$Da' \frac{\partial S}{\partial \tau} = \beta_s \frac{1}{\xi^2} \frac{\partial}{\partial \xi} \left( \xi^2 \frac{\partial S}{\partial \xi} \right) - Da' \tilde{R}_s \quad (3.15a)$$

$$\text{or,} \quad \frac{\partial S}{\partial \tau} = \frac{1}{\theta \phi^2} \frac{1}{\xi^2} \frac{\partial}{\partial \xi} \left( \xi^2 \frac{\partial S}{\partial \xi} \right) - \tilde{R}_s \quad (3.15b)$$

and similarly the product concentration in immobilized enzyme particles is given by,

$$\frac{\partial P}{\partial \tau} = \frac{1}{\alpha_p \theta \phi^2} \frac{1}{\xi^2} \frac{\partial}{\partial \xi} \left( \xi^2 \frac{\partial P}{\partial \xi} \right) + \tilde{R}_p \quad (3.16)$$

Dimensionless reversible Michaelis – Menten kinetics can be written as:

$$\tilde{R}_s = \tilde{R}_p = \frac{S - K_E P}{\theta(1 + \gamma P) + S} \quad (3.17)$$

Equations (15) and (16) are subject to the following boundary conditions:

$$\text{at } \xi = 0, \quad \left. \frac{\partial S}{\partial \xi} \right|_{\xi=0} = \left. \frac{\partial P}{\partial \xi} \right|_{\xi=0} = 0 \quad (3.18)$$

$$\text{at } \xi = 1, \quad \left. \frac{\partial S}{\partial \xi} \right|_{\xi=1} = Bi_S (S_b - S|_{\xi=1}), \quad \left. \frac{\partial P}{\partial \xi} \right|_{\xi=1} = \alpha_p Bi_P (P_b - P|_{\xi=1}) \quad (3.19)$$

## 3.2 Effects of External Mass Transfer Limitation

The effects of external diffusional effects on enzymatic reaction in an immobilized enzyme reactor is studied by considering a packed bed enzyme immobilized reactor of length,  $L$ , fluid velocity,  $u$ , with  $C_{S0}$  and  $C_{P0}$  as the substrate and product inlet concentrations respectively.

### 3.2.1 Assumptions

The mathematical equations that describe the behavior of a packed bed immobilized enzyme reactor have been formulated using the same assumptions described in section (3.1.1) of internal and external mass transfer model. Only the fourth assumption is relaxed by assuming the enzyme is immobilized evenly inside non-porous spherical particles instead of porous, which are uniformly packed in the reactor. The kinetic equation of reversible Michaelis – Menten has been considered in section (3.1.2).

### 3.2.2 Dispersed Plug Flow Reactor Model.

Under the relaxed assumptions, the steady state differential mass balance in the liquid bulk phase for the substrate and the product can be written respectively,

$$0 = D_{S_z} \frac{\partial^2 C_{Sb}}{\partial z^2} - u \frac{\partial C_{Sb}}{\partial z} - K_L a (C_{Sb} - C_S|_{r=R}) \quad (3.20)$$

$$0 = D_{P_z} \frac{\partial^2 C_{Pb}}{\partial z^2} - u \frac{\partial C_{Pb}}{\partial z} - K_L a (C_{Pb} - C_P|_{r=R}) \quad (3.21)$$

where,  $D_{S_z}$ ,  $D_{P_z}$  are effective substrate and product axial diffusivity (or axial dispersion

coefficients),  $m^2/h$  and  $K_L a$  is mass transfer coefficient in liquid,  $h^{-1}$

Equations (3.20) and (3.21) are subject to the following boundary conditions that require continuity of fluxes at both ends of the reactor (Danckwerts, 1953) for both substrate and product.

$$\text{at } z = 0^+, \quad C_{Sb}|_{z=0^+} = C_{Sb}|_{z=0^-} + \frac{D_{Ss}}{u} \frac{\partial C_{Sb}}{\partial z} \Big|_{z=0^+} \quad (3.22a)$$

$$C_{Pb}|_{z=0^+} = C_{Pb}|_{z=0^-} + \frac{D_{Pz}}{u} \frac{\partial C_{Pb}}{\partial z} \Big|_{z=0^+} \quad (3.22b)$$

$$\text{at } z = L, \quad \frac{\partial C_{Sb}}{\partial z} \Big|_{z=L} = \frac{\partial C_{Pb}}{\partial z} \Big|_{z=L} = 0 \quad (3.23)$$

At steady state the rate of substrate consumption is equal to the rate of substrate mass transfer:

$$K_L a (C_S - C_{S_i}) = \frac{v_{\max} C_{S_i}}{K_m \left( 1 + \frac{C_{P_i}}{K_i} \right) + C_{S_i}} \quad (3.23a)$$

$$K_L a (C_{P_i} - C_P) = \frac{v_{\max} C_{S_i}}{K_m \left( 1 + \frac{C_{P_i}}{K_i} \right) + C_{S_i}} \quad (3.23b)$$

From material balance, the inter-phase concentrations can be written as

$$C_{S_i} + C_{P_i} = C_{S_0}$$

### 3.2.3 Governing Equations in Dimensionless Form

Equation (3.20) to (3.23) can be reduced to the corresponding dimensionless forms by introducing the following dimensionless parameters:

Dimensionless axial coordinate, substrate and product concentration variables

$$\zeta = \frac{z}{L}, S_i = \frac{C_{Si}}{C_{S0}}, S_b = \frac{C_{Sb}}{C_{S0}}, P_i = \frac{C_{Pi}}{C_{S0}}, P_b = \frac{C_{Pb}}{C_{S0}} \quad (3.24)$$

The model can be described by the following dimensionless parameters

$$\theta = \frac{K_m}{C_{S0}}, \gamma = \frac{C_{S0}}{K_p}, K_E = 1/K_e, Pe = \frac{Lu}{D_{Sz}},$$

$$\alpha_z = \frac{D_{Sz}}{D_{Pz}}, St = K_L a \frac{L}{u}, Da = \frac{v_{max}}{K_m K_L a} \quad (3.25)$$

Equations (3.20) to (3.23) can be written in dimensionless form as follows,

$$0 = \frac{1}{Pe} \frac{d^2 S_b}{d\zeta^2} - \frac{dS_b}{d\zeta} - St(S_b - S_i) \quad (3.26)$$

$$0 = \frac{1}{\alpha_z Pe} \frac{d^2 P_b}{d\zeta^2} - \frac{dP_b}{d\zeta} - St(P_b - P_i) \quad (3.27)$$

with the following boundary conditions

$$\text{at } \zeta = 0^+, S_b|_{\zeta=0^+} = 1 + \frac{1}{Pe} \frac{dS_b}{d\zeta} \Big|_{\zeta=0^+} \quad (3.28a)$$

$$P_b|_{\zeta=0^+} = P_b|_{\zeta=0^-} + \frac{1}{\alpha_z Pe} \frac{\partial P_b}{\partial \zeta} \Big|_{\zeta=0^+} \quad (3.28b)$$

$$\text{at } \zeta = 1, \quad \left. \frac{dS_b}{d\zeta} \right|_{\zeta=1} = \left. \frac{dP_b}{d\zeta} \right|_{\zeta=1} = 0 \quad (3.29)$$

The dimensionless reversible Michaelis – Menten kinetics can be written as:

$$\tilde{R}_S = \tilde{R}_P = \frac{S - K_E P}{\theta(1 + \gamma P) + S} \quad (3.30)$$

At steady state condition

$$(S_b - S_i) = \theta Da \frac{S_i - K_E P_i}{\theta(1 + \gamma P_i) + S_i} \quad (3.31a)$$

$$-(P_b - P_i) = \theta Da \frac{S_i - K_E P_i}{\theta(1 + \gamma P_i) + S_i} \quad (3.31b)$$

Equation (3.31) can be arranged as quadratic equation in  $S_i$  as follows,

$$(\theta \gamma - 1)S_i^2 + [(1 - \theta \gamma)S_b - \theta(\gamma + 1 + Da)]S_i + \theta S_b(\gamma + 1) = 0$$

The dimensionless substrate concentration at the enzyme surface is calculated by the following equation

$$S_i = \frac{1}{2(\theta \gamma - 1)} [\theta(Da + \gamma + 1) + S_b(\theta \gamma - 1) \pm \Delta] \quad (3.31c)$$

$$\text{where } \Delta^2 = (1 - \theta \gamma)^2 S_b^2 - 2\theta(\theta \gamma - 1)[Da - \gamma - 1]S_b + \theta^2 [(1 + \gamma)^2 + Da(3 + 2\gamma)]$$

Equation (3.31c) can be used provided that  $\theta \gamma \neq 1$ . However, when  $\theta \gamma = 1$  (i.e.  $K_m = K_p$ ) the following equation can be used instead

$$S_i = \frac{S_b(\theta + 1)}{\theta(Da + 1) + 1} \quad (3.31d)$$



Numerical solution of the above non-linear differential equation can be obtained by using reverse shooting method, Galerkin's method and orthogonal collocation on a finite element. It is clear from the above equations that the reactor performance depends on the dimensionless parameters:  $Da$ ,  $St$ ,  $Pe$ ,  $\gamma$  and  $\theta$ .

### 3.2.3.1 Plug Flow Reactor ( $Pe \rightarrow \infty$ )

When Peclet number is infinity, equations (3.26) and (3.29) will be reduced to the plug flow reactor equation:

$$\frac{dS_b}{d\zeta} = St(S_i - S_b) \quad (3.32a)$$

$$\zeta = 0, \quad S_b = 1 \quad (3.32b)$$

Substituting for  $S_i$  from equation (3.29) into equation (3.32), the resulting differential equation can be solved using Runge-Kutta method or Matlab using `ode45` function.

### 3.2.3.2 Continuous Stirred Tank Reactor ( $Pe \rightarrow 0$ )

To derive the performance equation for CSTR, a similar procedure is used. Substrate mass balance around the reactor at steady state gives:

$$\frac{F}{V}(C_{s0} - C_s) = K_L a(C_s - C_{s_i}) \quad (3.33a)$$

where,  $F$  = Liquid flow rate, l/h

$V$  = Reactor Volume, l.

Using dimensionless variables, this equation reduces to:

$$St(S_b - S_i) = 1 - S_b \quad (3.33b)$$

where,  $St = K_L a \frac{V}{F}$ , for CSTR

Equations (3.29) and (3.33b) can be solved simultaneously to obtain the exit dimensionless substrate concentration.

### 3.2.3.3 Mass transfer limitations ( $S_i \approx 0$ )

For the case of external mass transfer limitations,  $C_{si}$  is very small compared to  $C_{sb}$ . For this case, the dimensionless substrate concentration at the reactor exit is given by:

$$S_{b,L} \approx e^{-St}, \text{ for PFR} \quad (3.34)$$

$$S_{b,L} = \frac{1}{1 + St}, \text{ for CSTR} \quad (3.35)$$

## 3.3 CSTR Model

### 3.3.1 Assumptions

The mathematical equations, which describe the behavior of, stirred – tank reactors have been formulated following the assumptions of Bodalo *et al.*, 1993:

- (1) The reactor is assumed to be perfectly mixed and isothermal conditions are maintained.
- (2) The enzyme is immobilized evenly inside the spherical particles, which are suspended in the stirred vessel in a uniform manner
- (3) The mass transfer resistance between solution and particle external surface is negligible
- (4) The substrate and product diffusion inside the catalytic particle can be modeled by Fick's first law, and the effective diffusivity does not change throughout the particle.

### 3.3.2 CSTR Mathematical Model

With these assumptions, the differential mass balances for the substrate and the product are respectively,

$$\frac{dC_{sb}}{dt} + \left(\frac{1-\varepsilon}{\varepsilon}\right) \frac{d\langle C_s \rangle}{dt} + \frac{F}{\varepsilon V} (C_{sb} - C_{sb0}) + \left(\frac{1-\varepsilon}{\varepsilon}\right) \langle R_s \rangle = 0 \quad (3.36)$$

$$\frac{dC_{pb}}{dt} + \left(\frac{1-\varepsilon}{\varepsilon}\right) \frac{d\langle C_p \rangle}{dt} + \frac{F}{\varepsilon V} (C_{pb} - C_{pb0}) - \left(\frac{1-\varepsilon}{\varepsilon}\right) \langle R_p \rangle = 0 \quad (3.37)$$

where,  $F$  = volumetric flow rate and  $V$  = total reactor volume. Equations (3.36) and (3.37)

are subjected into the following initial conditions,

$$\text{At } t = 0, \quad C_{Sb} = C_{Sb0} \quad \text{and} \quad C_{Pb} = C_{Pb0} \quad (3.38)$$

Equation (3.36) and (3.37) contain some terms, which depend on the average concentrations in the catalyst particles and average reaction rates. In order to calculate these values, the diffusion reaction equations within the particles must be solved. The differential mass balance for substrate within the immobilized enzyme particles in spherical coordinates is given by:

$$\frac{\partial C_s}{\partial t} = D_{sp} \frac{1}{r^2} \frac{\partial}{\partial r} \left( r^2 \frac{\partial C_s}{\partial r} \right) - R_s \quad (3.39)$$

and for the product is

$$\frac{\partial C_p}{\partial t} = D_{pp} \frac{1}{r^2} \frac{\partial}{\partial r} \left( r^2 \frac{\partial C_p}{\partial r} \right) - R_p \quad (3.40)$$

The initial conditions are as follows,

$$t = 0, \quad 0 \leq r < R, \quad C_s = C_p = 0 \quad (3.41)$$

$$t = 0, \quad r = R, \quad C_s = C_{Sb0}, \quad C_p = C_{Pb0} \quad (3.42)$$

The boundary conditions are,

$$t \geq 0, \quad r = 0, \quad \frac{\partial C_s}{\partial r} = \frac{\partial C_p}{\partial r} = 0 \quad (3.43)$$

$$t \geq 0, \quad r = R, \quad -D_{sp} \frac{\partial C_s}{\partial r} = k_L (C_{sb} - C_s) \quad (3.44)$$

$$r = R, \quad -D_{pp} \frac{\partial C_p}{\partial r} = k_L (C_{pb} - C_p) \quad (3.45)$$

### 3.3.3 Normalized Mathematical Model

In order to solve the reactor design equations or, in other words, to calculate the substrate and product conversions at reactor outlet (for CSTR) or the variation of the conversions as a function of time, equations (3.36) through (3.45) must be solved simultaneously. Analytical solutions cannot be obtained due to nonlinearity of the kinetic expression. To facilitate the numerical procedure, it is convenient to introduce a series of dimensionless parameters and variables:

$$\langle S \rangle = \frac{\langle C_S \rangle}{C_{Sb0}}, \quad \langle P \rangle = \frac{\langle C_P \rangle}{C_{Sb0}}, \quad Da' = \frac{V\varepsilon v_{\max}}{FC_{Sb0}} \quad (3.46)$$

Other dimensionless variables are defined in the previous sections. Taking into account the dimensionless variables, the reactor design equations, diffusion reaction equations, average concentration and conversions have been rewritten in their dimensionless forms. Reactor design equations (3.36) and (3.37) can be normalized as given in the following equations

$$\frac{dS_b}{d\tau} + \left( \frac{1-\varepsilon}{\varepsilon} \right) \frac{d\langle S \rangle}{d\tau} + \frac{1}{Da'} (S_b - 1) + \left( \frac{1-\varepsilon}{\varepsilon} \right) \langle \tilde{R}_s \rangle = 0 \quad (3.47)$$

$$\frac{dP_b}{d\tau} + \left( \frac{1-\varepsilon}{\varepsilon} \right) \frac{d\langle P \rangle}{d\tau} + \frac{1}{Da'} (P_b - P_{b0}) - \left( \frac{1-\varepsilon}{\varepsilon} \right) \langle \tilde{R}_s \rangle = 0 \quad (3.48)$$

with the following initial condition at  $\tau = 0$ ,  $S_b = 1$ ,  $P_b = P_{b0}$

Equation (3.39) and (3.40) represent diffusion reaction equations:

$$\frac{\partial S}{\partial \tau} = \frac{1}{\theta \phi^2} \frac{1}{\xi^2} \frac{\partial}{\partial \xi} \left( \xi^2 \frac{\partial S}{\partial \xi} \right) - \tilde{R} \quad (3.49)$$

$$\frac{\partial P}{\partial \tau} = \frac{1}{\alpha_p \theta \phi^2} \frac{1}{\xi^2} \frac{\partial}{\partial \xi} \left( \xi^2 \frac{\partial S}{\partial \xi} \right) + \tilde{R} \quad (3.50)$$

The initial conditions are as follows,

$$\tau = 0, \quad 0 \leq \xi < 1, \quad S = P = 0 \quad (3.51)$$

$$\tau = 0, \quad \xi = 1, \quad S = 1, P = P_{b0} \quad (3.52)$$

The boundary conditions are,

$$\tau \geq 0, \quad \xi = 0, \quad \frac{\partial S}{\partial \xi} = \frac{\partial P}{\partial \xi} = 0 \quad (3.53)$$

$$\tau \geq 0, \quad \xi = 1, \quad \frac{\partial S}{\partial \xi} = Bi(S_b - S|_{\xi=1}) \quad (3.54)$$

$$\xi = 1, \quad \frac{\partial P}{\partial \xi} = \alpha_p Bi_p (P_b - P|_{\xi=1}) \quad (3.55)$$

The average substrate and product concentrations, (refer to section 3.5) are,

$$\langle C_S \rangle = \frac{3}{R^2} \int_0^R C_S r^2 dr \quad \text{or} \quad \langle S \rangle = 3 \int_0^1 S \xi^2 d\xi \quad (3.56)$$

$$\langle C_P \rangle = \frac{3}{R^2} \int_0^R C_P r^2 dr \quad \text{or} \quad \langle P \rangle = 3 \int_0^1 P \xi^2 d\xi \quad (3.57)$$

Also, average reaction rate is given by the following equations,

$$\langle \tilde{R}_S \rangle = \frac{3}{R^2} \int_0^R R_S r^2 dr = 3 \int_0^1 \tilde{R}_S \xi^2 d\xi \quad (3.58)$$

## 3.4 Criteria for Reactor Performance

### 3.4.1 Average Concentrations and Average Reaction Rate

The calculations of the substrate and product profile along the radial and axial coordinates were obtained from the solution of the diffusion reaction equations. The average concentrations in the spherical particle can be obtained from the following expressions

$$\langle C_S \rangle = \frac{3}{R^2} \int_0^R C_S r^2 dr \text{ or } \langle S \rangle = 3 \int_0^1 S \xi^2 d\xi \quad (3.59)$$

$$\langle C_P \rangle = \frac{3}{R^2} \int_0^R C_P r^2 dr \text{ or } \langle P \rangle = 3 \int_0^1 P \xi^2 d\xi \quad (3.60)$$

The average reaction rates are defined as:

$$\langle \tilde{R}_S \rangle = \frac{3}{R^2} \int_0^R R_S r^2 dr = 3 \int_0^1 \tilde{R}_S \xi^2 d\xi \quad (3.61)$$

### 3.4.2 Effectiveness Factor

The internal diffusional limitations can be quantitatively expressed by the effectiveness factor,  $\eta$ , defined as the ratio of the average reaction rate to the rate which would be obtained if all enzyme molecules inside the particle were exposed to the same substrate concentration as that at the surface, i.e., in the absence of diffusional effects. The bulk reaction rate is the reaction rate at the bulk concentrations. Alternatively, the effectiveness factor may be defined as the ratio of the average reaction rate to the average

bulk reaction rate,  $R_b$ . This relation is expressed by the following equation:

$$\eta = \frac{\langle R_S \rangle}{R_S(C_{SR}, C_{PR})} = \frac{\langle \tilde{R}_S \rangle}{\tilde{R}_b(S_b, P_b)} = \frac{3 \int_0^1 \tilde{R}_S \xi^2 d\xi}{\tilde{R}_b} \quad (3.62)$$

However, the external diffusional limitations can be quantitatively expressed by the external effectiveness factor,  $\eta_E$ , defined as the ratio of the observed reaction rate (i.e. concentration at the surface of the particles) to the rate evaluated at the bulk concentrations. This relation is expressed by the following equation:

$$\eta = \frac{\langle R_S \rangle}{R_S(C_{SR}, C_{PR})} = \frac{\langle \tilde{R}_S \rangle}{\tilde{R}_b(S_b, P_b)} = \frac{3 \int_0^1 \tilde{R}_S \xi^2 d\xi}{\tilde{R}_b} \quad (3.62)$$

$$\eta_E = \frac{R_S(C_{S_i}, C_{P_i})}{R_S(C_{S_b}, C_{P_b})} = \frac{\tilde{R}_S(S_i, P_i)}{\tilde{R}_b(S_b, P_b)}, \quad \eta_E = \frac{(S_b - S_i) \left( 1 + \gamma \frac{P_b}{S_b} + \frac{1}{\theta} \right)}{Da} \quad (3.63a)$$

Equation (3.63a) is used provided that  $\theta\gamma \neq 1$ , otherwise the external effectiveness factor is calculated using equation (3.31d) when  $\theta\gamma = 1$ . For this case  $\eta_E$  is given by

$$\eta_E = \frac{\theta + 1}{\theta(Da + 1) + 1} \quad (3.63b)$$

The external effectiveness factor is a numerical measure of the influence of external mass transfer resistance on the observed reaction rate. If it is very low below unity, mass transfer resistance is restricting the supply of substrate to the surface and thus limiting the catalytic activity of the immobilized enzyme, whereas, the reaction is not limited by external mass transfer if the effectiveness factor is unity.



### 3.4.3 Fractional Conversion and Yield

Conversion is a convenient variable and it is often used in place of concentration in engineering work. It is defined as the ratio between the total moles of substrate converted into product and the total moles of substrate fed into the reactor per unit time for a continuous reactor.

The following apparent conversions for the substrate and product can also be defined:

$$X = 1 - \frac{C_{Sb}}{C_{Sb0}} = 1 - S_b \quad (3.64)$$

for CSTR, 
$$X = \frac{1}{FC_{Sb0}} (1 - \varepsilon) V_R \langle R_S \rangle \quad (3.65)$$

Yield is defined as the ratio of the substrate converted to the maximum amount that could be converted during one residence time. Yield is used to measure the efficiency of enzyme utilization. It can be expressed as:

$$\text{Yield, } Y = \frac{C_{S0} - C_{SL}}{v_{\max} \frac{\varepsilon L}{u}} = \frac{1 - S_{b,L}}{Da'} = \frac{1 - S_{b,L}}{\theta Da St} = \frac{1 - S_{b,L}}{\theta \beta_s \phi^2} = \frac{Bi}{\theta \phi^2 St} \left( \frac{1 - \varepsilon}{\varepsilon} \right) X \quad (3.65)$$

# 4

---

## NUMERICAL SIMULATION

### 4.1 Introduction

The Michaelis – Menten kinetic terms in the model equations makes it impossible to derive analytical solutions. Employment of numerical technique is therefore inevitable. Often, the Method of Lines (MOL), Nicholson or other finite-difference numerical techniques are used for solving a set of PDEs. This method lumps the PDE to a coupled system of ordinary differential equations (ODE). The number of ODE required is thought to be generally quite large for stiff problems to guarantee stability and good accuracy. The classical MOL technique, however, with an accuracy of  $\Delta z^2$  can be developed using Taylor series expansions (Shirashi *et al.*, 1996; Lee *et al.*, 1999a and 1999b). A mixture of central finite difference, forward finite difference and backward finite difference is employed to lump the governing PDE systems to a set of ODE and the Danckwerts boundary conditions are reduced to simple algebraic equations. Lee *et al.* (1999b) use global orthogonal collocation for solving activated sludge, in their work in which small

Peclet numbers (0.1–1) have been investigated where the solutions are generally stable. For moderate to large Peclet numbers up to 50, concentration gradient of species with respect to time may be very steep such that large number of collocation points is required. In such case, the orthogonal collocation on finite elements (OCFE) may be employed, to reduce the number of differential equations required that produce DAE system to be solved. It is recognized that there exists a host of other numerical techniques in the literature that may be employed to solve coupled differential-algebraic equations (DAE) (Finlayson, 1980, Villadsen & Michelsen, 1978).

Boundary-value problems, however, in relatively simple geometries define an important class of models describing chemical engineering process systems. This class of models falling between highly simplified, lumped-models and those models generated by complete, highly detailed analyses generating BVPs defined in complex physical domains. In deciding what degree of modeling is necessary for a particular application, a balance must be struck between the level of detail that is attempted to be captured in the model under development and uncertainty in the physical and chemical mechanisms defining the model, and so these BVP models can provide a great deal of utility in many engineering applications.

There have been a large number of important contributions to the numerical techniques available for solving BVPs and PDEs by different method of weighted residual. Most of the computational techniques are based on a globally defined and spatially-localized trial

function method. Traditionally, Fortran-based programs developed to implement these methods, are written for a specific implementation of one element of weighted residual solution procedure. The Fortran programs **JACOBI.f**, **INTRP.f**, **DFOPR.f** and **RADAU.f** written by Villadsen and Michelsen (1978) are set of subroutines for solving PDEs with orthogonal collocation method. These subroutines are used to compute the differentiation and quadrature arrays, and for interpolating solutions between collocation points. Many of the chemical engineering studies making use of the orthogonal collocation method of Villadsen and Michelsen (1978) relied on the collocation discretization array. A Significant portion of recent efforts have gone into developing Matlab-based for PDE and BVP systems. Examples include the 2D Matlab PDE toolbox, the weighted residual method tools developed by Lin *et al.* (1999), recently object-oriented programming for MWR suite developed by Adomaitis (2002) and a number of new functions are built into Version 6 of Matlab for solving 1-dimensional BVPs using collocation on cubic splines using **bvp4c.m** function.

## **4.2 The Spectral Methods**

Spectral methods involve representing the solution to a differential equation model in terms of a truncated series of known smooth, global, orthogonal trial functions of the independent variables. Most applications have been to time dependent mixed initial-boundary-value problems with finite-difference or other time-stepping schemes to provide integration in time. The choice of an appropriate spectral method is governed by accuracy and efficiency.

*Accuracy* of spectral method should be designed to give results of greater accuracy than can be obtained by more conventional difference methods using similar spatial resolution or degrees of freedom. The choice of appropriate spectral representation depends on the kind of boundary conditions involved in the problem.

*Efficiency* of the spectral methods should be at least as efficient as difference methods with comparable numbers of degrees of freedom. Therefore, for similar amounts of work, the spectral methods should produce more accurate results than a finite-difference method.

The accuracy and efficiency of a spectral method depends on making the correct choice for the test and trial functions. The proper choice depends on the problem and on the nature of the boundary conditions. When an appropriate choice is made, spectral methods provide a very high rate of convergence once sufficient trial functions are included to adequately represent the underlying problem. If an inappropriate choice is made, the result can be poor accuracy or even convergence to a spurious solution.

The finite-difference formulation may appear to offer a more direct approach to the numerical solution of partial differential equations than does a spectral method. It simply replaces the derivatives with finite-difference expansions and demands that the resulting algebraic equations be satisfied exactly at the grid points. However, difficulties can arise in imposing boundary conditions, and low order finite-difference formulations are often inaccurate, particularly on a coarse grid.

Spectral discretization methods do, however, have some drawbacks: they can be difficult

to code and may be inflexible compared to finite-difference or finite element methods. The finite-difference methods require relatively little algebraic manipulation and relatively straightforward programming. Finite-element methods require some preliminary algebraic manipulation and more programming effort than finite-difference methods. However, the modularity of the finite element method lends itself to efficient programming. In solving a new problem, relatively few changes need be made in an existing computer package. Spectral methods require substantial preliminary algebraic manipulation and programming if an efficient code is to be generated. Also, the solution of a new problem typically requires a new set of trial functions, new boundary-condition specification, and so on, in short, a complete new program.

All spectral methods computation procedures are almost the same by posing solutions in the form of trial function expansion defined over the entire physical domain and its boundaries. Then the residual function is formed by substituting the truncated trial functions and then projected into the trial function expansion using weighted inner product. The method of projection operation or weight function differentiates among various spectral methods. Eigenfunction expansion are based on expressing the solution in terms of trial function defined by the eigenfunctions of Sturm – Liouville problem related to reduced BVP to be solved. The Galerkin method is based on choosing a trial function expansion and projecting the residual onto each function by making the residual orthogonal to the sequence of trial functions. The method is applicable to nonlinear problem. The least squares projection is the optimal discretization technique for a given trial function expansion and is derived from minimizing the residual function norm,

normally is used for steady state problem. Finally, orthogonal collocation method is a pseudospectral technique based on a specific collocation point selection procedure.

#### **4.2.1 Numerical Algorithms**

There has been a considerable amount of research devoted to developing numerical techniques for solving boundary-value problems and PDEs involving in modeling chemical and biochemical processes. This reflects the prevalence of BVPs in chemical engineering modeling problems involving transport and distributions defined on finite domains. For many of these problems, it is natural to pose solutions in the form of trial function expansions, where each trial function is defined over the entire physical domain and its boundaries. The residuals are formed by substituting the trial function expansions into the modeling PDEs and boundary conditions. The different method of weighted residual such as numerical eigenfunction expansion, Galerkin, and orthogonal collocation discretization techniques are distinguished by the form of the projection operation used to determine the mode amplitude coefficients that minimize the residuals. Because the trial functions sequences can be defined by polynomials, trigonometric functions, Bessel's functions, or any other special function, the key concept that made possible an interchangeable set of residual computational tools was establishing a numerical technique for accurately representing these functions while retaining the maximum flexibility in choosing the form of the functions (Adomaitais, 2001). Essentially all the method of weighted residual solution procedure operations reduces to matrix operations. These operations are performed by the weighted inner product function. Other operations,

such as the Gram-Schmidt orthogonalization of a sequence, solution of Sturm-Liouville problems, and computing collocation arrays from general sequences of orthogonal functions, all used naturally on the weighted inner product and other elemental operations.

Computing an eigenfunction expansion solution require posing the solution in terms of a trial function expansion using the Laplacian operator eigenfunctions that satisfy the boundary conditions. Projecting the residual onto each eigenfunction minimizes the residual formed by substituting the trial function expansion into the nonhomogeneous differential equation model. Each of these solution steps translates into a mathematical operation that involves solving a Sturm-Liouville problem, normalizing a set of trial functions, projecting one function onto another with an inner product computations that can be solved numerically.

#### **4.2.2 Eigenfunction Expansion**

Eigenfunction expansion solution procedures can be used for linear, nonhomogeneous problems where the nonhomogeneous terms appear in the modeling equation or the boundary conditions. By choosing trial functions as the eigenfunctions of the linear operator decouples the modes, thus, solutions can be computed term-by-term until a specified residual error tolerance is satisfied. This method is employed by substituting the trial function expansion into the modeling equation to form the residual and then projecting the residual onto each normalized eigenfunction.



### **4.2.3 Galerkin's Method**

Galerkin discretization procedure represents the solution in terms of an orthogonal function expansion where each trial function satisfies the boundary conditions. The residual is projected onto these trial functions in a process similar to the eigenfunction expansion method. However, this discretization procedure does not necessarily produce a modal decomposition generating a decoupled set of ordinary differential equations in time; in fact, the mode amplitudes coefficients may be coupled in a nonlinear manner for nonlinear problems. This method is employed by substituting the trial function expansion into the PDE equation and projecting the residual onto each trial function using the inner product.

### **4.2.4 Orthogonal Collocation Method**

The orthogonal collocation method was developed originally as a stable, predictable, and simple to implement pseudo-spectral technique. Because of its reliability, it has become a standard method for solving boundary-value problems by polynomial trial function expansions (Lin *et al.*, 1999, Fernalyson, 1980, Villadsen & Michelsen, 1978). The interior formulation of this method (Villadsen and Stewart, 1967) is based on choosing a set of trial functions from an orthogonal polynomial sequence, with the discretization points computed as the roots of the polynomial next in the sequence. In most applications, this approximates the Galerkin procedure, because the residual is forced to have as its primary component the polynomial used to determine the collocation points. However, for some linear problems where the residual can be expressed exactly in terms of the chosen set of

trial functions, the two methods give identical results. The mixed collocation formulation is commonly used for problems with nonhomogeneous and nonlinear boundary conditions, and for BVPs defined by a set of differential equations with different boundary conditions (Adomaitis and Lin, 1998 ; Adomaitis and Lin, 2000). As in the case of the interior collocation formulation, the residual at  $N$  interior points is forced to vanish making the residual defined in the domain of interest approximately orthogonal to the first  $N$  trial functions; additional collocation points are placed at the boundaries to satisfy the  $N_{BC}$  boundary condition residuals, resulting in an overall trial function truncation number of  $N + N_{BC}$ . The result is that the mixed collocation method is a discrete approximation.

In the original orthogonal collocation reference (Villadsen and Stewart, 1967), the authors had illustrated three example tables for collocation point locations, quadrature weights, and first and second discrete derivative arrays. Collocation-based on Orthogonal Polynomials such as Jacobi and Legendre polynomials as the truncated trial function expansion using only even powers of  $x$  and these trial functions satisfy the boundary condition at  $x = 0$ ; the factor  $(1-x^2)$  forces the trial functions to also satisfy the boundary condition at  $x = 1$ . The polynomials are constructed as the normalized Jacobi polynomials defined by a sequence of  $2^{\text{nd}}$  order polynomials orthonormal with respect to weighted inner product.

#### **4.2.5 Orthogonal Collocation on Finite Element (OCFE )**

The OCFE technique, first developed by Carey and Finlayson (1975) has been employed successfully to simulate chromatographic column (Ma & Guiochon, 1991; Suwondo *et al.*, 1991) where the global orthogonal collocation, GOC, technique failed. The basic idea of the OCFE technique as its name implies, is introduction of fixed elements or junction points within two ends or outlet boundaries, thus forming subdomains. Collocation is then applied to each subdomain instead of fixing the position of junction point, Gardini *et al.* (1985) proposed that positions of the elements to be dependent on time such that discretization grid of the space variable is maintained with respect to the position of the moving front. Excellent results on the application of the orthogonal collocation on moving finite element were reported by Kill *et al.* (1995), Kaczmariski (1997) and Kaczmariski *et al.* (1997) but they require that the time-dependent space variable to be known and calculated a priori, which is a major disadvantage. Furthermore, improvement in the numerical accuracy and/or computation time of the modified OCFE applied to a fixed-bed adsorption column reported by Kaczmariski *et al.* (1997) are thought to be insignificant. Due to these problems only the fixed element OCFE technique is considered to study the dynamics of continuous bioreactors.

However, for high Thiele modulus or Peclet number the solution has steep gradient in radial coordinate. The solution is more advantageous to use trial functions that are defined only over part of the region. If the domain is divided into NE elements, in each element the orthogonal collocation method can be applied. This result of N internal collocation points was chosen in each element. A numerically stiff catalyst problem (high

Thiele modulus or Peclet number) has been discussed in collocation literature (Villadsen and Michelsen, 1978, Finalyson, 1980, Lin *et al.*, 1999) as a test case for evaluating different collocation procedures. Attempts at computing a solution in the slab geometry by a global collocation method were shown to fail (Villadsen and Michelsen, 1978, Rice and Do, 1995) for discretizations performed using a moderate number of collocation points. An orthogonal collocation on finite element (OCFE), however, was shown to produce convergent results, measured in terms of the convergence of the effectiveness factor.

#### **4.2.6 High Degree-Orthogonal and Special Polynomials**

High degree-orthogonal polynomial method has been shown to be effective for solving stiff problem (Guertin *et al.*, 1977, Sorensen *et al.*, 1973, Adomaitis and Lin, 1998, Chang and Adomaitis, 1999). Lin *et al.* (1999) implemented high-degree orthogonal polynomial in slab geometry. This method based on exponential trial functions was used to provide rapid convergence of the boundary flux. Implementation procedure for the high degree orthogonal polynomial methods for example when  $N$  is large, the high-degree functions  $x^n$  can not be evaluated accurately by discretized function algorithm due to ill-conditioned Vandermonde matrix. Chebyshev polynomial formulation, however, can be used to generate the basis function. The shifted Chebyshev function can be used by replacing  $x$  by  $x^2$ . The sequences  $\psi_n(x)$ ,  $\{\psi_n(x) = \cos(n \cos^{-1}(2x^2 - 1))\}$  for  $n = 0, 1, 2, \dots, N\}$ , are generated and then orthonormalized with respect to weight function  $w = (1 - x^2)$  using Gram-Schmidt. These polynomials are generated in the same way that

Villadsen and Michelsen (1978) did and recently employed by MWRtools by Lin *et al.* (1999).

Collocation procedure, however, can be used as a high-degree method by employing exponential trial functions (Guertin *et al.*, 1977; Lin *et al.*, 1999). This method was used to provide rapid convergence of the boundary flux. The trial functions used in their work, to generate high-degree orthogonal collocation given for stiff-catalyst problem, is given in equation (4.1).

$$\psi_j(x) = \frac{(1-x)^{j-1}}{2} e^{(x-1)\theta} + \frac{(1+x)^{j-1}}{2} e^{-(x-1)\theta} \quad \text{for } j = 1, 2, \dots, N \quad (4.1)$$

The collocation points were chosen based on the orthogonality condition of this trial function sequences and  $Q(x)$  function where the later is defined as,

$$Q(x) = \psi_N(x) + \sum_{j=1}^{N-1} \psi_j(x) b_j \quad (4.2)$$

by solving the orthogonality condition  $\langle Q(x), \psi_k(x) \rangle = 0$  for  $k = 1, 2, \dots, N-1$ , then the amplitude  $b$ ,

$$b_j = \frac{\left\langle \sum_{j=1}^{N-1} \psi_j(x), \sum_{j=1}^{N-1} \psi_j(x) \right\rangle}{\left\langle \psi_N(x), \sum_{j=1}^{N-1} \psi_j(x) \right\rangle} \quad (4.3)$$

where collocation points were computed as the roots of  $Q(x)$ .

To perform orthogonal collocation for stiff catalyst problem  $N = 10$ , collocation points can be chosen as the root of the exponential trial functions as follows,

$$x = \{ 0, 0.9697, 0.9799, 0.9852, 0.9896, 0.9932, 0.9960, 0.9981, 0.9999, 1.0000 \}$$

A multiple-grid collocation method was used to generate truncated trial function expansion solution to boundary-value problem (BVP) with polynomial nonlinearities. Adomaitis and Lin (1998) formulated a true discrete to Galerkin projection applicable to study the convergence behavior of a nonlinear second order reaction – diffusion as a function of Thiele modulus. This problem gives multiple steady states at high Thiele modulus. They showed that a second solution, physically meaningless, could be obtained at saddle-node bifurcation. The residual computations using Galerkin technique was developed (Adomaitis and Lin, 1998) to examine each solution convergence. They found, using perturbation analysis, that if sum of all quadrature second differentiation matrix,

$$\sum_{i=1}^N B_{i,j} > 0, \text{ for any value of } i, \text{ no solution can exist for large Thiele modulus and fixed } N.$$

On the other hand, solution will exist if the sum of the row elements of B are all negative numbers. Thus solution will exist large Thiele modulus for one-point collocation solution. Thus, solving this problem by increasing the number of fine discretization points allows analysis of high-degree nonlinearities. Also a high-degree polynomial discretization can be employed (Lin *et al.*, 1999).

### 4.3 Galerkin Numerical Solution

Application of the eigenfunction expansion technique is limited to certain linear distributed parameters system. Its applicability is increased by choosing to express the solution in terms of trial function other than the eigenfunction of the linearized system. The Galerkin technique can be seen as an extension of the eigenfunction expansion method to nonlinear systems. The Galerkin method is based on choosing a trial function expansion and projecting the residual onto each function, making the residual orthogonal to the sequence of trial functions. In this work, the Galerkin method is used to spatially discretize the partial differential equations governing the immobilized enzyme reactor design equations to a set a ordinary differential equation. The resulting ODEs set is integrated by differential algebraic equations integrator.

#### 4.3.1 Expansion of Solution

The bulk phase substrate, product concentrations are expressed in terms of the trial function expansions  $\phi$ ,

$$S_b(\zeta, \tau) = 1 + \sum_{j=1}^M a_j(\tau) \phi_{1j}(\zeta) \quad (4.4)$$

$$P_b(\zeta, \tau) = P_{b0} + \sum_{j=1}^M b_j(\tau) \phi_{2j}(\zeta) \quad (4.5)$$

The substrate and product concentration inside enzyme particles are expressed in terms of the trial function expansions  $\eta(\xi)$  and  $\psi(\zeta)$ , this is because of nonhomogeneous boundary condition. Where, the substrate and product concentration can be expressed as

sum of homogeneous and nonhomogeneous term due to boundary condition,  $S = S_{hm} + S_{BC}$ .

$$S(\xi, \zeta, \tau) = \sum_{j=1}^M \sum_{i=1}^N c_{ij}(\tau) \eta_{1i}(\xi) \psi_j(\zeta) + \sum_{j=1}^M e_j \xi^2 \psi_j(\zeta) \quad (4.6)$$

$$P(\xi, \zeta, \tau) = \sum_{j=1}^M \sum_{i=1}^N g_{ij}(\tau) \eta_{2i}(\xi) \psi_j(\zeta) + \sum_{j=1}^M h_j \xi^2 \psi_j(\zeta) \quad (4.7)$$

In these truncated trial function expansions,  $a$ ,  $b$ ,  $c$ ,  $e$ ,  $g$  and  $h$  are the mode amplitude coefficients and  $\phi_1(\zeta)$ ,  $\phi_2(\zeta)$ ,  $\eta_1(\xi)$ ,  $\eta_2(\xi)$  and  $\psi(\zeta)$  are the trial functions. The means by which the trial functions are represented and computed is described in the following section.

### 4.3.2 Quadrature Projection Methods

The discretization point positions are based on the modified Gaussian quadrature method (Gauss-Lobatto method). The two end points are preassigned and interior positions are the roots of the  $(M-2)^{th}$  Jacobi polynomial  $J_{M-2}(1, \alpha + 1)(x)$  where  $\alpha$  is the geometry factor. This choice of fine-scale discretization points also guarantees that the quadrature weights  $w$  result in exact integral evaluations when the degree of function is less than  $q = 2M-3$ . On the fine grid, differentiation also reduces to a matrix operation.

The numerical discretization techniques described for constructing the fine-grid quadrature weights, differentiation arrays, and collocation point locations build on the computational techniques of Villadsen and Michelsen (1978) are employed by Lin *et al.* (1999). The effect of such finely discretized function representations is that numerical



computations on this grid can be treated as (and under some circumstances are) exact, within the limits set by the number of discretization points. It is possible to use nonpolynomial trial functions in the various residual methods solution procedures, including collocation based on nonpolynomial trial functions. It also provides a means of estimating, or, for some problems computing exactly, discretization truncation errors and makes possible the development of exact discrete analogs to the Galerkin technique and other methods. We also note that some of the most computationally-intensive steps, such as Newton-Raphson iterations and the time integration of the discretized equations, depend primarily of the mode truncation number and not the number of fine-scale discretization points.

Well-known quadrature weight formulas exist for computing  $w$  and further modifications to improve the accuracy for high-degree interpolating polynomials have been discussed in the literature (Lin *et al.*, 1999). The Gauss-Lobatto quadrature guarantees that the quadrature weights,

$$\int_{\mathbb{J}} f(\xi) \xi^\alpha d\xi = w^T f \quad (4.8)$$

used to compute result in numerically exact integral evaluations if  $f$  is a polynomial with degree less than  $q = 2n - 3$ . Therefore, in the inner product definition,

$$\int_{\mathbb{J}} \phi_i(\xi) \phi_j(\xi) \xi^\alpha d\xi = \langle \phi_i, \phi_j \rangle \quad (4.9)$$

In general, spectral discretization methods approximate solutions to a boundary – value problem are represented by the truncated trial function expansion. The one-dimensional basis function components can be represented as vectors of the function values at a set of

quadrature points. The quadrature points are defined as the combination of the unit interval endpoints and the roots of a shifted orthogonal Jacobi polynomial  $J^{\alpha+1, \beta+1}(x)$ , a polynomial sequence orthogonal with respect to inner product weight  $x^\alpha (1-x)^\beta$  where  $J_0^{\alpha+1, \beta+1} = 1$ , where,  $\alpha = 0, 1$ , or  $2$ , corresponds to the slab, cylindrical, or spherical geometries, respectively. Numerical computation of the quadrature points can be carried out using several approaches (Adomaitis, 2002, Lin *et al.*, 1999).

The first step is to define the discretized physical domain and the differentiation and quadrature operators according to the specific domain geometry. The fine-scale discretization point locations are chosen as the fixed end points as 0 and 1, and the interior points as the roots of the Jacobi polynomial. Thus, the fine-grid discretization point density increase towards each end of the interval. Discretizing the coordinate system on each ( $\xi$  and  $\zeta$ ) direction to obtain distribution of the discretization points on  $\xi$  and  $\zeta$  directions, weight matrix  $w_r$  and  $w_z$  and linear differential operator to store the discrete first order differentiation and Laplacian operator arrays ( $d\xi$ ,  $d\zeta$ ,  $d^2\xi$  and  $d^2\zeta$ ). Choosing the trial function  $\psi(\zeta)$  expansion is not confirmed by a boundary conditions to satisfy. Because this function makes the substrate and product concentration inside enzyme particle not fixed, the trial solution is assumed as polynomial,

$$\psi(\zeta) = \zeta^j \quad (4.10)$$

where,  $j = 1, 2, 3, \dots, M$

This trial function can be used after orthogonalization by making this trial function orthonormal with respect to weight function in  $z$  – direction.

### 4.3.3 Trial Functions

Because of analytical nature of Galerkin method, the most time-consuming step in the implementation of Galerkin solution procedure is the actual computation of the trial functions. The trial functions satisfy the following ordinary differential equations that fits the Sturm – Liouville standard form for  $0 < \xi < 1$ ,

$$\frac{1}{\xi^\alpha v(\xi)} \frac{d}{d\xi} \left( \xi^\alpha p(\xi) \frac{d\phi}{d\xi} \right) + q(\xi) \frac{d\phi}{d\xi} + r(\xi)\phi = \lambda\phi \quad (4.11)$$

The solution is subjected to the following boundary conditions,

$$a \frac{d\phi(0)}{d\xi} + b\phi(0) + a_1 \frac{d\phi(1)}{d\xi} + b_1\phi(1) = 0 \quad (4.12)$$

$$c \frac{d\phi(1)}{d\xi} + d\phi(1) + c_1 \frac{d\phi(0)}{d\xi} + d_1\phi(0) = 0 \quad (4.13)$$

The trial function corresponding to equations (4.4) through (4.7) can be written as the following ODEs with homogeneous boundary conditions to impose solution to modeling equations (3.12) to (3.19)

$$\lambda_1 \phi_1 = \frac{d^2 \phi_1}{d\xi^2}, \quad \phi_1'(0) = Pe \phi_1(0) \quad \text{and} \quad \phi_1'(1) = 0 \quad (4.14)$$

$$\lambda_2 \phi_2 = \frac{d^2 \phi_2}{d\xi^2}, \quad \phi_2'(0) = \alpha_2 Pe \phi_2(0) \quad \text{and} \quad \phi_2'(1) = 0 \quad (4.15)$$

$$\lambda_3 \eta_1 = \frac{d^2 \eta_1}{d\xi^2}, \quad \eta_1(0) = 0 \quad \text{and} \quad \eta_1'(1) = -Bi \eta_1(1) \quad (4.16)$$

$$\lambda_4 \eta_2 = \frac{d^2 \eta_2}{d\xi^2}, \quad \eta_2(0) = 0 \quad \text{and} \quad \eta_2'(1) = -\alpha_p Bi \eta_2(1) \quad (4.17)$$

Numerical solution to solve Sturm – Liouville systems equations (4.14) through (4.17)

yield all eigenfunctions expansion  $\phi_1(\zeta)$ ,  $\phi_2(\zeta)$ ,  $\eta_1(\xi)$ ,  $\eta_2(\xi)$   $\psi(\zeta)$  and eigenvalues  $\lambda$ .

#### 4.3.4 Discretization of the PDEs

The unknown mode amplitude coefficients  $a$ ,  $b$ ,  $c$ ,  $e$ ,  $g$  and  $h$  can be written in time-discretized form by extending the number of dimensions of each array by one in each array's final dimension. To discretize the PDE system, by substituting the trial function expansion solution into the PDE equations, then project the resulting functions onto each trial function using weighted inner product to obtain a residual matrix. Substitute bulk substrate concentration trial function equation (4.4) into modeling equation (3.12), the semi-discrete form of equation (3.12) becomes

$$\left\langle Da' \frac{\partial S_b}{\partial \tau}, \phi_1 \right\rangle = \left\langle \frac{1}{Pe} \frac{\partial^2 S_b}{\partial \zeta^2} - \frac{\partial S_b}{\partial \zeta} - St(S_b - S|_{\xi=1}), \phi_1 \right\rangle \quad (4.18)$$

where, the left hand side of the above equation can be written as,

$$\left\langle Da' \frac{\partial S_b}{\partial \tau}, \phi_1 \right\rangle = Da' \left\langle \frac{\partial}{\partial \tau} \left( 1 + \sum_{j=1}^M a_j(\tau) \phi_j(\zeta) \right), \phi_1 \right\rangle = \frac{da_j}{d\tau} \quad (4.19)$$

Thus equation (4.18) can be written in differential form as,

$$\frac{da_j}{d\tau} = \left\langle \frac{1}{Pe} \frac{\partial^2 S_b}{\partial \zeta^2} - \frac{\partial S_b}{\partial \zeta} - St(S_b - S|_{\xi=1}), \phi_1 \right\rangle \quad (4.20)$$

In similar analysis the bulk product concentration equation (3.12b) can be written in the following form,

$$\frac{db_j}{d\tau} = \left\langle \frac{1}{\alpha_z Pe} \frac{\partial^2 P_b}{\partial \zeta^2} - \frac{\partial P_b}{\partial \zeta} - St(P_b - P|_{\xi=1}), \phi_2 \right\rangle \quad (4.21)$$

To obtain substrate and product concentration inside enzyme particle, the trial function expansion equation (4.4) to (4.7) into the modeling equations and boundary conditions equations (3.12) through (4.19). Equation (4.21) can be written after projecting the trial function onto the residual in the following form,

$$\left\langle \frac{\partial S}{\partial \tau}, \eta_1 \psi \right\rangle = \left\langle \frac{1}{\theta \Phi^2} \frac{1}{\xi^2} \frac{\partial}{\partial \xi} \left( \xi^2 \frac{\partial S}{\partial \xi} \right) - \tilde{R}_s, \eta_1 \psi \right\rangle \quad (4.22)$$

where the left-hand side equation can be simplified as,

$$\left\langle \frac{\partial}{\partial \tau} \left( \sum_{j=1}^M \sum_{i=1}^N c_{ij}(\tau) \eta_i(\xi) \psi_j(\zeta) + \sum_{j=1}^M e_j(\tau) \xi^2 \psi_j(\zeta) \right), \eta_1 \psi \right\rangle = \frac{dc_{i,j}}{d\tau} + \left\langle \frac{\partial}{\partial \tau} \left( \sum_{j=1}^M e_j(\tau) \xi^2 \psi_j(\zeta) \right), \eta_1 \psi \right\rangle \quad (4.23)$$

Equation (4.22) and product concentration can be written as,

$$\frac{dc_{i,j}}{d\tau} + \left\langle \frac{\partial}{\partial \tau} \left( \sum_{j=1}^M e_j(\tau) \xi^2 \psi_j(\zeta) \right), \eta_1 \psi \right\rangle = \left\langle \frac{1}{\theta \Phi^2} \frac{1}{\xi^2} \frac{\partial}{\partial \xi} \left( \xi^2 \frac{\partial S}{\partial \xi} \right) - \tilde{R}_s(S, P), \eta_1 \psi \right\rangle \quad (4.24)$$

$$\frac{dg_{i,j}}{d\tau} + \left\langle \frac{\partial}{\partial \tau} \left( \sum_{j=1}^M h_j(\tau) \xi^2 \psi_j(\zeta) \right), \eta_2 \psi \right\rangle = \left\langle \frac{1}{\alpha_p \theta \Phi^2} \frac{1}{\xi^2} \frac{\partial}{\partial \xi} \left( \xi^2 \frac{\partial P}{\partial \xi} \right) + \tilde{R}_p(S, P), \eta_2 \psi \right\rangle \quad (4.25)$$

Boundary condition, at  $\xi = 1$ , equation (3.19)

$$\left\langle \frac{\partial S}{\partial \xi} \Big|_{\xi=1}, \xi^2 \psi \right\rangle = \left\langle Bi_s (S_b - S|_{\xi=1}), \xi^2 \psi \right\rangle \quad (4.26)$$

$$\left\langle \frac{\partial P}{\partial \xi} \Big|_{\xi=1}, \xi^2 \psi \right\rangle = \left\langle \alpha_p Bi_p (P_b - P|_{\xi=1}), \xi^2 \psi \right\rangle \quad (4.27)$$

Weighted inner product of right-hand side of equations (4.20), (4.21), (4.24) and (4.25) are calculated numerically. The mode amplitude coefficients can be obtained by solving

the Differential Algebraic Equations (DAE) resulted from Galerkin discretization ODEs equations (4.20), (4.21), (4.24), (4.25) and algebraic equations (4.26) and (4.27).

## 4.4 OCFE Numerical Simulation

The system of coupled partial differential equations with their boundary conditions given by equations (3.12) through (3.19) has been solved by the method of orthogonal collocation. This can be solved by choosing appropriate collocation polynomial based on the symmetry and boundary conditions. Semi-Legendre polynomials with N collocation points have been chosen for the interior nodes in the radial direction of the spherical particles because of symmetrical boundary condition at the center. M collocation points were taken in the axial direction for the external fluid by Semi-Legendre polynomial. The solution can be represented by truncated trial function expression, bulk phase and microenvironment phase concentrations of substrate and product can be represented with the following trial function,

$$S_b(\zeta, \tau) = \sum_{j=1}^M b_j(\tau) (1 - \nu \zeta^\sigma) \eta_j(\zeta^\sigma) = \sum_{j=1}^M b_j(\tau) \psi_j(\zeta) \quad (4.28)$$

where,  $\nu$  and  $\sigma$  are positive integers, and  $\eta$  and  $\psi$  are test and trial functions respectively.

The vector of trial functions is defined as

$$\psi(\zeta) = (1 - \nu \zeta^\sigma) [\eta_1(\zeta^\sigma) \quad \eta_2(\zeta^\sigma) \quad \dots \quad \eta_M(\zeta^\sigma)] \quad (4.29)$$

with amplitude coefficient  $b(\tau)$ , by using only even power of dependent variable, the trial function  $\psi$  satisfy the boundary condition at  $\zeta = 0$ , the factor  $(1 - \zeta^2)$  forces the trial functions to also satisfy the second boundary condition at  $\zeta = 1$ . The polynomials  $\eta$  are constructed as the normalized Jacobi polynomials (with  $\nu = 1$  and  $\sigma = 2$ ) defined with respect to weighted inner product with weight function  $w = (1 - \zeta^2)$ . Semi-Legendre

polynomial (with  $\nu = 0$ ,  $\sigma = 1$ ) are constructed with  $w = 1$ , and they are a function of  $\zeta$  only.

#### 4.4.1 Steady State Solution

With  $NE$  number of elements in the radial coordinate of spherical enzyme particle and  $N$  number of collocation points in each element. By choosing  $x$  in the radial coordinate as shown in Figure 4.1

$$m = 1, 2, \dots, NE$$

$$I = 2, 3, \dots, N+1$$

$$i = (m-1)(N+1) + I$$

$$K = 1, 2, \dots, N+2$$

$$k = (m-1)(N+1) + K, \quad j = 1, 2, \dots, M+2$$

$$h_m = x_{m+1} - x_m$$

$$x_i = x_m + x_I h_m$$

Collocation matrix  $D$  can be defined,

$$D_{I-1,K} = \frac{B_{I,K}}{h_m^2} + \frac{2A_{I,K}}{h_m(x_m + h_m x_{1,I})} \quad (4.30)$$

where,  $A, B$  are the first and second derivative matrices of Semi-Legendre polynomial with  $N$  collocation points ( $x_I$ )

$W$  quadrature weight matrix of Semi-Legendre polynomial

Equations (3.12) through (3.19) can be written in terms of these polynomials at the radial



and axial collocation points. The orthogonal collocation equations on each element can be written as,

$$\text{PDE.1} \quad \frac{dS_{i,j}}{d\tau} = \frac{1}{\theta \phi^2} \sum_{K=1}^{N+2} D_{I-1,K} S_{k,j} - R_{i,j} \quad (4.31)$$

$$\text{where, } R_{i,j} = \frac{S_{i,j} - K_E P_{i,j}}{\theta (1 + \gamma P_{i,j}) + S_{i,j}}$$

$$\text{PDE.2} \quad \frac{dP_{i,j}}{d\tau} = \frac{1}{\alpha_p \theta \phi^2} \sum_{K=1}^{N+2} D_{I-1,K} P_{k,j} + R_{i,j} \quad (4.32)$$

The average reaction rate is given by,

$$\langle R_j \rangle = 3 \int_0^1 \xi^2 R_j d\xi = \sum_{m=1}^{NE} 3 \int_0^1 h_m x_m^2 R_j dx = 3 \sum_{m=1}^{NE} \sum_{K=1}^{N+2} q_{K,m} R_{k,j} \quad (4.33)$$

$$\text{where, } q_{p,m} = h_m W_p (x_m + h_m x_{1p})^2$$

for  $p = 1, 2, \dots, N+2$  and  $m = 1, 2, \dots, NE$

The bulk reaction rate is defined with respect to bulk concentrations as

$$R_{b,j} = \frac{S_{b,j} - K_E P_{b,j}}{\theta (1 + \gamma P_{b,j}) + S_{b,j}} \quad (4.34)$$

The effectiveness factor,  $\eta$ , is defined as

$$\eta_j = \frac{\langle R_j \rangle}{R_{b,j}} \quad (4.35)$$

The boundary conditions for substrate and product can be written as

$$\text{B.C.1: at } \xi = 0, m = 1, \quad \frac{1}{h_1} \sum_{K=1}^{N+2} A_{1,K} S_{k,j} = 0, \quad (4.36)$$

$$\text{B.C.2: at } \xi = 1, m = NE, \quad \frac{1}{h_{NE}} \sum_{K=1}^{N+2} A_{N+2,K} S_{k,j} = Bi_S (S_{b,j} - S_{NE(N+1)+1,j}) \quad (4.37a)$$

$$\frac{1}{h_{NE}} \sum_{K=1}^{N+2} A_{N+2,K} P_{k,j} = \alpha_p Bi_S (P_{b,j} - P_{NE(N+1)+1,j}) \quad (4.37b)$$

The continuity of flux across element boundaries between element  $m-1$  and  $m$

$$\text{Since,} \quad \left. \frac{\partial S}{\partial x_{m-1}} \right|_{x=x_{m-1}} = \left. \frac{\partial S}{\partial x_m} \right|_{x=x_m} \quad \text{for } m = 2, 3, \dots, NE$$

$$\text{Then,} \quad \frac{D_{Sp,N+2}}{h_{m-1}} \left( \sum_{K=1}^{N+2} A_{N+2,K} S_{k-(N+1),j} \right) = \frac{D_{Sp,1}}{h_m} \left( \sum_{K=1}^{N+2} A_{1,K} S_{k,j} \right) \quad (4.38a)$$

$$\frac{D_{Pp,N+2}}{h_{m-1}} \left( \sum_{K=1}^{N+2} A_{N+2,K} P_{k-(N+1),j} \right) = \frac{D_{Pp,1}}{h_m} \left( \sum_{K=1}^{N+2} A_{1,K} P_{k,j} \right) \quad (4.38b)$$

If it is assumed that diffusivities are uniform throughout the particles this gives the flux continuity at the elements boundaries as follows,

for  $m = 2, 3, \dots, NE$

$$\frac{1}{h_{m-1}} \left( \sum_{K=1}^{N+2} A_{N+2,K} S_{k-(N+1),j} \right) = \frac{1}{h_m} \left( \sum_{K=1}^{N+2} A_{1,K} S_{k,j} \right) \quad (4.39a)$$

$$\frac{1}{h_{m-1}} \left( \sum_{K=1}^{N+2} A_{N+2,K} P_{k-(N+1),j} \right) = \frac{1}{h_m} \left( \sum_{K=1}^{N+2} A_{1,K} P_{k,j} \right) \quad (4.39b)$$

For the external bulk phase differential mass balance,

$$Da' \frac{dS_{b,j}}{d\tau} = \frac{1}{Pe} \sum_{k=1}^{M+2} Bz_{j,k} S_{b,k} - \sum_{k=1}^{M+2} Az_{j,k} S_{b,k} - St(S_{b,j} - S_{NE(N+1)+1,j}) \quad (4.40)$$

$$Da' \frac{dP_{b,j}}{d\tau} = \frac{1}{\alpha_z Pe} \sum_{k=1}^{M+2} Bz_{j,k} P_{b,k} - \sum_{k=1}^{M+2} Az_{j,k} P_{b,k} - St(P_{b,j} - P_{NE(N+1)+1,j}) \quad (4.41)$$

with the appropriate boundary condition (continuity of the flux)

$$\text{at } \zeta = 0^+, \quad S_{b,1} = 1 + \frac{1}{Pe} \sum_{k=1}^{M+2} Az_{1,k} S_{b,k} \quad (4.42a)$$

$$\text{at } \zeta = 0^+, \quad P_{b,1} = P_{b0} + \frac{1}{\alpha_z Pe} \sum_{k=1}^{M+2} Az_{1,k} P_{b,k} \quad (4.42b)$$

$$\text{at } \zeta = 1, \quad \sum_{k=1}^{M+2} Az_{M+2,k} S_{b,k} = 0 \quad (4.43a)$$

$$\text{at } \zeta = 1, \quad \sum_{k=1}^{M+2} Az_{M+2,k} P_{b,k} = 0 \quad (4.43b)$$

where,  $Az$ ,  $Bz$  are the first and second derivative matrices of Semi-Legendre polynomial with M collocation points ( $x_2$ ). Matrices  $A$  and  $B$  are the first and second derivative matrices of Semi-Legendre polynomial with N collocation points ( $x_1$ ).  $W$  is weight matrix of Semi-Legendre polynomial in slab geometry. These matrices generated using the same procedure developed by Villadsen and Michelsen (1978), Finlayson (1980) and Lin *et al.* (1999). Steady state solution of equations (4.31) to (4.43) can be obtained by solving this nonlinear system using Newton – Raphson's method.

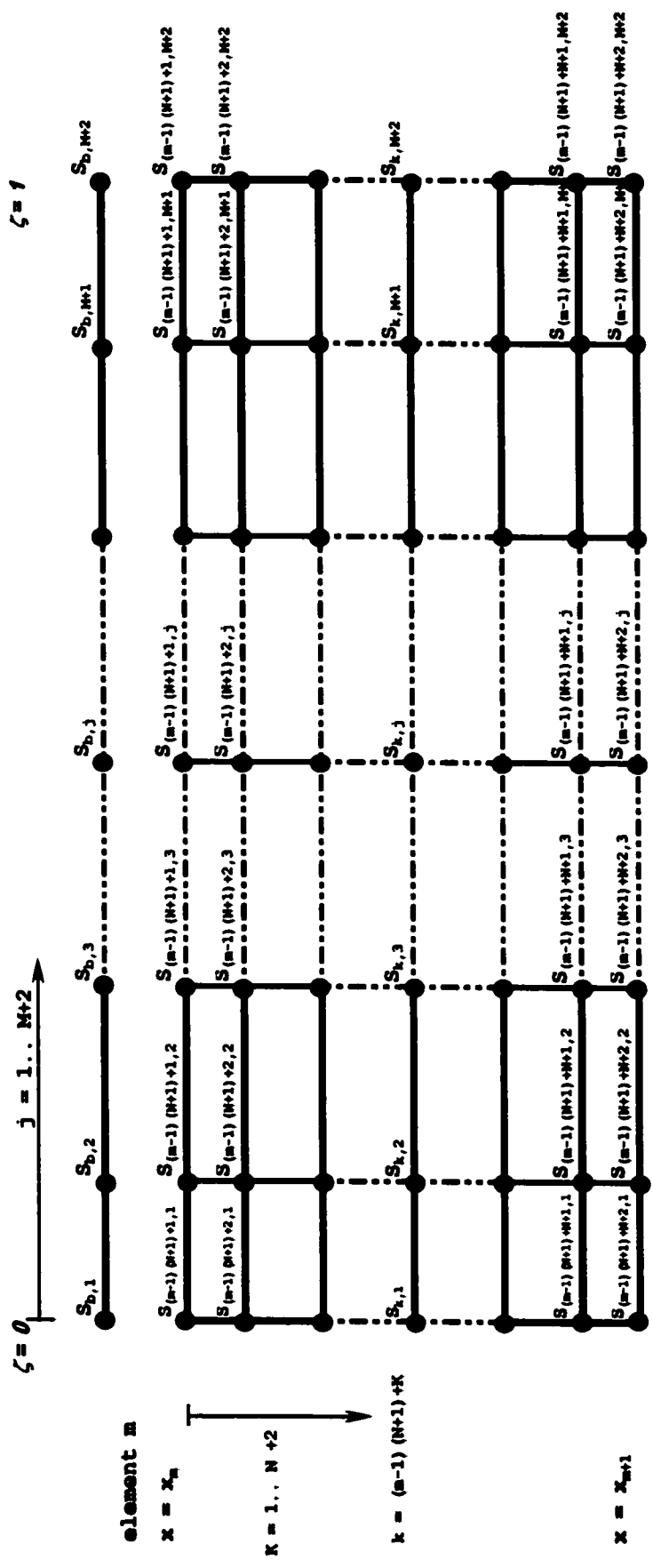


**Figure 4.1: OCFE Numerical Scheme for discretization in bulk phase and spherical particle for element  $m$**

#### 4.4.2 Unsteady State Solution

Unsteady state solution converts the partial differential equations to ordinary differential equations. The first order differential equations (4.44), (4.45) and (4.46) with (4.49) and (4.50) resulted in collocation form. Using global orthogonal collocation, this system can be solved by choosing appropriate collocation polynomial based on the symmetry and boundary conditions. Jacobi polynomials with N collocation points have been chosen for the interior nodes in the radial direction of the spherical particles because of symmetrical boundary condition at the center. M collocation points were taken in the axial direction for the external fluid by Semi-Legendre polynomial. Using stiff integration algorithm with sparse Jacobian utilizing `ode15s` from MATLAB package.

$$\text{PDE.1} \quad \frac{dS_{i,j}}{d\tau} = \frac{1}{\theta \phi^2} \left[ \sum_{k=1}^N B_{i,k} S_{k,j} + B_{i,N+1} S_{N+1,j} \right] - R_{i,j} \quad (4.44)$$

$$\text{PDE.2} \quad \frac{dP_{i,j}}{d\tau} = \frac{1}{\alpha_p \theta \phi^2} \left[ \sum_{k=1}^N B_{i,k} P_{k,j} + B_{i,N+1} P_{N+1,j} \right] + R_{i,j} \quad (4.45)$$

where  $i = 2, 3, \dots, N$  and  $j = 2, 3, \dots, M+1$

where, the average rate of reaction can be written as follows,

$$\langle R_j \rangle = 3 \left[ \sum_{k=1}^N W_k R_{k,j} + W_{N+1} R_{N+1,j} \right] \text{ and } R_{i,j} = \frac{S_{i,j} - K_E P_{i,j}}{\theta (1 + \gamma P_{i,j}) + S_{i,j}} \quad (4.46)$$

where,  $A$ ,  $B$  are the first and second derivative matrices of Jacobi polynomial with N collocation points ( $x_l$ ) and  $W$  is the quadrature weight matrix of Jacobi polynomial. The symmetrical boundary conditions for substrate and product at the center is satisfied by

*Jacobi polynomial*, and the remaining boundary condition can be written as:

$$\text{B.C.2 S at } \xi = 1, \quad \sum_{k=1}^N A_{N+1,k} S_{k,j} + A_{N+1,N+1} S_{N+1,j} = Bi_S (S_{b,j} - S_{N+1,j}) \quad (4.47)$$

$$\text{B.C.2 P at } \xi = 1, \quad \sum_{k=1}^N A_{N+1,k} P_{k,j} + A_{N+1,N+1} P_{N+1,j} = \alpha_P Bi_P (P_{b,j} - P_{N+1,j}) \quad (4.48)$$

where  $i = 2, 3, \dots, N$  and  $j = 2, 3, \dots, M+1$

For the external fluid,

$$Da' \frac{dS_{b,j}}{d\tau} = \frac{1}{Pe} \left[ Bz_{j,1} S_{b,1} + \sum_{k=1}^M Bz_{j,k} S_{b,k} + Bz_{j,M+2} S_{b,M+2} \right] - \left[ Az_{j,1} S_{b,1} + \sum_{k=1}^M Az_{j,k} S_{b,k} + Az_{j,M+2} S_{b,M+2} \right] - St (S_{b,j} - S_{N+1,j}) \quad (4.49)$$

$$Da' \frac{dP_{b,j}}{d\tau} = \frac{1}{\alpha_2 Pe} \left[ Bz_{j,1} P_{b,1} + \sum_{k=1}^M Bz_{j,k} P_{b,k} + Bz_{j,M+2} P_{b,M+2} \right] - \left[ Az_{j,1} P_{b,1} + \sum_{k=1}^M Az_{j,k} P_{b,k} + Az_{j,M+2} P_{b,M+2} \right] - St (P_{b,j} - P_{N+1,j}) \quad (4.50)$$

with the following boundary conditions,

B.C.3 S at  $\zeta = 0^+$ ,

$$S_{b,1} = 1 + \frac{1}{Pe} \left[ Az_{1,1} S_{b,1} + \sum_{k=1}^M Az_{1,k} S_{b,k} + Az_{1,M+2} S_{b,M+2} \right] \quad (4.51)$$

B.C.3 P at  $\zeta = 0^+$ ,

$$P_{b,1} = P_{b0} + \frac{1}{\alpha_2 Pe} \left[ Az_{1,1} P_{b,1} + \sum_{k=1}^M Az_{1,k} P_{b,k} + Az_{1,M+2} P_{b,M+2} \right] \quad (4.52)$$

$$\text{B.C.4 S at } \zeta = 1, \quad Az_{M+2,1} S_{b,1} + \sum_{k=1}^M Az_{M+2,k} S_{b,k} + Az_{M+2,M+2} S_{b,M+2} = 0 \quad (4.53)$$

$$\text{B.C.4 P at } \zeta = 1, \quad Az_{M+2,1}P_{b,1} + \sum_{k=1}^M Az_{M+2,k}P_{b,k} + Az_{M+2,M+2}P_{b,M+2} = 0 \quad (4.54)$$

where,  $Az$ ,  $Bz$  are the first and second derivative matrices of Semi-Legendre polynomial with M collocation points ( $x_2$ )

The solution of boundary condition node variables for interparticle and bulk concentration for both substrate ( $S_{b, M+2}$ ,  $S_{b,1}$ ,  $S_{N+1,j}$ ) and product ( $P_{b, M+2}$ ,  $P_{b,1}$ ,  $P_{N+1,j}$ ) as follows,

$$S_{b,M+2} = \frac{a_{1S} - a_{2S}}{b_{2S} - b_1} \quad P_{b,M+2} = \frac{a_{1P} - a_{2P}}{b_{2P} - b_1} \quad (4.55)$$

$$S_{b,1} = a_{1S} + b_1 S_{b,M+2} \quad P_{b,1} = a_{1P} + b_1 P_{b,M+2} \quad (4.56)$$

$$S_{N+1,j} = \frac{Bi_S S_{b,j} - \sum_{k=1}^N A_{N+1,k} S_{k,j}}{A_{N+1,N+1} + Bi_S} \quad P_{N+1,j} = \frac{\alpha_P Bi_P P_{b,j} - \sum_{k=1}^N A_{N+1,k} P_{k,j}}{A_{N+1,N+1} + \alpha_P Bi_P} \quad (4.57)$$

where,

$$a_{1S} = -\frac{\sum_{k=2}^{M+1} Az_{M+2,k} S_{b,k}}{Az_{M+2,1}} \quad a_{1P} = -\frac{\sum_{k=2}^{M+1} Az_{M+2,k} P_{b,k}}{Az_{M+2,1}} \quad (4.58)$$

$$b_1 = -\frac{Az_{M+2,M+2}}{Az_{M+2,1}} \quad \Delta_S = 1 - \frac{Az_{1,1}}{Pe} \quad \Delta_P = 1 - \frac{Az_{1,1}}{\alpha_P Pe} \quad (4.59)$$

$$a_{2S} = \frac{1 + \frac{1}{Pe} \sum_{k=2}^{M+1} Az_{1,k} S_{b,k}}{\Delta_S} \quad a_{2P} = \frac{P_{b0} + \frac{1}{\alpha_P Pe} \sum_{k=2}^{M+1} Az_{1,k} P_{b,k}}{\Delta_P} \quad (4.60)$$

$$b_{2S} = \frac{Az_{1,M+2}}{Pe \Delta_S} \quad b_{2P} = \frac{Az_{1,M+2}}{\alpha_P Pe \Delta_P} \quad (4.61)$$

## 4.5 Numerical Solution of External Mass Transfer Model

For external diffusional limitation, the system of coupled ordinary differential equations with their boundary conditions given by equations (4.26) through (4.31) has been solved by the method of orthogonal collocation. This can be solved by choosing appropriate collocation polynomial based on the symmetry and boundary conditions. Semi-Legendre polynomials with  $M$  collocation points have been chosen for the interior nodes in the axial direction of the reactor, by choosing  $x$  in the radial coordinate as shown in Figure 4.1. For the external fluid for steady state solution, from equation (4.40) and (4.41)

for  $j = 1, 2, \dots, M+2$

$$0 = \frac{1}{Pe} \sum_{k=1}^{M+2} Bz_{j,k} S_{b,k} - \sum_{k=1}^{M+2} Az_{j,k} S_{b,k} - St(S_{b,j} - S_{int}) \quad (4.62)$$

$$0 = \frac{1}{\alpha_z Pe} \sum_{k=1}^{M+2} Bz_{j,k} P_{b,k} - \sum_{k=1}^{M+2} Az_{j,k} P_{b,k} - St(P_{b,j} - P_{int}) \quad (4.63)$$

with the appropriate boundary condition

$$\text{at } \zeta = 0^+, \quad S_{b,1} = 1 + \frac{1}{Pe} \sum_{k=1}^{M+2} Az_{1,k} S_{b,k} \quad (4.64a)$$

$$\text{at } \zeta = 0^+, \quad P_{b,1} = P_{b0} + \frac{1}{\alpha_z Pe} \sum_{k=1}^{M+2} Az_{1,k} P_{b,k} \quad (4.64b)$$

$$\text{at } \zeta = 1, \quad \sum_{k=1}^{M+2} Az_{M+2,k} S_{b,k} = 0 \quad (4.65a)$$



at  $\zeta = 1$ ,

$$\sum_{k=1}^{M+2} Az_{M+2,k} P_{b,k} = 0 \quad (4.65b)$$

where,  $Az$ ,  $Bz$  are the first and second derivative matrices of Semi-Legendre polynomial with M collocation points ( $x_l$ ). Equations (3.31) can be written for all points in z-direction, when steady state prevails. Equation (3.31) written in discretized form as,

$$(S_{b,j} - S_{int,j}) = \theta Da \frac{S_{int,j} - K_E P_{int,j}}{\theta (1 + \gamma P_{int,j}) + S_{int,j}} \quad (4.66a)$$

$$-(P_{b,j} - P_{int,j}) = \theta Da \frac{S_{int,j} - K_E P_{int,j}}{\theta (1 + \gamma P_{int,j}) + S_{int,j}} \quad (4.66b)$$

where  $Az$ ,  $Bz$  are the first derivative and second derivative matrices of Semi-Legendre polynomial in slab geometry. These matrices can be generated using the same procedure developed by Villadsen and Michelsen (1978), Finlayson (1980), Lin *et al.* (1999). Steady state solution of equations (4.62) to (4.66) can be obtained by solving this nonlinear system using Newton – Raphson's method.



# 5

---

## RESULTS AND DISCUSSIONS

The objectives of this thesis are to investigate the characteristics and behavior of packed bed immobilized enzyme reactors. These objectives can be achieved explicitly by studying the effects of kinetics parameters, internal and external mass transfer parameters, effects of reactor hydrodynamics and the effects of simultaneous diffusional effects.

In addition, preliminary studies were conducted to investigate the unsteady-state behavior of immobilized enzyme reactor. Reactor conversion, yield and internal effectiveness factor are calculated as a function of dimensionless parameters Thiele modulus,  $\phi$ ,  $St$ ,  $Pe$ ,  $\theta$ , and  $\gamma$ . Peclet number,  $Pe$ , which measures the degree of dispersion is assumed to be 2.0 for DPFR model, since at higher  $Pe$  numbers the reactor performance tends to approach the PFR model. In order to evaluate the performance of packed bed immobilized enzyme reactors performance of packed bed immobilized enzyme reactors, numerical values of the process parameters were obtained from the literature (Carrara *et al.*, 2002; Xiu *et al.*,

2001; Abu-Reesh, 1997; Carrara and Rubiolo, 1997 and 1995; Hassan *et al.*, 1995; Lortie, 1994; Bodalo *et al.*, 1993; Hassan and Beg, 1987; Park *et al.*, 1984). Since a wide range of such values have been reported, the range of dimensionless Michaelis modulus,  $\theta$ , and Stanton number,  $St$  used in this simulation study of conversion, yield and internal effectiveness factor, was varied from 0.1 to 10. Similarly the range of product inhibition modulus,  $\gamma$ , used in this analysis varies from  $\gamma = 0$ , corresponding to Michaelis – Menten kinetics, to  $\gamma = 10$ . The developed model of immobilized enzyme reactor has been analyzed by taking into account the effect of kinetic parameters ( $\theta, \gamma, K_E$ ); external mass transfer limitations ( $St, Da$ ) and / or internal mass transfer limitation ( $\phi, \alpha_p$ ) and axial dispersion on external fluid side characterized by  $Pe$  and  $\alpha_z$  which represent reactor hydrodynamic. In addition, Biot number represents simultaneous interaction between internal and external mass transfer.

The differential mass balance equations have been written and normalized for both substrate and product in both external bulk phase and microenvironment phase (inside IME particles). The normalized PDEs are then solved using orthogonal collocation on finite elements (OCFE) and Galerkin's method. The number of collocation points and number of finite elements were chosen to give satisfactory convergence. Numerical simulation was performed to analyze the effect of transport and kinetic parameters on the reactor performance. The model equations were solved using the orthogonal collocation method. 12 internal collocation points were chosen for the reactor bed axial direction and 5 collocation points were used inside enzyme particle. It is found that with these points a good accuracy can be obtained compared to those results with 15 collocation points.

## 5.1 Effects of kinetic parameters with intraparticle diffusion

The effect of kinetic parameters have been studied in terms of Michaelis, product inhibition modulus for irreversible Michaelis – Menten with competitive product inhibition kinetic rate equation for enzymatic reaction, i.e.  $K_E = 0$ .

### 5.1.1 Effect of Michaelis Modulus, $\theta$

Michaelis modulus,  $\theta$ , is a dimensionless Michaelis – Menten constant. It is defined as the ratio of Michaelis – Menten constant,  $K_m$ , to the inlet substrate concentration,  $C_{S0}$ . Michaelis – Menten kinetic with competitive product inhibition represented by equation (3.17), is of variable reaction order between zero and first order kinetics. Zero order kinetic can be obtained when the Michaelis modulus,  $\theta$ , approaches zero, while when the Michaelis modulus approaches very high values (i.e.  $\theta \rightarrow \infty$ ), the kinetic rate equation can be represented by first order. Instead of discussing the reactor behavior under special kinetic such as first and zero order,  $\theta$  is used to exaggerate this interval to be more practically  $\theta \geq 0$  ( Carrara *et al.*, 2002; Xiu *et al.*, 2001; Bodalo *et al.*, 1993; Hassan and Beg, 1987). The value of  $\theta$  depends on the reaction nature. Furthermore, it varies not only due to the reaction Michaelis constant,  $K_m$ , but also with the inlet substrate concentration. Thus, it can be used to investigate the kinetic parameter,  $K_m$ , by varying the inlet substrate concentration.

Figure 5.1 illustrates the effects of product inhibition modulus on the substrate conversion for varying Thiele and Michaelis modulus with  $Pe = 2.0$ ,  $Bi = 0.1$  and  $St =$

1.0. The square of the Thiele modulus,  $\phi^2$ , has the physical interpretation of a first order reaction rate to the intraparticle diffusion rate (Blanch and Clark, 1997; Bailey and Ollis, 1986). The  $\phi^2$  is a measure of whether the process is reaction rate controlled at low  $\phi$  or diffusion rate controlled (high  $\phi$ ). Mixed – regime, however, happens when the two controlling processes are dominating. It is evident from Figure 5.1 that when the process is reaction rate controlled, the substrate conversion increases rapidly upon increasing the Thiele modulus. However, when the process is diffusion rate controlled, the substrate conversion increases slowly with increasing Thiele modulus until it reaches asymptotically higher conversion.

Figure 5.2 illustrates the effects of Michaelis modulus on the substrate conversion as a function of Thiele modulus. It shows that when the process is reaction rate controlled, higher conversion can be predicted for higher Michaelis modulus. Therefore, the first – order reaction indicates higher conversion than Michaelis – Menten and zero – order. It is clear from this figure that zero order kinetics gives the lowest conversion. Another point to note from Figure 5.2 is that all different  $\theta$  curves collapse into one curve when the process is diffusion rate controlled. This takes place when the process is independent of kinetic parameters.

On the other hand, Figures 5.3 and 5.4 show the effects of Michaelis modulus on the internal effectiveness factor as a function of Thiele modulus with  $St = 1$ ,  $Bi = 0.1$  and  $Pe = 2.0$  for  $\gamma = 0, 1, 10$ . When the process is reaction rate controlled, the internal effectiveness factor,  $\eta$ , approaches unity where the reaction rate approaches the intrinsic

one. However, the effectiveness factor decreases rapidly when the value of Thiele modulus increases. The smaller the effectiveness factor, the more serious the intraparticle limitations when the process is diffusion rate controlled. The effect of Michaelis modulus,  $\theta$ , on the internal effectiveness factor is illustrated in Figure 5.4. It shows that the intraparticle diffusion limitation is more significant for high Michaelis modulus and it is the highest for first order reaction. As  $\theta$  increases the reaction rate decreases compared to intraparticle diffusion implying lower effectiveness factor. Therefore, the higher the Michaelis modulus,  $\theta$ , is a lower effectiveness factor,  $\eta$ , can be expected.

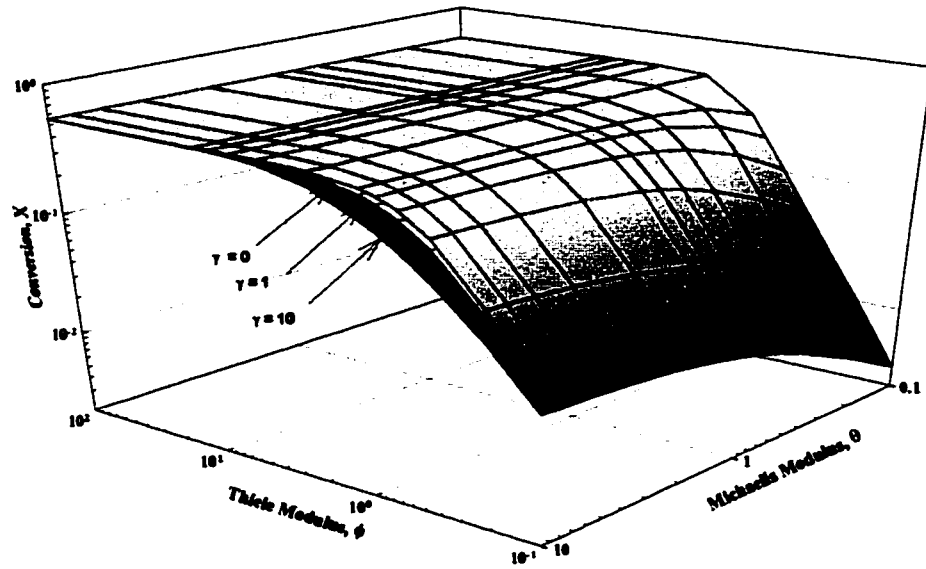


**Figure 5.1: Effects of product inhibition modulus,  $\gamma$ , on substrate conversion for varying Thiele and Michaelis modulus with  $Pe = 2.0$ ,  $Bi = 0.1$  and  $St = 1.0$**

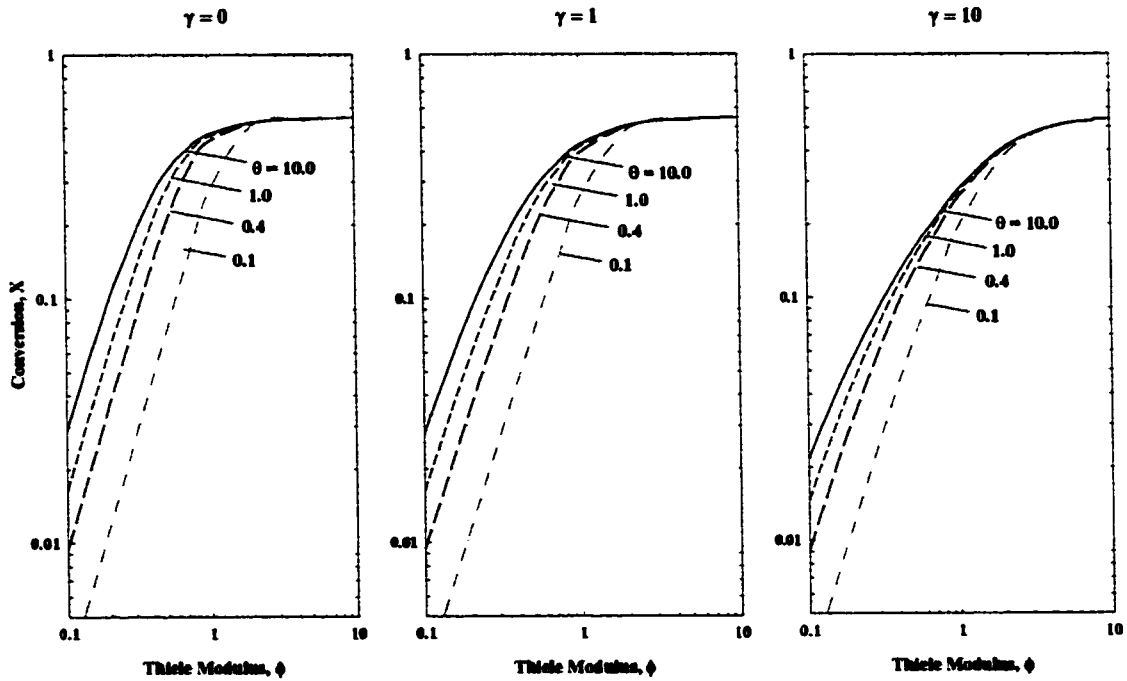


**Figure 5.2: Effects of Michaelis modulus on substrate conversion as a function of Thiele modulus for  $\gamma = 0, 1, 10$ ;  $Pe = 2.0$ ,  $Bi = 0.1$  and  $St = 1.0$**



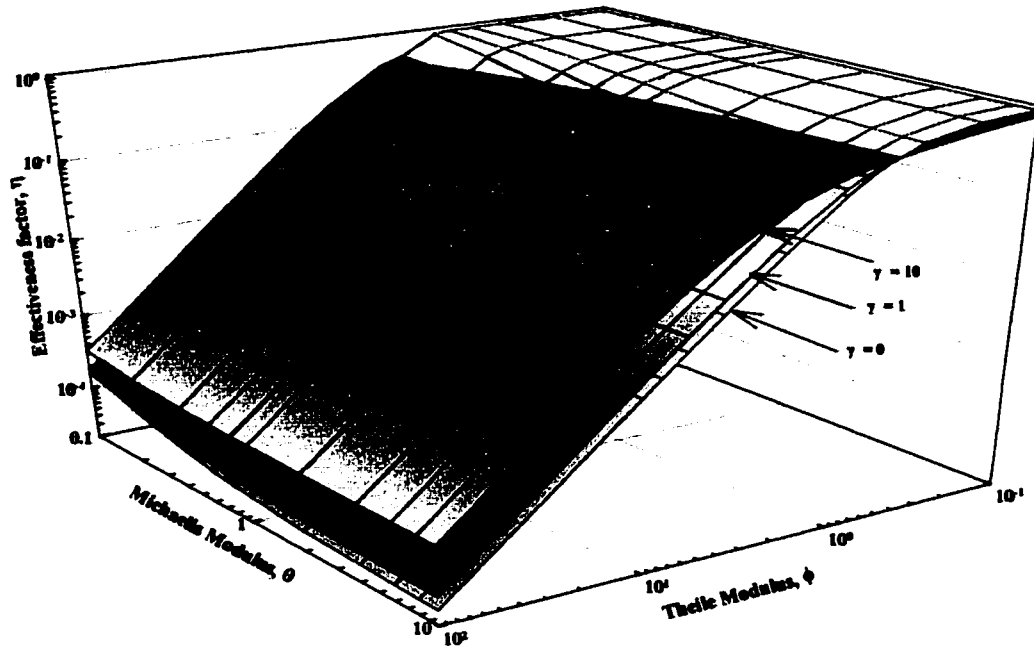


**Figure 5.3:** Effects of product inhibition  $\gamma$  on internal effectiveness factor for varying Michaelis and Thiele modulus for  $\gamma = 0, 1, 10$ ;  $Pe = 2.0$ ,  $Bi = 0.1$  and  $St = 1.0$

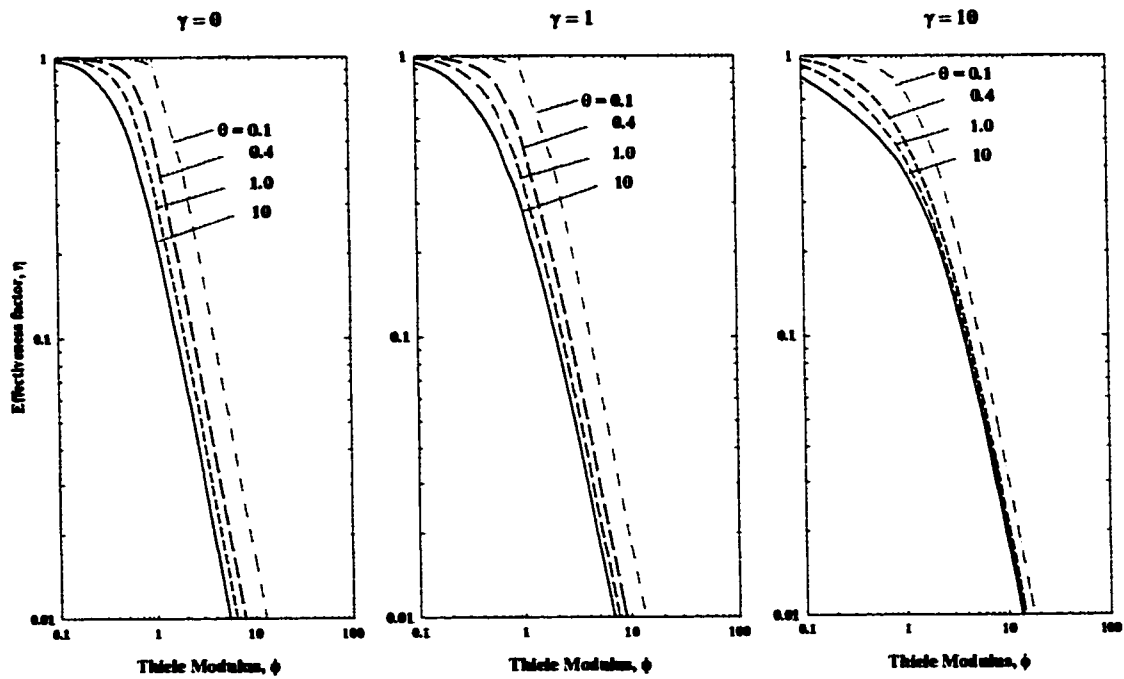


**Figure 5.4:** Effects of Michaelis modulus on internal effectiveness factor as a function of Thiele modulus for  $\gamma = 0, 1, 10$ ;  $Pe = 2.0$ ,  $Bi = 0.1$  and  $St = 1.0$

### **5.1.2 Effect of product inhibition modulus, $\gamma$**

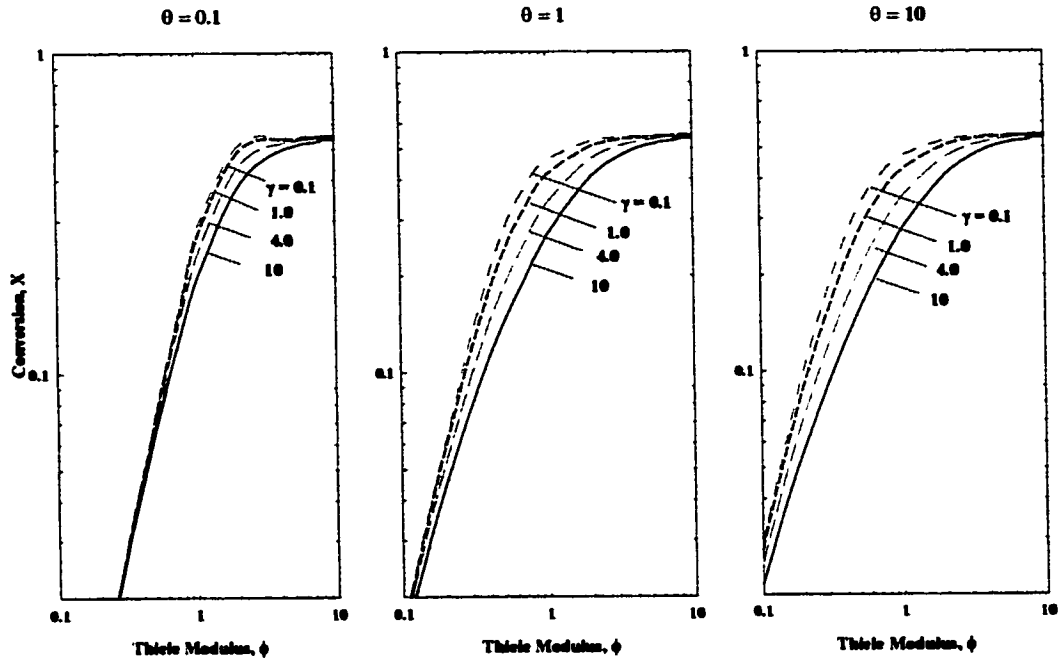
Product inhibition modulus,  $\gamma$ , is defined as the ratio of inlet substrate concentration,  $C_{S0}$ , to the product inhibition constant. It is a direct way to measure the importance of product inhibition on the enzyme reaction kinetic. This parameter can be varied from  $\gamma = 0$ , which represent the Michaelis – Menten kinetics to  $\gamma > 0$  which represents the competitive product inhibition effects on Michaelis – Menten kinetics. In this analysis, the  $\gamma$  value is varied from 0 and 10 (i.e.  $0 \leq \gamma \leq 10$ ).

Figure 5.5 illustrates the relationship between the product inhibition modulus on reactor conversion at different Thiele modulus for  $\theta = 0.1, 1, 10$  at  $Pe = 2.0, Bi = 0.1$  and  $St = 1.0$ . It shows that the substrate conversion increases with decreasing the product inhibition  $\gamma$  when the process is kinetically controlled. Yet, substrate conversion is independent of product inhibition when the process is mass transfer controlled. It is clear from Figure 5.5 that the conversion is higher at higher Michaelis modulus ( $\theta = 10$ ) compared to the conversion for  $\theta = 1.0$  and  $\theta = 0.1$ . The difference in conversion between  $\gamma = 0$  (i.e. Michaelis – Menten kinetics) and higher  $\gamma$  values is directly proportional to the Michaelis modulus. It is shown that for lower value of  $\theta$ , the conversion is less sensitive to product inhibition  $\gamma$ , and the conversion is independent of  $\gamma$  when the Michaelis modulus,  $\theta \rightarrow 0$ , where zero – order reaction prevails.

Figure 5.6 illustrates the effects of product inhibition on internal effectiveness factor as a function of Thiele modulus for  $\theta = 0.1, 1, 10$  at  $Pe = 2.0, Bi = 0.1$  and  $St = 1.0$ . It shows

that there exist a crossover point at which all  $\gamma$  curves intersect at certain  $\phi$ , where  $\phi_{xo}$  is found at around 1.5, 0.75 and 0.5 at  $\theta_{xo} = 0.1, 1$  and  $10$  respectively. Thus,  $\phi$  - crossover point,  $\phi_{xo}$ , is a function of Michaelis modulus where it increases with decreasing Michaelis modulus at crossover point,  $\theta_{xo}$ . It is evident that the effectiveness factor is independent of product inhibition,  $\gamma$ , at  $\phi$  - crossover point. Below  $\phi_{xo}$ , i.e. when the process is reaction rate controlled; the increase in product inhibition reduces the effectiveness factor because it reduces the reaction rate. However, the increase in product inhibition modulus,  $\gamma$ , increases the effectiveness factor when the process is diffusion rate controlled at which  $\phi > \phi_{xo}$ . At this regime, the intraparticle diffusion is less severe when the process is associated with competitive product inhibition, where Michaelis – Menten kinetic showed higher intraparticle diffusion limitations compared to Michaelis – Menten with  $\gamma = 10$ . Product inhibition effects (when  $\phi > \phi_{xo}$ ) have reduced the effect of  $\theta$  by reducing the bulk reaction rate,  $R_b$ , and thereby increasing the internal effectiveness factor. A possible explanation for such behavior is that for higher  $\gamma$ ,  $K_p$  is lower and slows the product reaction rate (i.e. lower product has been formed). Since the mass – transfer limitations is less severe for the case of higher  $\gamma$ , lower product is transferred to the bulk phase compared to that reaction without product inhibition at which high product is transferred under mass transfer controlling process.

It is concluded that the Thiele modulus at crossover point,  $\phi_{xo}$ , can be used to characterize the limit below which the process is kinetically controlled and above which the process is diffusion rate controlled.



**Figure 5.5: Effects of product inhibition on reactor conversion as a function of Thiele modulus for  $\theta = 0.1, 1, 10$ ;  $Pe = 2.0$ ,  $Bi = 0.1$  and  $St = 1.0$**

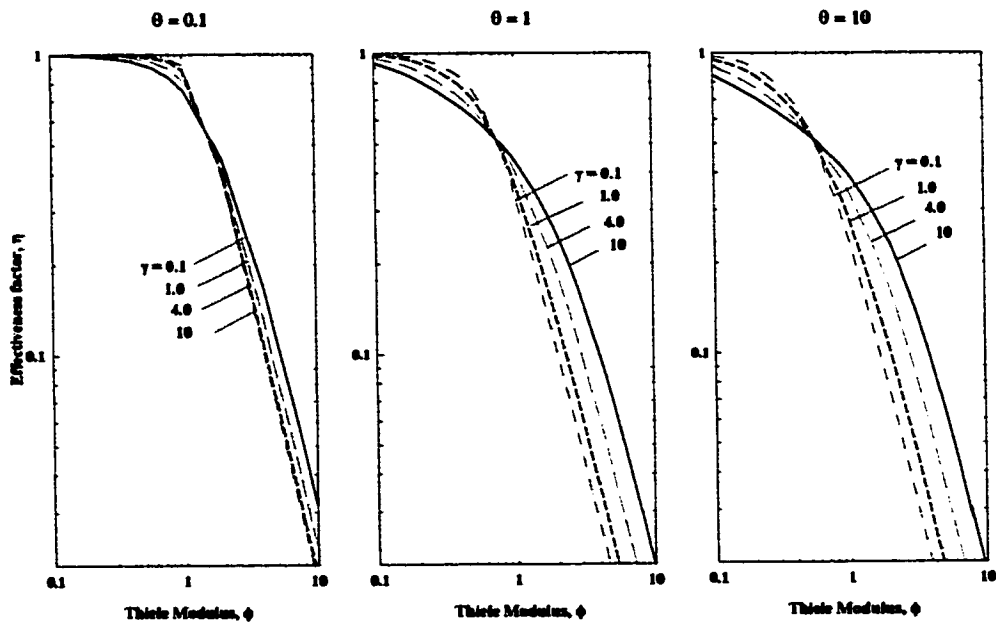


**Figure 5.6: Effects of product inhibition on internal effectiveness factor as a function of Thiele modulus for  $\theta = 0.1, 1, 10$ ;  $Pe = 2.0$ ,  $Bi = 0.1$  and  $St = 1.0$**

## 5.2 Effect of Transport Parameters

In this section the combined effect of Stanton number with intraparticle diffusion and the effect of Stanton number with kinetic parameters will be studied.

### 5.2.1 Effects of Stanton number and Thiele modulus

Stanton number,  $St$ , is a measure of how the external mass transfer resistance compares to the residence time. Figure 5.7 shows the effects of product inhibition on the substrate conversion as a function of Stanton number and Thiele modulus for  $\theta = 1$ ,  $\gamma = 1.0$ ,  $Pe = 2.0$  and  $Bi = 0.1$ . It shows that the trend of substrate conversion versus Thiele modulus is the same for the entire range of Stanton number. The trend is a function of Stanton number, where the relation between the conversions versus  $\phi$  increases substrate conversion with increases in Stanton number. It is noticed that there exist a relationship relating external mass transfer and intraparticle diffusion limitations. At very low Stanton number (i.e.  $St = 0.1$ ), the  $\phi \leq 3.0$  represents the process at which the reaction rate is dominated compared to  $\phi \leq 1.0$  for  $St = 10$ . Higher substrate conversion is achieved with increasing Stanton number because increases in Stanton number will increase external mass transfer which implies lower bulk substrate concentration and thereby it will reduce external mass transfer resistance.

Figure 5.7 also shows the effects of Thiele modulus on the substrate conversion as a function of  $St$ . As can be seen, the substrate conversion increases with increasing  $St$  when

the process is reaction rate controlled (low  $\phi$ ). However, the same relationship is weak when the process is diffusion rate controlled as clearly shown in Figure 5.8.

Although the substrate conversion increases as the  $St$  increases at  $\theta = 1$  and  $\gamma = 1.0$ , the effectiveness factor is independent of  $St$  at this condition for the entire range of Thiele modulus. This behavior is clear as shown in Figure 5.9. This behavior is further explored and discussed with different kinetic and transport parameters in sections 5.2 and 5.3.

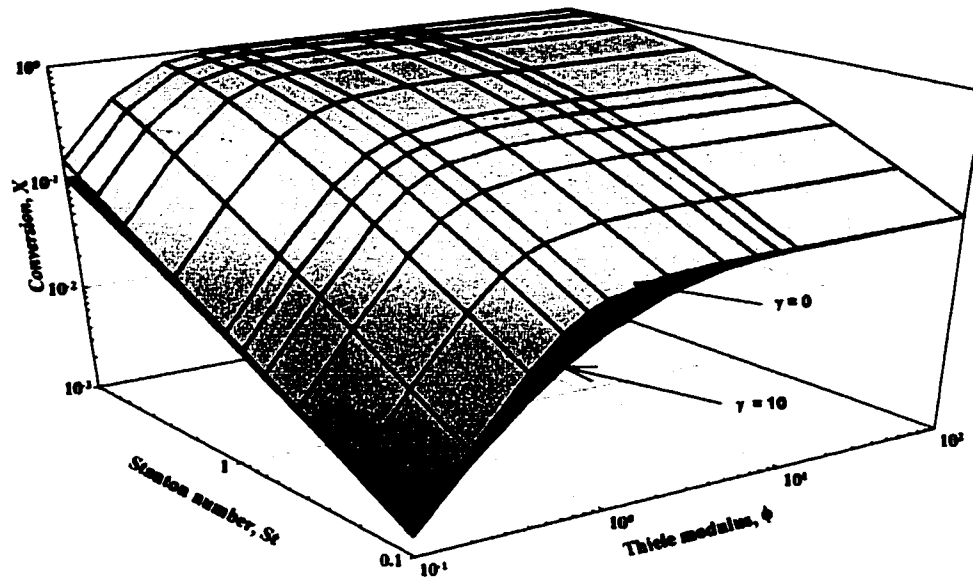


**Figure 5.7:** Effects of product inhibition on reactor conversion for varying Stanton number and Thiele modulus with  $\theta = 1$ ,  $\gamma = 1$ ;  $Pe = 2.0$  and  $Bi = 0.1$

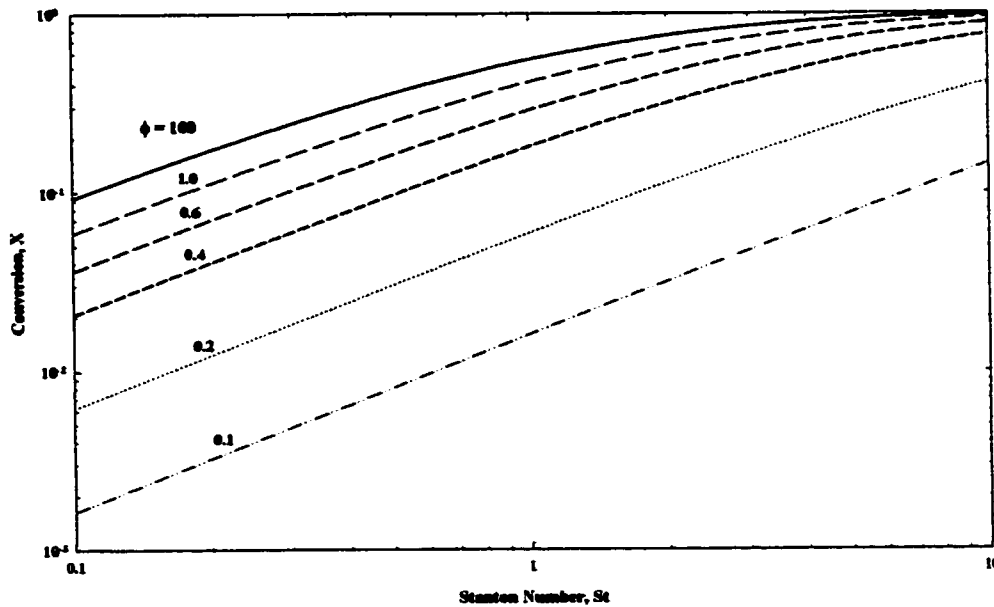


**Figure 5.8:** Effects of Thiele modulus on reactor conversion as a function of Stanton number with  $\theta = 1$ ,  $\gamma = 1$ ;  $Pe = 2.0$  and  $Bi = 0.1$

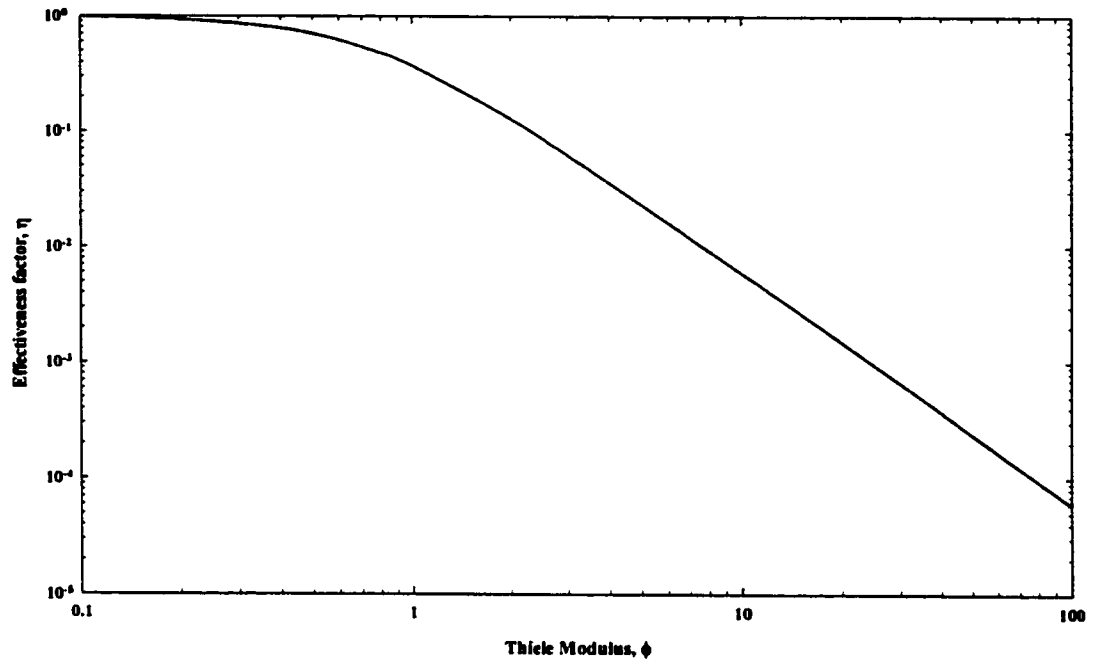


**Figure 5.9: Dependence of effectiveness factor on Thiele modulus with  $0.1 < St < 10$  for  $\theta = 1, \gamma = 1; Pe = 2.0$  and  $Bi = 0.1$**

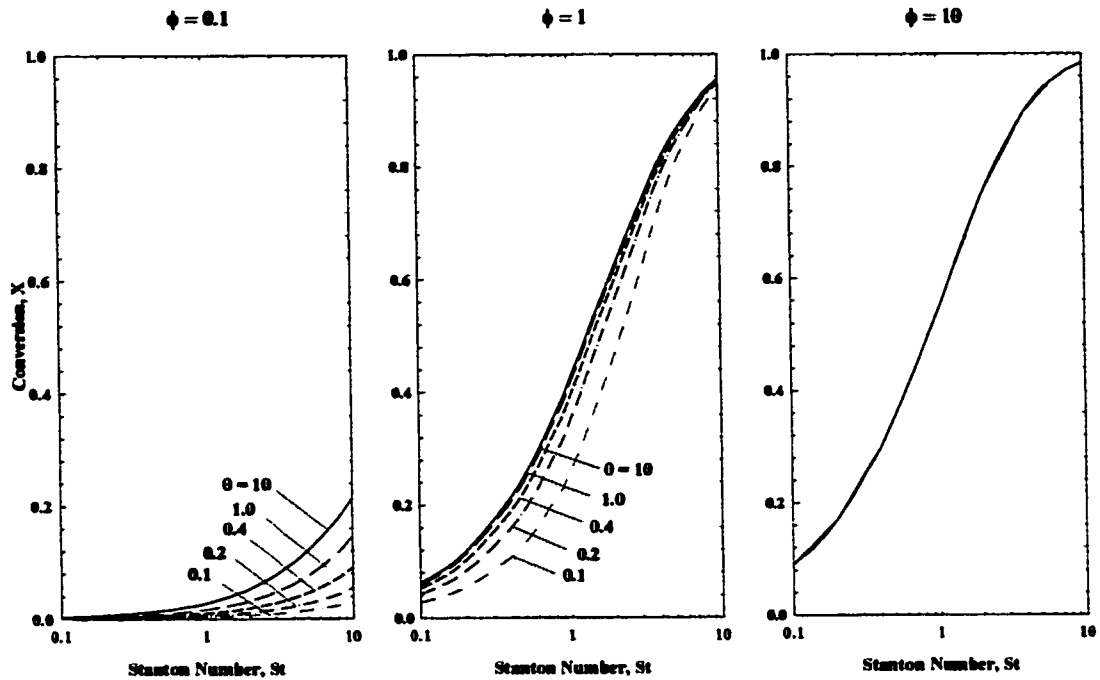


## 5.2.2 Effect of $St$ and $\theta$

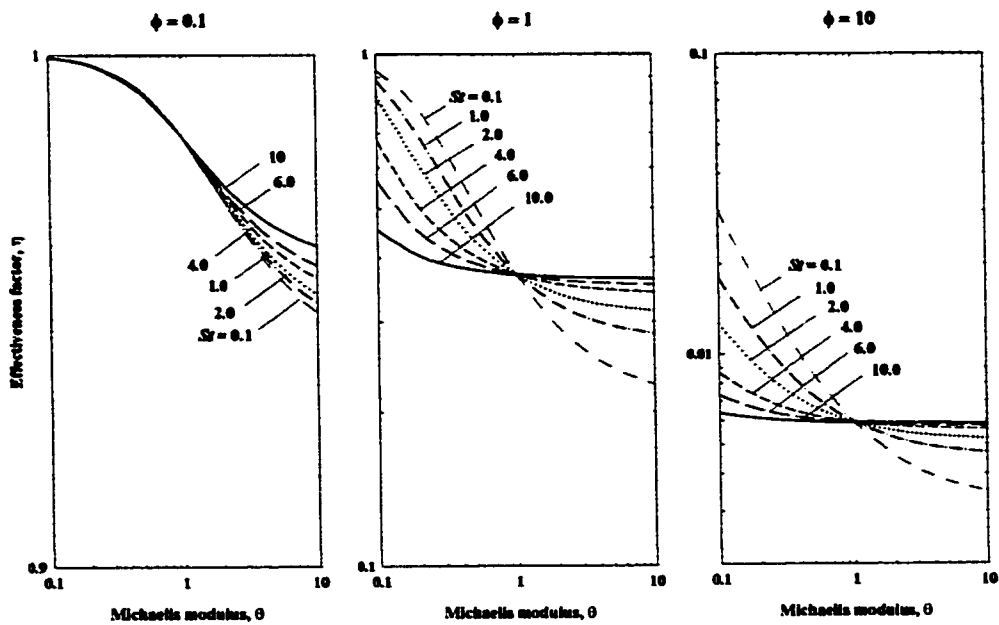
The dependence of substrate conversion on Stanton number was studied for different Michaelis modulus for three cases of intraparticle diffusion  $\phi = 0.1, 1$  and  $10$ . The result is shown in Figure 5.10. In this figure, the substrate conversion increases with increasing  $St$  for the three cases. It is evident that as Stanton number increases substrate conversion increases regardless of  $\theta$  when the process is mass transfer controlled as shown in Figure 5.10 at  $\phi = 10$ . However, substrate conversion increases strongly with increasing  $\theta$  and  $St$  when the process is kinetically controlled, whereas, this relation becomes weak in the mixed regime. Therefore, it can be concluded that the effect of  $\theta$  is significant when the process is controlled by kinetic limitations (i.e. when the intraparticle diffusion and external mass transfer resistances are negligible). However, at high  $\phi$  and high  $St$ , when the mass transfer limitations are dominating factors in determining the substrate conversion, the substrate conversion is independent of  $\theta$ .

Figure 5.11 shows the effects of  $St$  on the internal effectiveness factor as a function of  $\theta$  for  $\phi = 0.1, 1, 10$  at  $\gamma = 1.0, Pe = 2.0$  and  $Bi = 0.1$ . It is clear that when the process is reaction rate controlled at  $\phi = 0.1$ , the effectiveness factor is independent of  $St$  for  $\theta \leq 1$ . However, the effectiveness factor increases slightly as  $St$  increases and more dominant increase in effectiveness factor is found when  $\theta$  is high (i.e.  $\theta = 10$ ). Effect of Stanton number on the effectiveness factor shows a crossover point at  $\theta = 1$  and  $\gamma = 1$  at which effectiveness factor is independent of  $St$ . Above this point, when  $\theta > 1$ , increase in Stanton number favors  $\eta$  while a decrease in effectiveness factor is found when  $\theta < 1$ .

Again, as pointed out from Figure 5.11, increase in  $St$  is confined to certain value of  $St$  above which no further change in effectiveness factor has been found (e.g.  $St = 20$  at  $\phi = 1.0$  and  $St = 10$  at  $\phi = 10$ ). Also, Figure 5.12 illustrates the effect of  $\theta$  on effectiveness factor at different  $St$  for  $\phi = 0.1, 1, 10$  at  $\gamma = 1, Pe = 2$  and  $Bi = 0.1$ . The effectiveness factor is found to be independent of  $St$  not only when the process is reaction rate controlled but also when the process is mass transfer controlled at very high  $St$ . However, between these extreme cases it is found that the effectiveness factor is varying with  $St$  either increasing when  $\theta > 1$ , or decreasing when  $\theta < 1$ .



**Figure 5.10: Effects of Michaelis modulus on reactor conversion as a function of Stanton number for  $\phi = 0.1, 1, 10, \gamma = 1; Pe = 2.0$  and  $Bi = 0.1$**



**Figure 5.11: Effects of Stanton number on internal effectiveness factor as a function of Michaelis modulus for  $\phi = 0.1, 1, 10, \gamma = 1; Pe = 2.0$  and  $Bi = 0.1$**

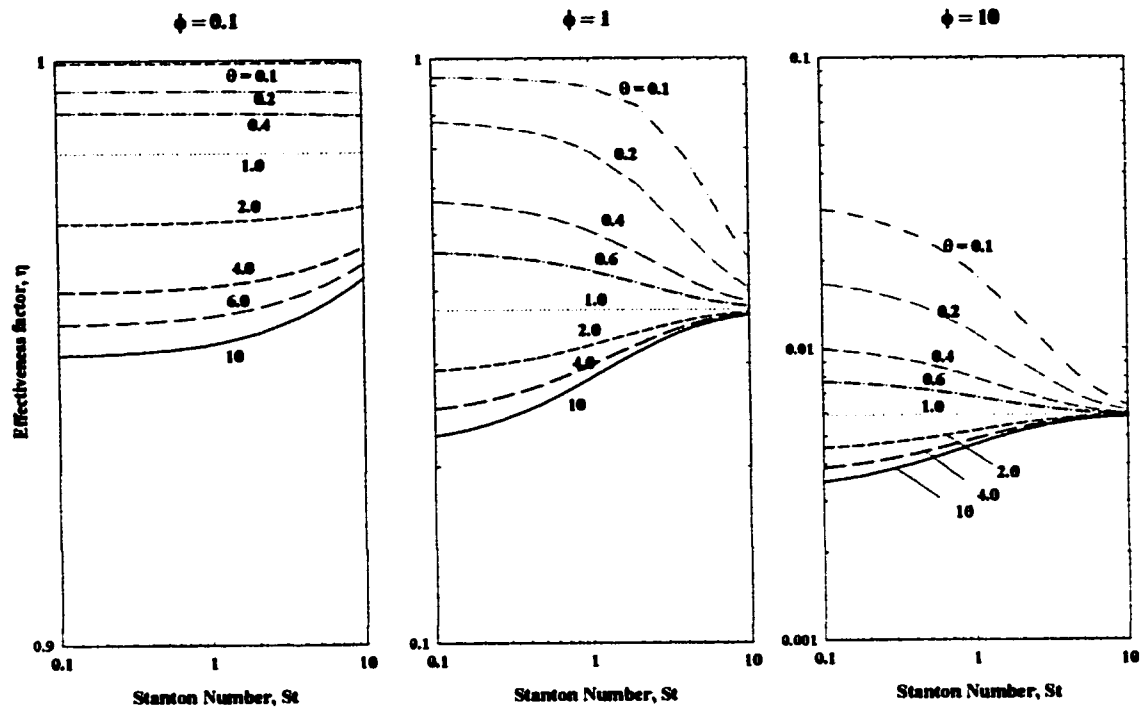


**Figure 5.12: Effects of Michaelis modulus on internal effectiveness factor as a function of Stanton number for  $\phi = 0.1, 1, 10$ ,  $\gamma = 1$ ;  $Pe = 2.0$  and  $Bi = 0.1$**

### 5.2.3 Effects of $St$ and $\gamma$

A similar study was carried out to study the effect of  $St$  for different product inhibition modulus,  $\gamma$ , and the simulation results are expressed in Figures 5.13, 5.14 and 5.15. Figure 5.13 shows the effects of product inhibition modulus on the substrate conversion as a function of Stanton number for  $\phi = 0.1, 1, 10$  at  $\theta = 1.0, Pe = 2.0$  and  $Bi = 0.1$ . It shows that the substrate conversion increases with increasing  $St$ . The effect of  $\gamma$  on substrate conversion is shown to decrease the conversion. Product inhibition modulus,  $\gamma$ , is shown to reduce the conversion and appreciable effect of  $\gamma$  is found at high  $St$  at  $\phi$  of 0.1 to 1.0. Figure 5.13 also shows that when the process is reaction rate controlled with low  $St$ , the substrate conversion is very low regardless of  $\gamma$ . When the process is mass transfer controlled (i.e.  $\phi = 10$ ) the substrate conversion is only a function of  $St$ . Higher external mass transfer (i.e. high  $St$ ) implies lower bulk substrate concentration,  $S_b$ , and consequently higher substrate conversion.

Figure 5.14 shows the effects of product inhibition modulus,  $\gamma$ , on the effectiveness factor as a function of  $St$  for  $\phi = 0.1, 1, 10$  at  $\theta = 1, Pe = 2.0$  and  $Bi = 0.1$ . It shows that for  $\phi = 0.1$  the internal effectiveness factor,  $\eta$ , approaches unity and is a function of  $\gamma$  only for very low Stanton number. However, effectiveness factor increases as  $St$  increases when  $\gamma > 1$ . Figure 5.14 also shows that at  $\phi = 1$ , the product inhibition forms crossover point at certain  $St$  at which effectiveness factor is independent of  $\gamma$ , and  $\eta$  is independent of  $St$  at  $\gamma = 1.0, \theta = 1.0$ . This crossover condition is found at  $St_{x_0} = 0.55, \theta_{x_0} = 1.0, \phi_{x_0} = 1.0$ . The

effect of  $St$  is more sensitive to the product inhibition when  $\gamma > 1$ . The  $\eta$  increases with increasing  $St$  when  $\gamma < 1$ . Yet, the effectiveness decreases with increasing  $St$  when  $\gamma > 1$  as shown in Figure 5.15. Again from Figure 5.14, it can be noted that the crossover point  $St_{x_0}$  is a function of  $\phi_{x_0}$  at  $\theta = 1.0$ , where it exists at very high values  $St_{x_0}$  for lower  $\phi = 0.1$ . For example,  $St_{x_0} = 0.55$  for  $\phi = 1.0$  and very low  $St_{x_0}$  for  $\phi = 10$ .

The effects of both kinetic parameters  $\theta$  and  $\gamma$  were studied in Figure 5.16 with the external mass transfer on the internal effectiveness factor for  $St = 0.1, 1, 2.0$  and  $10$  at  $\phi = 2.0$  and  $Bi = 0.1$ . Two distinct regions are shown to have different behavior, first region when  $\theta \gamma < 1$ , and the second when  $\theta \gamma > 1$ . As can be seen when  $\theta \gamma > 1$ , the effectiveness factor increases with  $St$  increasing. On the other hand, the effectiveness factor increases with decreasing  $St$  when  $\theta \gamma < 1$ . These two regions intersect when  $\theta \gamma = 1$  at which the effectiveness factor is independent of  $St$ . This can be proved analytically for external mass transfer when  $\theta \gamma = 1$ , the reaction rate is independent of product concentration as given in equation (3.31d). Increases in  $St$  decreases both substrate and product bulk concentrations. This implies that  $R_b$  decreases with increasing  $St$ . Thus the effectiveness factor will consequently increases with increasing  $St$  in this region.

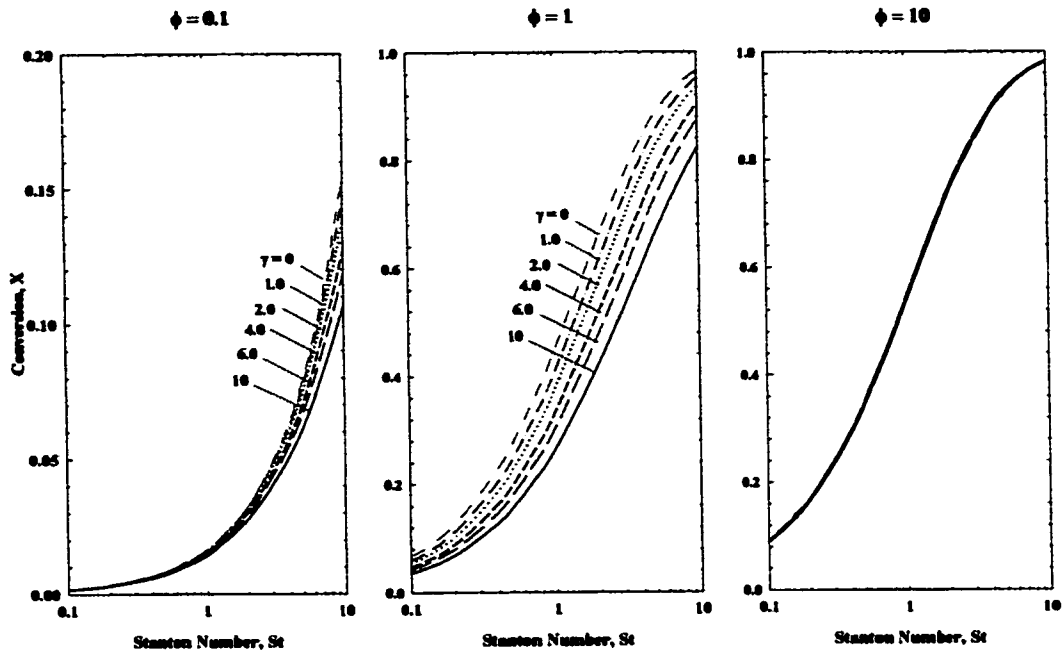


**Figure 5.13: Effects of product inhibition modulus on reactor conversion as a function of Stanton number for  $\phi = 0.1, 1, 10$ ,  $\theta = 1$ ;  $Pe = 2.0$  and  $Bi = 0.1$**

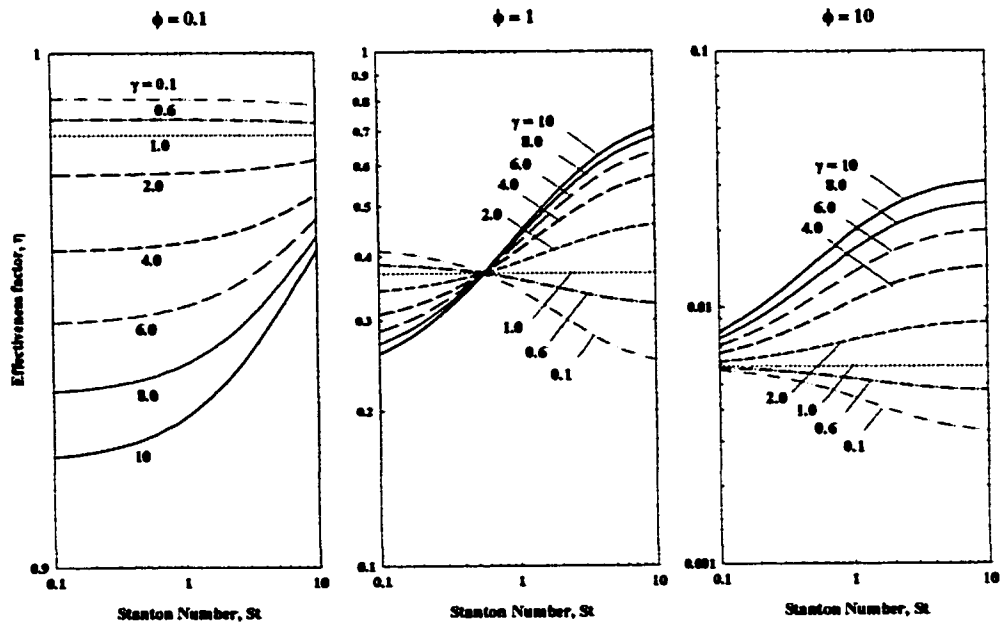


**Figure 5.14: Effects of product inhibition modulus on internal effectiveness factor as a function of Stanton number for  $\phi = 0.1, 1, 10$ ,  $\theta = 1$ ;  $Pe = 2.0$  and  $Bi = 0.1$**

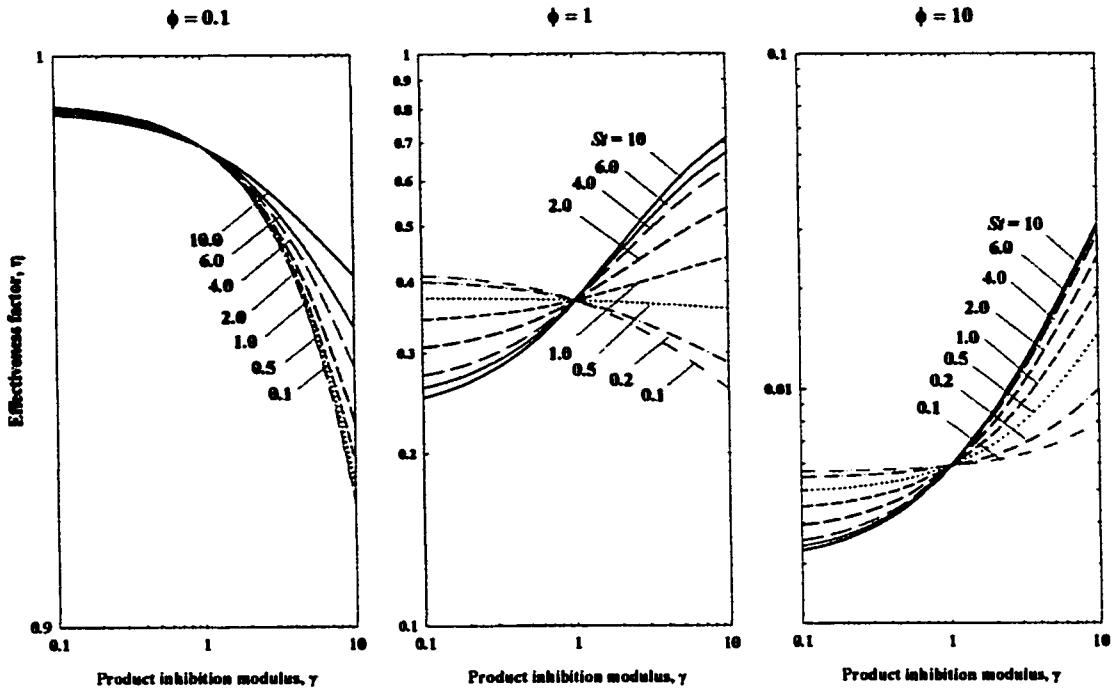


**Figure 5.15:** Effects of Stanton number on internal effectiveness factor as a function of product inhibition modulus for  $\phi = 0.1, 1, 10$ ,  $\theta = 1$ ;  $Pe = 2.0$  and  $Bi = 0.1$

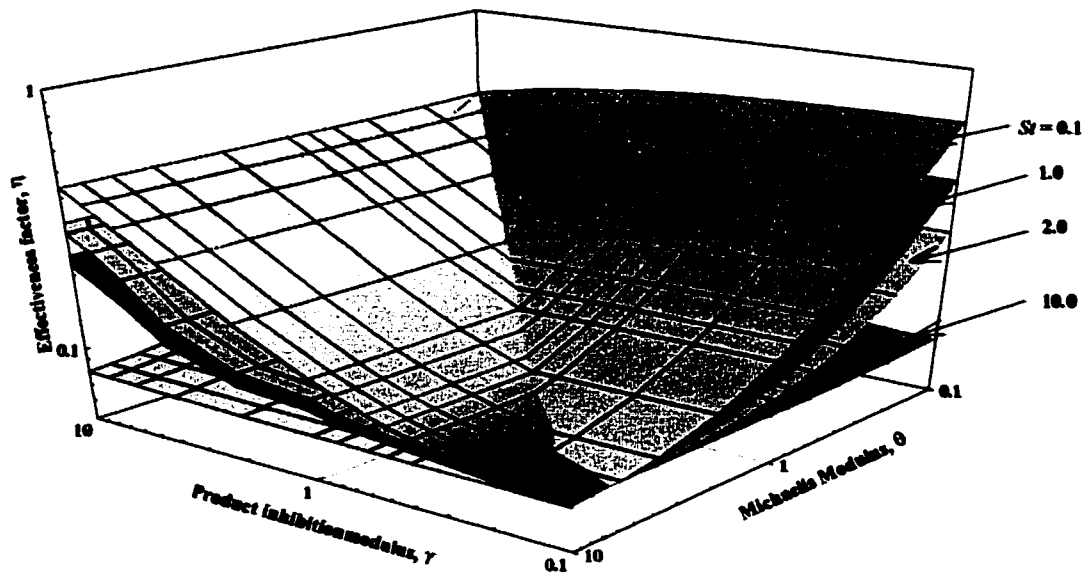


**Figure 5.16:** Effect of  $St$  on internal effectiveness factor for different  $\theta$  and  $\gamma$  at  $\phi = 2$  and  $Bi = 0.1$



### **5.3 Effects of Biot number, $Bi$**

Biot number is defined as the ratio of intraparticle diffusion resistance to external mass transfer resistance. The effects of Biot number on the substrate conversion will be studied with intraparticle limitations in section 5.3.1. Moreover, effects of  $Bi$  and external mass transfer limitations with kinetic parameters  $\theta$  and  $\gamma$  will be discussed in section 5.3.2 and 5.3.3, respectively.

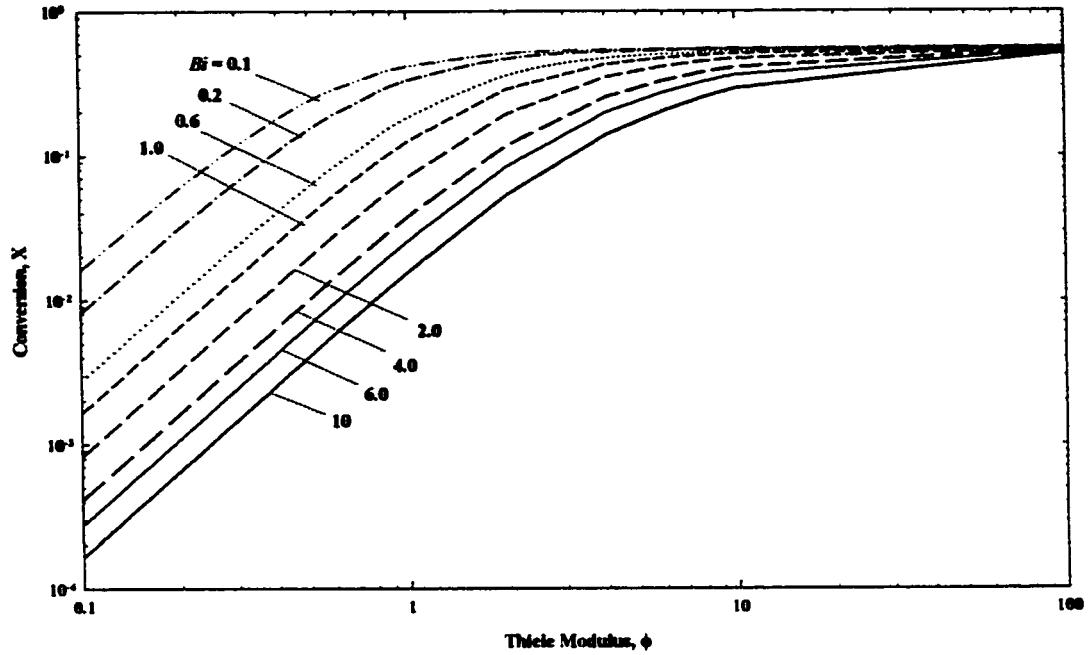
#### **5.3.1 Effects of Biot number and Thiele modulus**

Figure 5.17 demonstrates quantitatively the effects of Biot number on the substrate conversion as a function of Thiele modulus with  $\theta = 1$ ,  $\gamma = 1$ ,  $Pe = 2.0$  and  $St = 1.0$ . At low Thiele modulus, the effect of increasing Biot number on the substrate conversion is shown to reduce the substrate conversion. This takes place when the process is reaction rate controlled. At extremely high Thiele modulus, however, all curves of different  $Bi$  asymptotically approach constant value where the system becomes diffusion rate controlled.

Figure 5.18 shows the effects of Thiele modulus on the substrate conversion as a function of Biot number with  $\theta = 1.0$ ,  $\gamma = 1.0$ ,  $Pe = 2.0$  and  $St = 1.0$ . It shows that the substrate conversion increases as a result of decreasing  $Bi$  when the process is kinetically controlled. This relation becomes independent of  $Bi$  when the process is mass transfer controlled. However, a weak relation is shown when both intraparticle diffusion and kinetic processes are dominating (i.e. in the mixed regime).

Lower Biot number indicates the presence of strong external mass transfer resistance and hence both internal and external mass transfer resistances are important for the determination of substrate conversion. As the Biot number increases the external mass transfer resistance decreases in its importance. This occurs because the microenvironment substrate conversion approaches the bulk phase concentration and thereby the external mass transfer disappears. The effects of  $Bi$  are dominant in the reaction-controlled regime. However, the conversion is independent of Biot number when the process is diffusion rate controlled as quantitatively shown in Figure 5.18.

Figure 5.19 shows the effects of Biot number on the internal effectiveness factor as a function of Thiele modulus with  $\theta = \gamma = 1$ ,  $Pe = 2.0$  and  $St = 1.0$ . The trend of effectiveness factor versus Thiele modulus is shown to be a function of Biot number. The effectiveness factor approaches unity and it is independent of  $Bi$  when the process is kinetically controlled. Conversely, the effectiveness factor increases with increasing Biot number in the reaction controlled regime as quantitatively shown in Figure 5.20.



**Figure 5.17: Effects of Biot number on reactor conversion as a function of Thiele modulus with  $\theta = 1$ ,  $\gamma = 1$ ;  $Pe = 2.0$  and  $St = 1.0$**

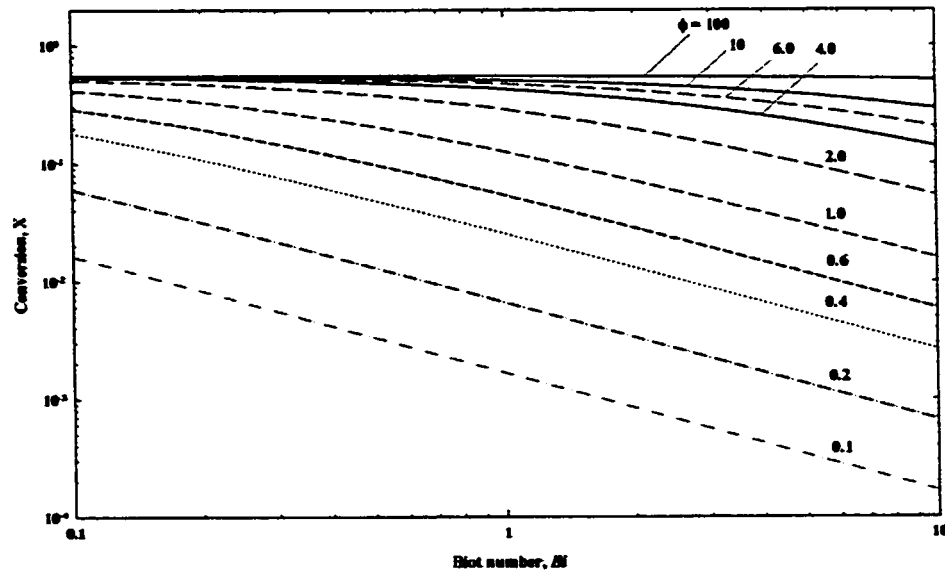


**Figure 5.18: Effects of Thiele modulus on reactor conversion as a function of Biot number with  $\theta = 1$ ,  $\gamma = 1$ ;  $Pe = 2.0$  and  $St = 1.0$**

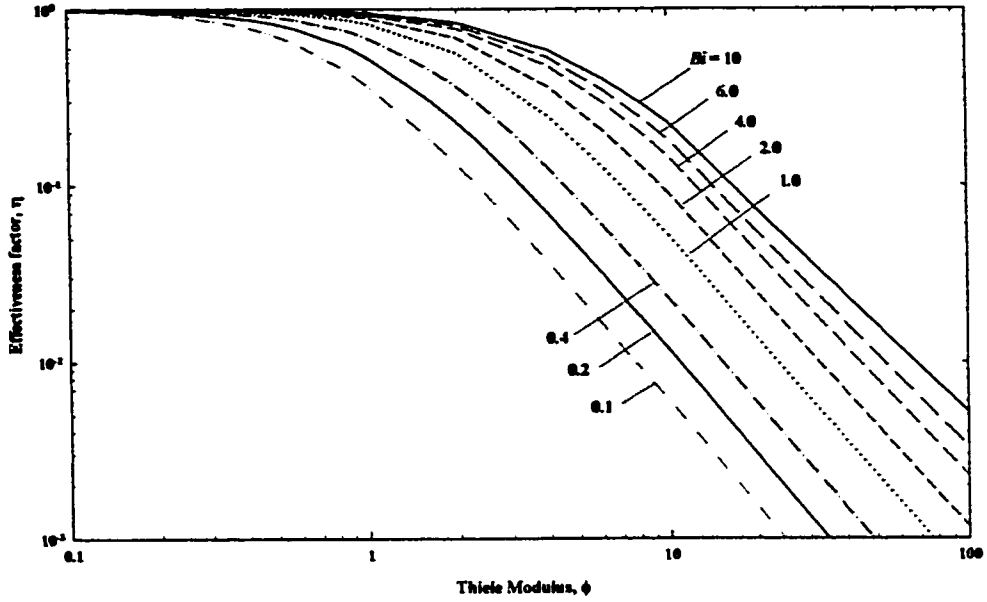


**Figure 5.19: Effects of Biot number on internal effectiveness factor as a function of Thiele modulus with  $\theta = 1$ ,  $\gamma = 1$ ;  $Pe = 2.0$  and  $St = 1.0$**

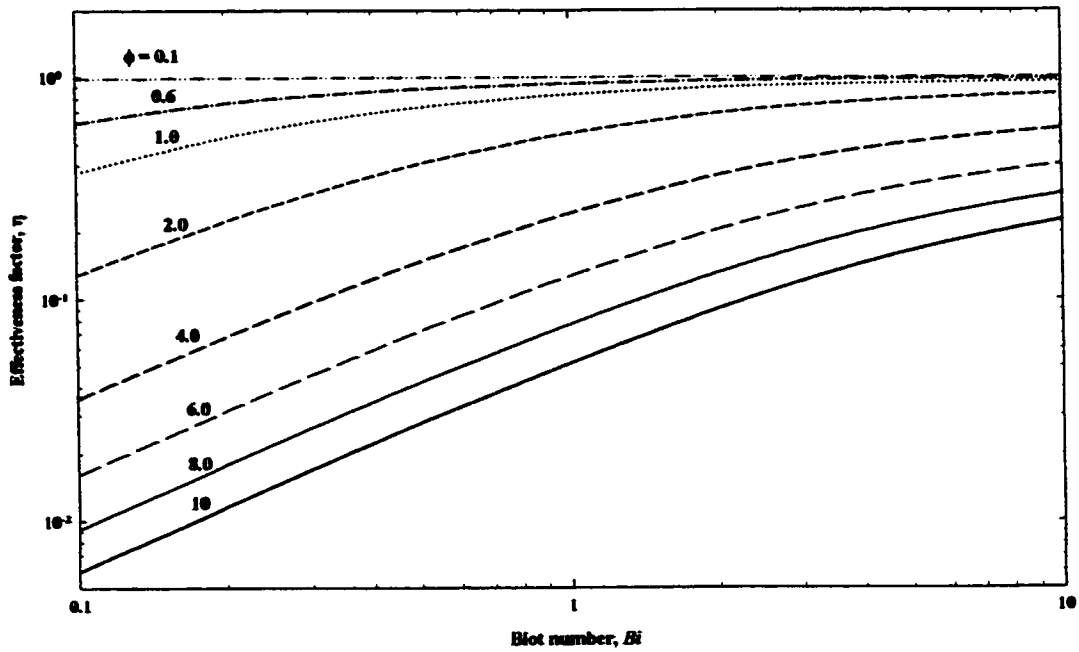


**Figure 5.20: Effects of Thiele modulus on internal effectiveness factor as a function of Biot number with  $\theta = 1$ ,  $\gamma = 1$ ;  $Pe = 2.0$  and  $St = 1.0$**

### 5.3.2 Effects of Biot, Michaelis modulus and $St$

Figure 5.21 shows quantitatively the effects of Michaelis modulus,  $\theta$ , and Stanton number on the substrate conversion as a function of Biot number with  $\gamma = 1.0$ ,  $\phi = 2.0$  and  $Pe = 2.0$ . It shows that the conversion decreases upon increasing Biot number at a given  $St$ . A further decrease in Biot number results in the substrate conversion becoming independent of Michaelis modulus and the substrate conversion asymptotically approaches constant value. Also, it depends on  $St$  because the diffusional resistance is dominating factors in determining the substrate conversion. Effects of external mass transfer on the substrate conversion at different Stanton number for different Michaelis modulus is shown in Figure 5.22. When the external mass transfer is very low (i.e.  $St = 0.1$ ), the substrate conversion is very low compared to higher  $St$ . In addition, the effect of Michaelis modulus is negligible for lower Biot number.

The effects of mass transfer limitations were measured quantitatively by internal effectiveness factor. These effects are shown in Figure 5.23, which illustrates the effects of Biot number and  $St$  on the effectiveness factor for three different Michaelis modulus  $\theta = 0.1, 1, 10$  and  $\gamma = 1.0$ . Although, the substrate conversion increases with decreasing Biot number, it is found in Figure 5.23 that the effectiveness factor increases upon increasing  $Bi$  up to certain value above which no further change is detected in effectiveness factor. In this regime, the reaction rate approaches the intrinsic value where the process is kinetically controlled. It is noticed that the increase in  $St$  in the reaction rate

regime will be approached at lower  $Bi$ . Therefore, at very high  $Bi$ , the effectiveness factor is a function of Michaelis modulus as shown in Figure 5.24.

The following results can be drawn from Figures 5.23, 5.24 and 5.25:

- At very low  $St$ , the effectiveness factor is characterized by Michaelis modulus and  $Bi$ , which is independent of  $St$ .
- An increase in  $St$  reduces the effectiveness factor when  $\theta < 1$  and increases the effectiveness factor when  $\theta > 1$ . However, the effectiveness factor is independent of  $St$  when  $\theta = 1$ .
- As can be seen from Figure 5.23 for a given  $Bi$ , increase  $St$  from  $\theta = 0.1$  and 1.0, causes the effectiveness factor to asymptotically approach a constant value at certain  $St$ . Above this value of  $St$ , the effectiveness factor is only a function of  $Bi$  regardless of  $St$  and  $\theta$ . Similarly for the case where  $\theta = 10$  and 1.0 the two curves approaches each other at a tangent point (i.e. cusp point). This cusp point forms earlier for the case of  $\theta = 10$  compared to  $\theta = 0.1$ .

It can be concluded that the effectiveness factor is only a function of  $\theta$  when the process is kinetically controlled at very high  $Bi$  and extremely low  $St$ . In this regime, upon increasing  $St$ , the effectiveness factor becomes independent of  $St$  and can be a function of  $Bi$  and  $\theta$ . However, at extremely high  $St$ , the effectiveness factor becomes independent of both  $St$  and  $\theta$  and is characterized by  $Bi$  when the process is mass transfer controlled. Between these two limiting cases, the effectiveness factor is a function of  $\theta$ ,  $Bi$  and  $St$  while other parameters remains constant.

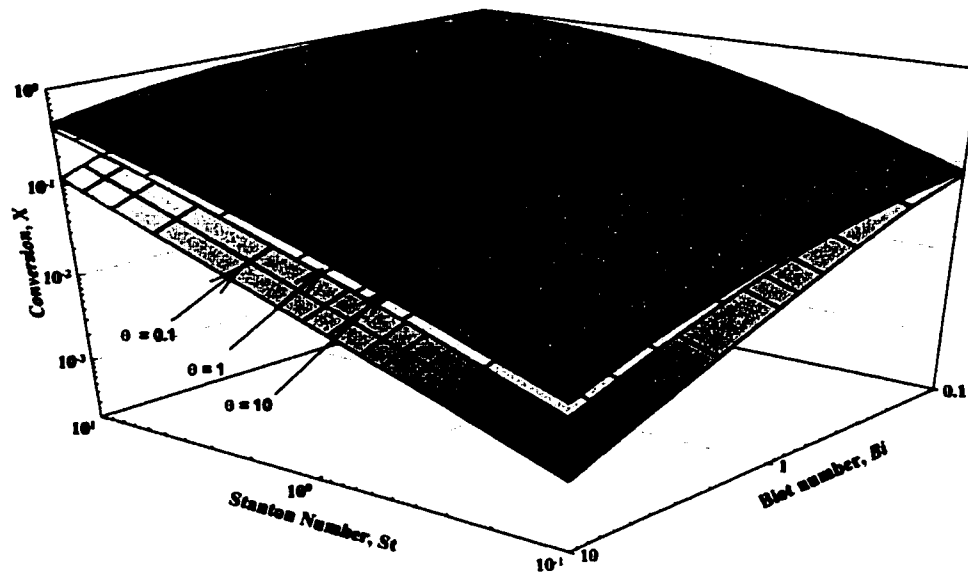


Figure 5.21: Effects of Michaelis modulus on reactor conversion for varying Biot number and Stanton number with  $\gamma = 1$ ,  $\phi = 2.0$  and  $Pe = 2.0$

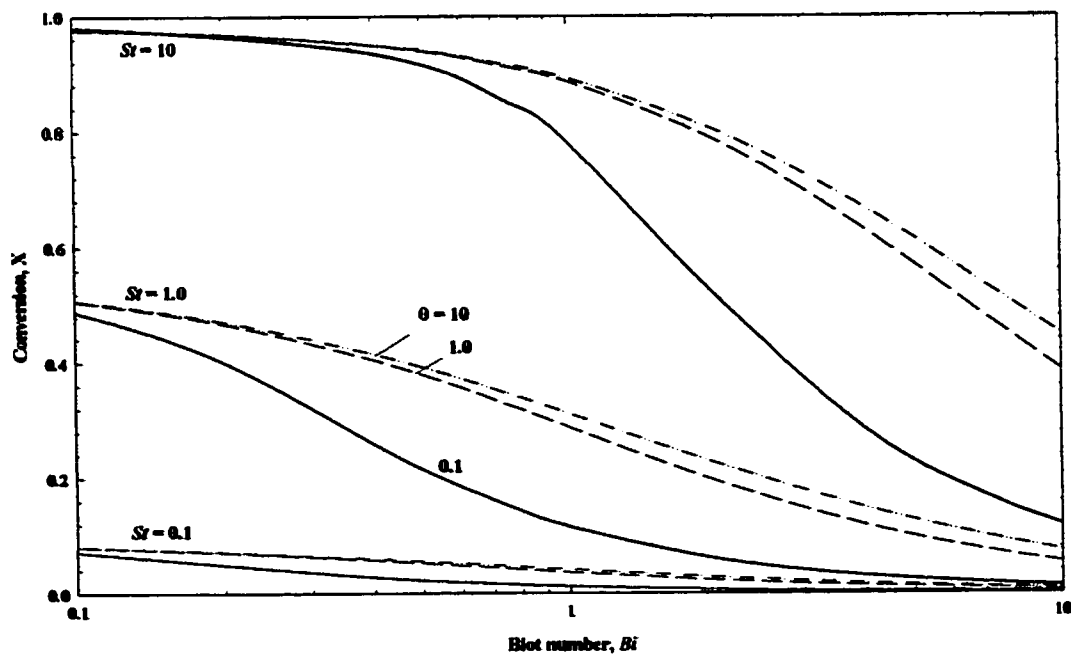
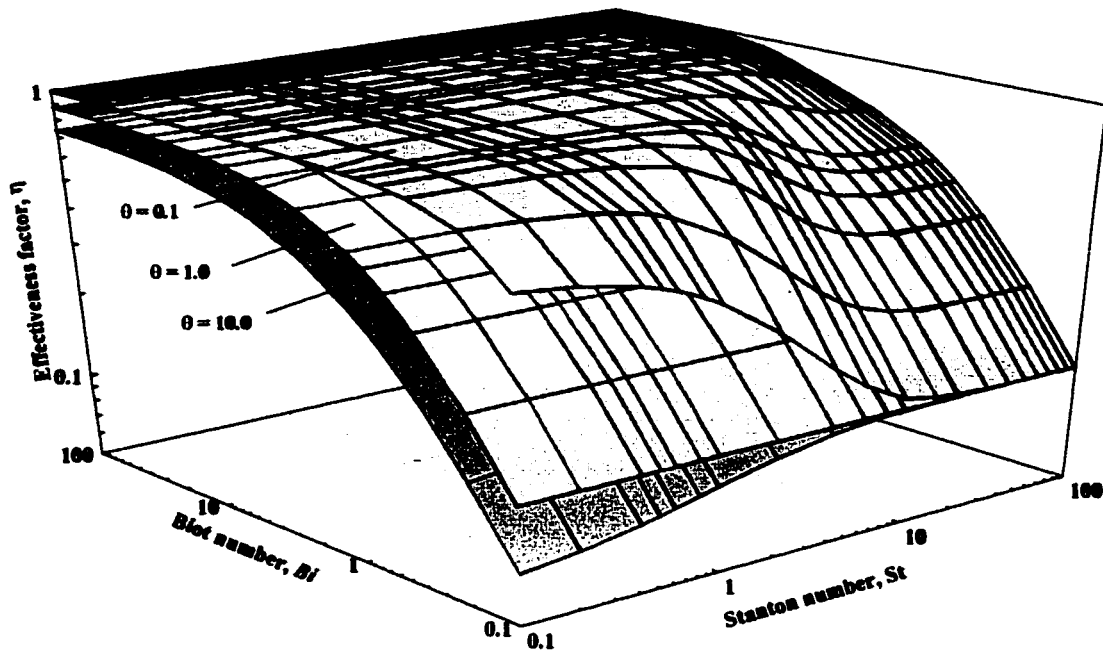
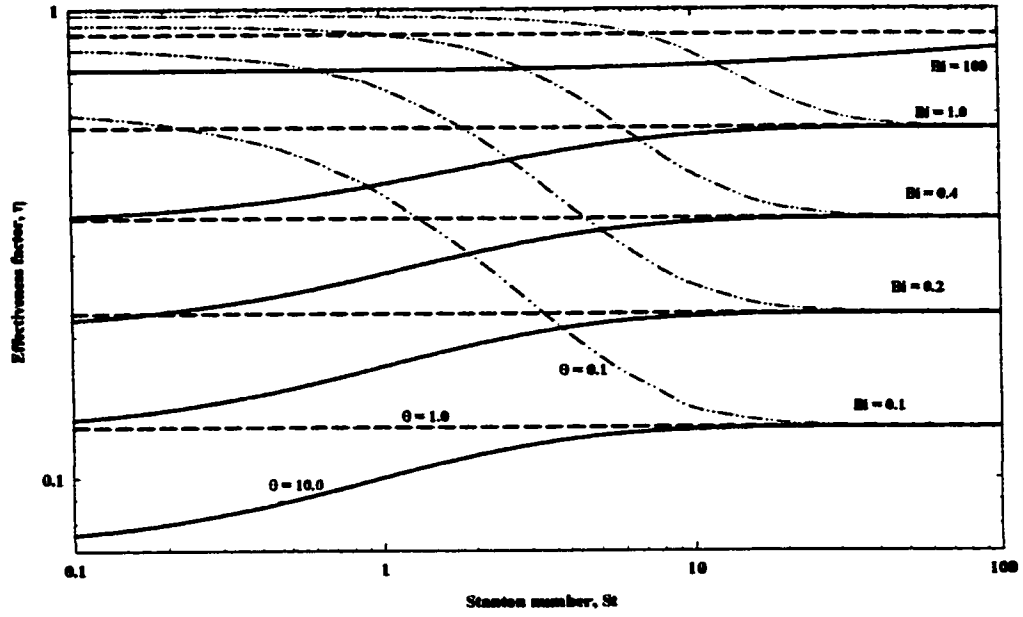


Figure 5.22: Effects of  $St$  number on reactor conversion as a function of Biot number with  $\theta = 0.1, 1, 10$ ,  $\gamma = 1$ ,  $\phi = 2.0$  and  $Pe = 2.0$

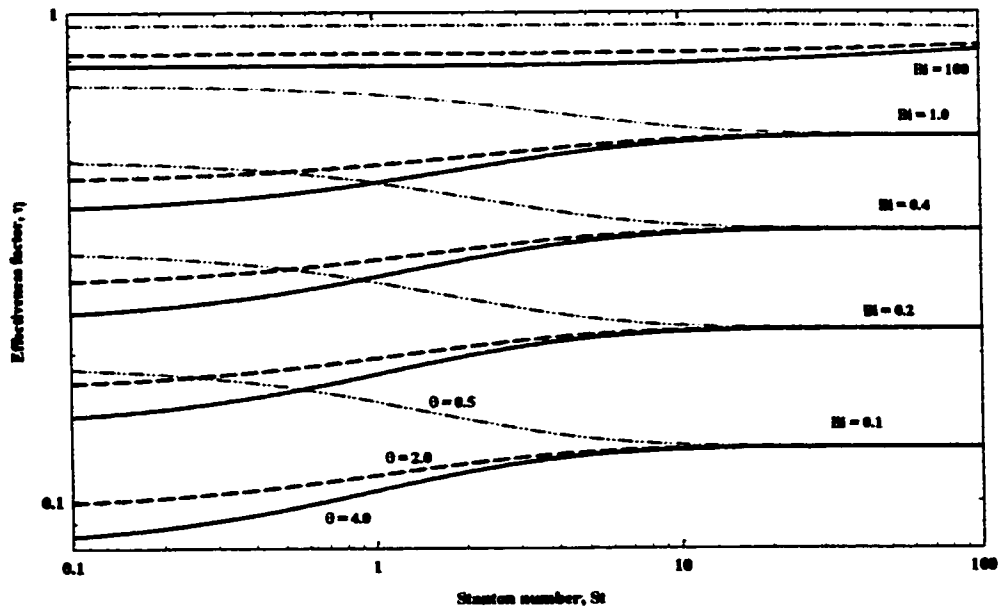


**Figure 5.23: Effects of  $\theta$  on internal effectiveness factor for varying Biot number and Stanton number with  $\theta = 0.1, 1, 10, \gamma = 1, \phi = 2.0$  and  $Pe = 2.0$**





(a)



(b)

**Figure 5.24: Effects of Biot number on internal effectiveness factor as a function of Stanton number with  $\gamma = 1$ ,  $\phi = 2.0$  and  $Pe = 2.0$  for (a)  $\theta = 0.1, 1, 10$  (b)  $\theta = 0.5, 2, 4$**

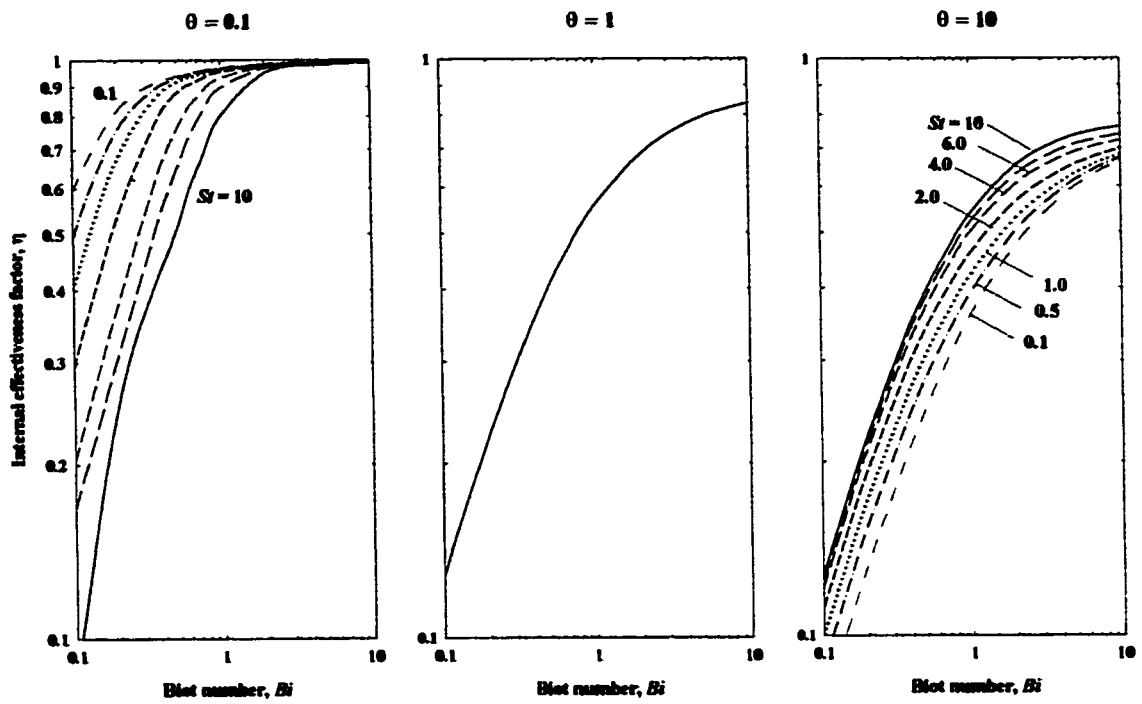


**Figure 5.25: Effects of Stanton number on internal effectiveness factor as a function of Biot number for  $\theta = 0.1, 1, 10, \gamma = 1, \phi = 2.0$  and  $Pe = 2.0$**

### **5.3.3 Effects of Biot number, $St$ and product inhibition**

A similar study was carried out to study the effects of Biot number for different product inhibition modulus,  $\gamma$ . The simulation results are shown in Figures 5.26 and 5.27 for substrate conversion. Figures 5.28, 5.29, 5.30 and 5.31 illustrate the effects of Biot number on the effectiveness factor.

Figure 5.26 shows the effects of  $\gamma$  on the substrate conversion for varying Biot number and Stanton number with  $\phi = 2.0$ ,  $\theta = 1.0$ ,  $Pe = 2.0$ . As discussed earlier in section 5.3.2, it can be concluded that the substrate conversion increases with decreasing Biot number. The effect of product inhibition reduces the substrate conversion, and more significant effects occur when both kinetic and mass transfer limitations are dominating factors i.e.  $Bi$  lies in the mixed regime as clearly shown in Figure 5.27.

Figure 5.28 shows the effects of  $\gamma$  on the internal effectiveness factor for varying Biot number and  $St$  with  $\theta = 1.0$ ,  $\phi = 2.0$  and  $Pe = 2.0$ . The trend can be characterized by three distinct regimes. First, the process is kinetically controlled when the mass transfer resistances are negligible at very high Biot number and low  $St$ . In this regime, the effectiveness factor is independent of both  $Bi$  and  $St$  but is a function of  $\gamma$  where the product inhibition reduces the effectiveness factor. Second, the kinetic and mass transfer are controlling the process when the effectiveness factor varies with  $St$  and it depends on  $\gamma$  and  $Bi$ . In this regime, the effectiveness factor increases with increasing  $St$  when  $\theta \gamma > 1$ , with decreasing  $St$  at  $\theta \gamma < 1$  and it is independent of  $St$  when  $\theta \gamma = 1$ . Third, the Stanton number is extremely high, when the effectiveness factor asymptotically reaches a

constant value regardless of  $St$  but depends on  $\gamma$ . It is shown that the product inhibition favor the effectiveness factor in this regime. Therefore, the effectiveness factor is independent of  $St$ ,  $Bi$  when the mass transfer is dominating factor in determining the effectiveness factor. This behavior is similar to the effect of product inhibition on the effectiveness factor discussed earlier. It can be concluded that the effect of product inhibition reduces the effectiveness factor when the process is reaction rate controlled but it favors the effectiveness factor when the process is mass transfer controlled. Although the internal effectiveness factor is a function of  $\gamma$  in these two regimes, the effectiveness factor is independent of both  $St$  and  $Bi$  as shown in Figure 5.28.

In the mixed regime, however, the effectiveness factor increases with increasing Biot number and the trend is proportional when  $\theta\gamma > 1$ . Whereas when  $\theta\gamma < 1$ , the trend is inversely proportional. Due to these two opposite trends shown in the effect of  $\gamma$  and  $St$  on  $\eta$ , it is found that effectiveness factor is independent of  $\gamma$  at certain values of  $St$  and  $Bi$  at crossover point. It is evident from Figure 5.28 that the crossover points trajectory can be represented by dimensionless parameters at crossover point  $\beta_{x0} = St_{x0} / Bi_{x0} = 1.5$ , at  $\theta = 1.0$  and  $\phi = 2.0$  that satisfied all crossover points trajectory.

Further to investigate the effects of  $\theta$  and  $\phi$  on the crossover points trajectory, a similar study was conducted for different combinations of  $\theta$  and  $\phi$  and the simulation results were plotted in Figure 5.29, 5.30 and 5.31. The results are summarized in Table 5.1

Furthermore, Figure 5.31b illustrates the effects of product inhibition on the internal effectiveness factor as a function of  $St$  and  $\phi$  with  $\theta = 1.0$ ,  $Bi = 0.1$  and  $Pe = 2.0$ . As can

be seen, the effects of product inhibition form a crossover points trajectory in  $St-\phi$  at given  $Bi = 0.1$ . Therefore, the  $\beta_s$  at crossover points can be given by equation 5.1 at  $\theta = 1.0$ ,

$$\beta_{x0} \approx \frac{6.0}{\phi_{x0}^2} \quad (5.1)$$

The following equation can be correlated from Table 5.1 which can be used to approximate the  $\beta_s$  at crossover point that relates to  $\theta$  and  $\phi$ ,

$$\beta_{x0} = \frac{St_{x0}}{Bi_{x0}} \approx \frac{6.0}{\theta^{\frac{1}{3}} \phi_{x0}^2} \quad (5.2)$$

Thus, the crossover points found in Figure 5.2 can also be approximated by equation (5.2) at  $\beta_{x0} = 10$ .

$$\phi_{x0} \approx \frac{0.776}{\theta^{\frac{1}{6}}} \quad (5.3)$$

Thus the mixed regime can be characterized by  $\beta_{x0}$  at which the effectiveness factor  $\beta_s > \beta_{x0}$ , whereas, when  $\beta_s < \beta_{x0}$  the effectiveness factor decreases as  $St$  increases. Therefore, when  $\beta_s < \beta_{x0}$ , the reaction kinetic factors are more significant where the effect of product inhibition has reduced the effectiveness factor by reducing reaction rate. However, when  $\beta_s < \beta_{x0}$ , the mass transfer limitations are dominant and the product inhibition favors the internal effectiveness factor since it reduces rate of mass transfer.

**Table 5.1: Calculated  $\beta_{x_0}$  from different simulation results**

<b>Source</b>	<b><math>\theta_{x_0}</math></b>	<b><math>\phi_{x_0}</math></b>	<b><math>\beta_{x_0}</math></b>
Figure 5.28	1.0	2.0	1.5
Figure 5.29a	1.0	0.5	20
Figure 5.29b	1.0	4.0	0.4
Figure 5.30a	0.1	2.0	6.0
Figure 5.30b	0.5	2.0	2.1
Figure 5.31a	5.0	2.0	0.95

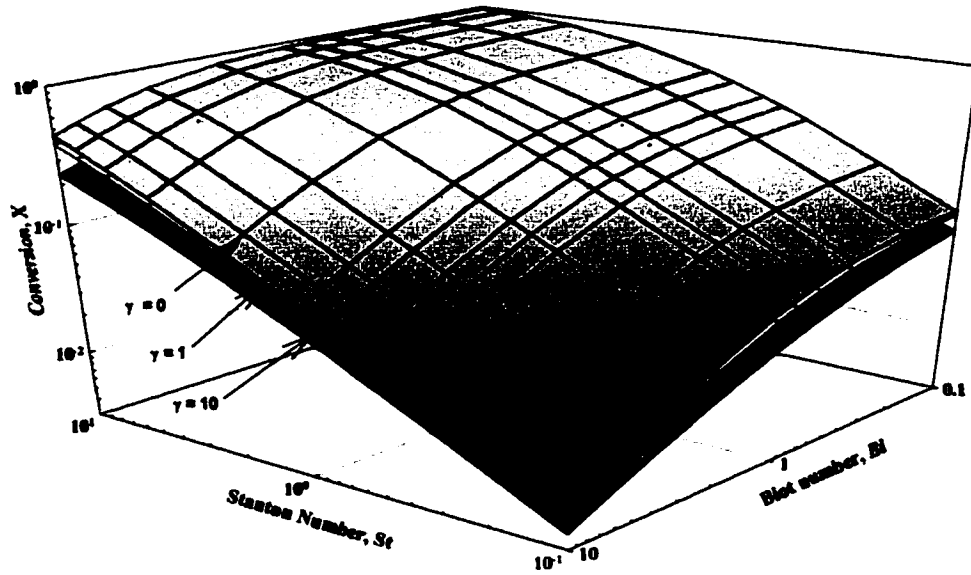


Figure 5.26: Effects of product inhibition on reactor conversion for varying Biot and Stanton number with  $\gamma = 0, 1, 10, \theta = 1, \phi = 2.0$  and  $Pe = 2.0$

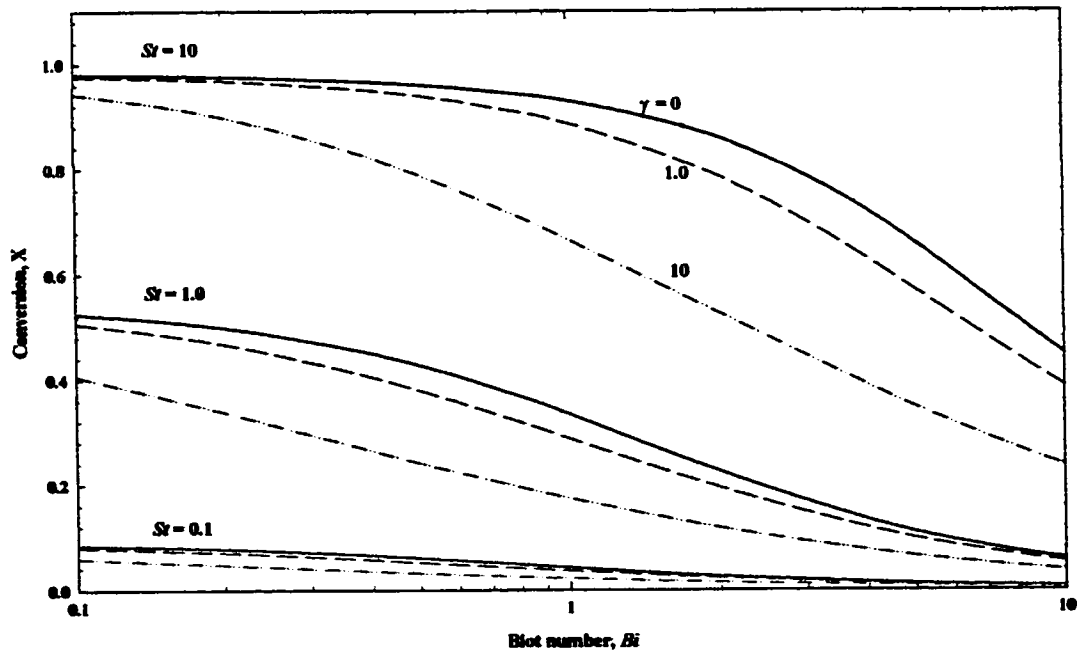
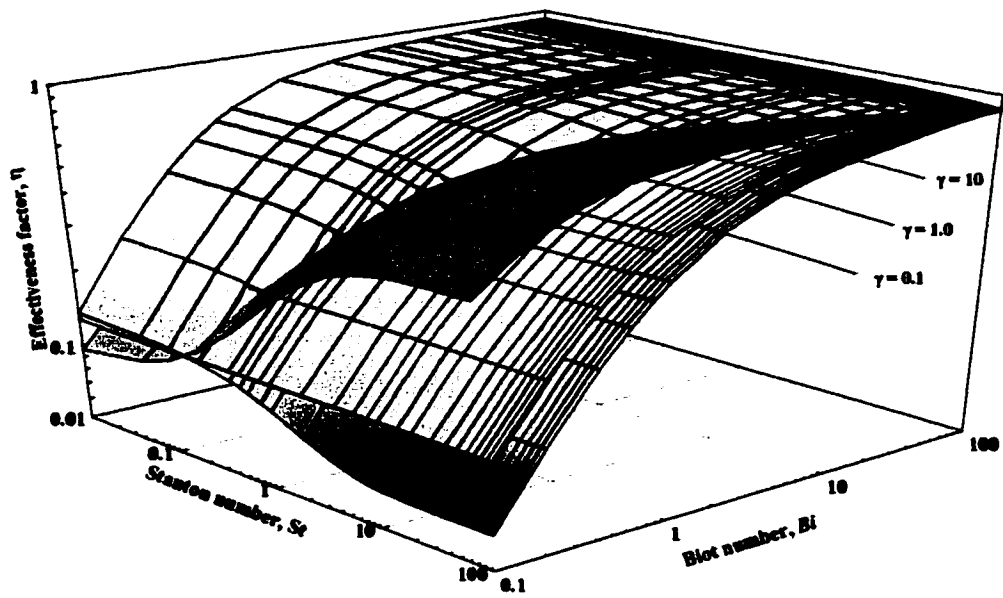
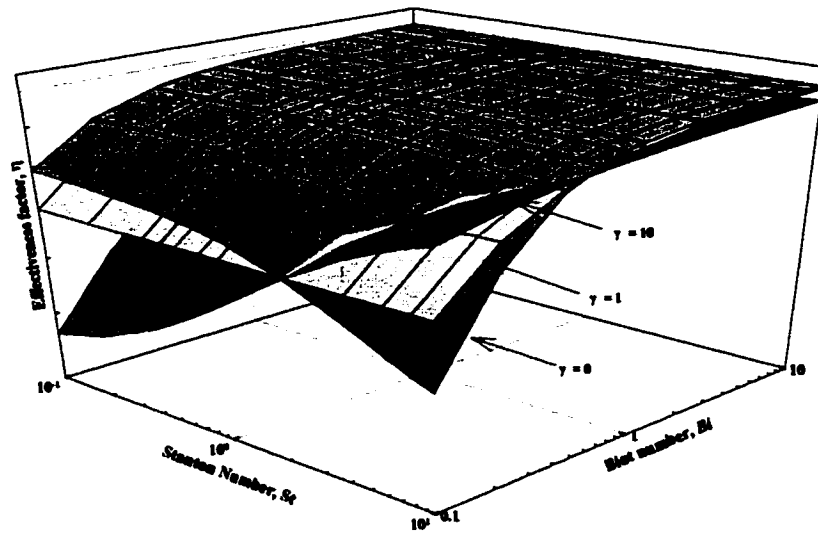


Figure 5.27: Effects of  $St$  number on reactor conversion as a function of Biot number with  $\gamma = 0, 1, 10, \theta = 1, \phi = 2.0$  and  $Pe = 2.0$

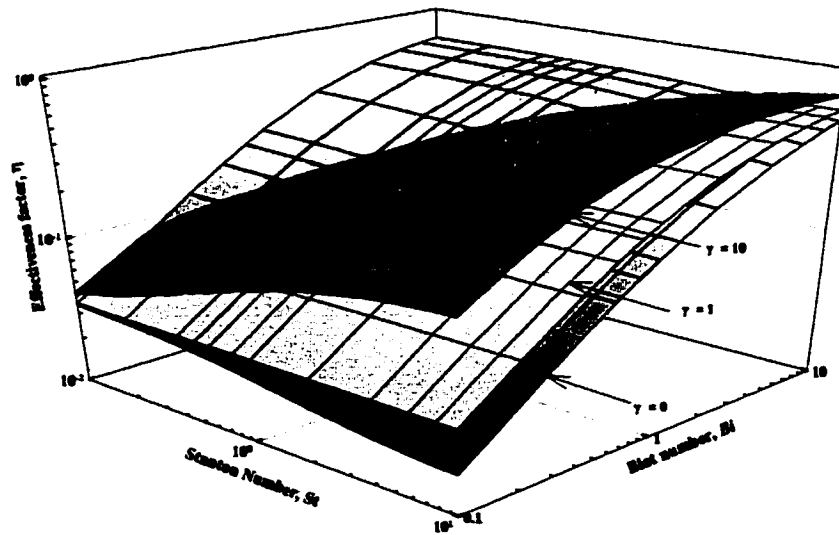


**Figure 5.28: Effects of product inhibition on internal effectiveness factor for varying Biot and Stanton number with  $\theta = 1$ ,  $\phi = 2.0$  and  $Pe = 2.0$**



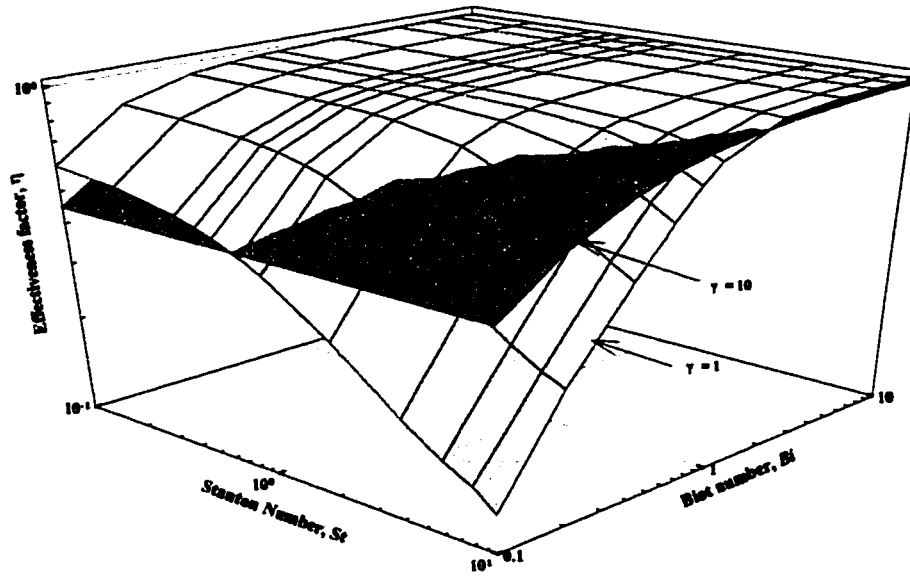


(a)

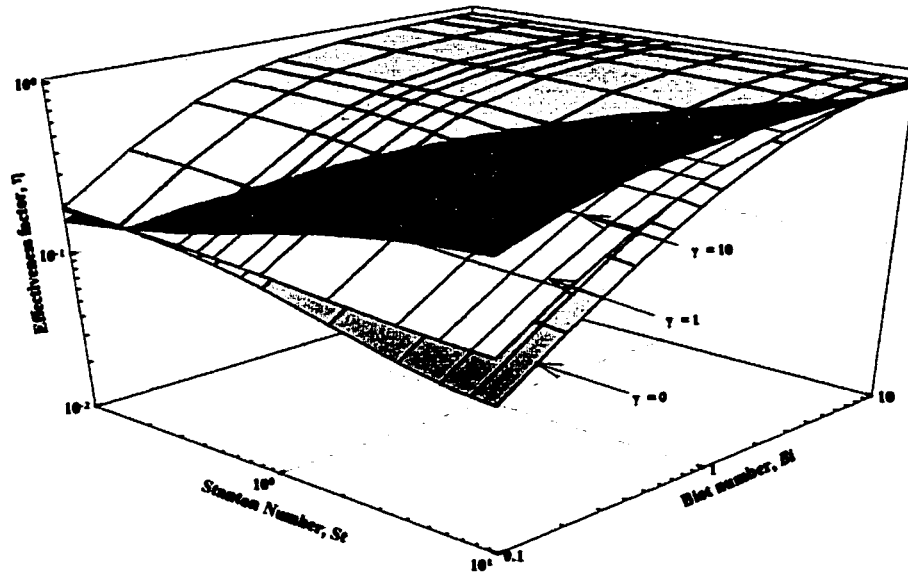


(b)

**Figure 5.29: Effects of product inhibition on internal effectiveness factor for varying Biot and Stanton number with  $\theta = 1$ ,  $Pe = 2.0$  for (a)  $\phi = 0.5$  (b)  $\phi = 4.0$**

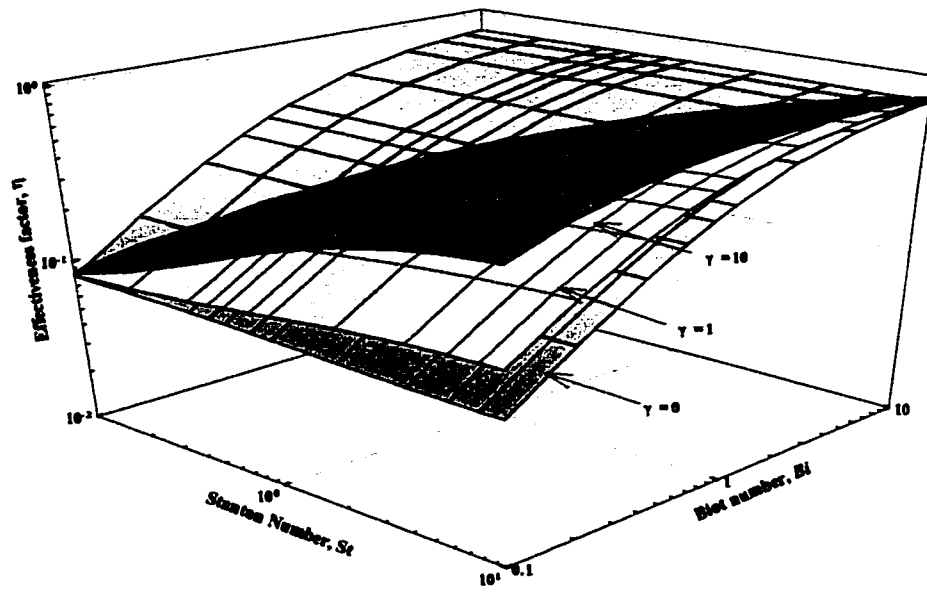


(a)

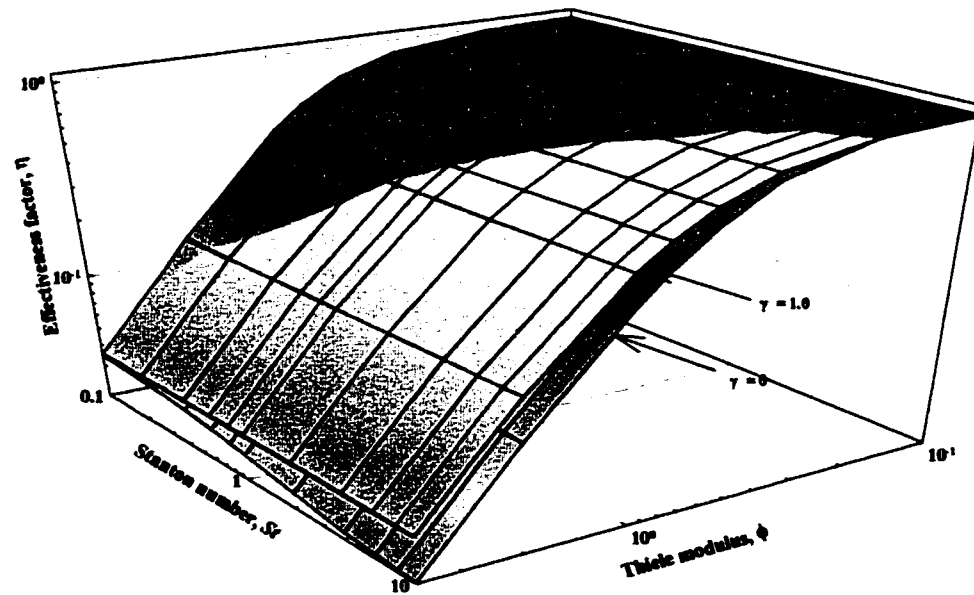


(b)

**Figure 5.30: Effects of product inhibition on internal effectiveness factor as a function of Biot number and Stanton number with  $\theta = 1$ ,  $Pe = 2.0$ ,  $\phi = 2.0$  for (a)  $\theta = 0.1$  (b)  $\theta = 5.0$**



(a)



(b)

**Figure 5.31: Effects of product inhibition on internal effectiveness factor with  $Pe = 2.0$ ;**  
**(a) varying  $Bi$  and  $St$  at  $\phi = 2.0$ ,  $\theta = 0.5$ ; (b) varying  $St$  and  $\phi$  at  $\theta = 5.0$ ,  $Bi = 0.1$**

## 5.4 Effect of Reactor Hydrodynamics

The effects of reactor hydrodynamics have been studied on the reactor performance in terms of substrate conversion and internal effectiveness factor. The reactor hydrodynamics is characterized by Peclet number to represent axial dispersion effects. Peclet number,  $Pe$ , is the ratio of backmixing time to residence time. It measures the effect of degree of mixing, for extremely low  $Pe$  (i.e.  $Pe = 0.001$ ) represent CSTR, for high  $Pe$  (i.e.  $Pe = 10^4$ ) represent PFR and dispersed plug flow reactor model (DFPR) characterized by finite  $Pe$ . The effects of axial dispersion were studied with intraparticle and external mass transfer in section 5.4.1. Moreover, the effects of Michaelis modulus and product inhibition on the axial dispersion was studied in section 5.4.2 and 5.4.3 respectively.

### 5.4.1 Effects of $Pe$ , $\phi$ and $St$

Figures 5.32 and 5.33 show the effects of  $Pe$  on the substrate conversion for varying  $St$  and Thiele modulus with  $\gamma = 1.0$ ,  $\theta = 1.0$  and  $Bi = 0.1$ . It shows that at given  $St$  the substrate conversion is independent of  $Pe$  when the process is kinetically controlled at low Thiele modulus and low  $St$ . However, when the process is diffusion rate controlled at high  $\phi$  and high  $St$ , the substrate conversion increases with increasing  $Pe$ .

Therefore, the substrate conversion increases as a result of increasing  $Pe$  when  $\beta_s > \beta_{x_0}$ . However, the substrate conversion is independent of  $Pe$  as shown clearly in Figure 5.32 when  $\beta_s \leq \beta_{x_0}$ . At high  $St$  (i.e. at high  $\beta_s$ ), the Thiele modulus at cross-over point,  $\phi_{x_0}$ ,

occurs at low value of  $\phi$ , whereas at low  $St$ , the cross-over  $\phi_{xo}$  occurs at high  $\phi$ .

Figures 5.34 and 5.35 show the effects of Peclet number on the substrate conversion as a function of  $St$  with various values of  $\phi$ . It shows that the substrate conversion is independent of Peclet number when the process is kinetically controlled at extremely low  $St$ .

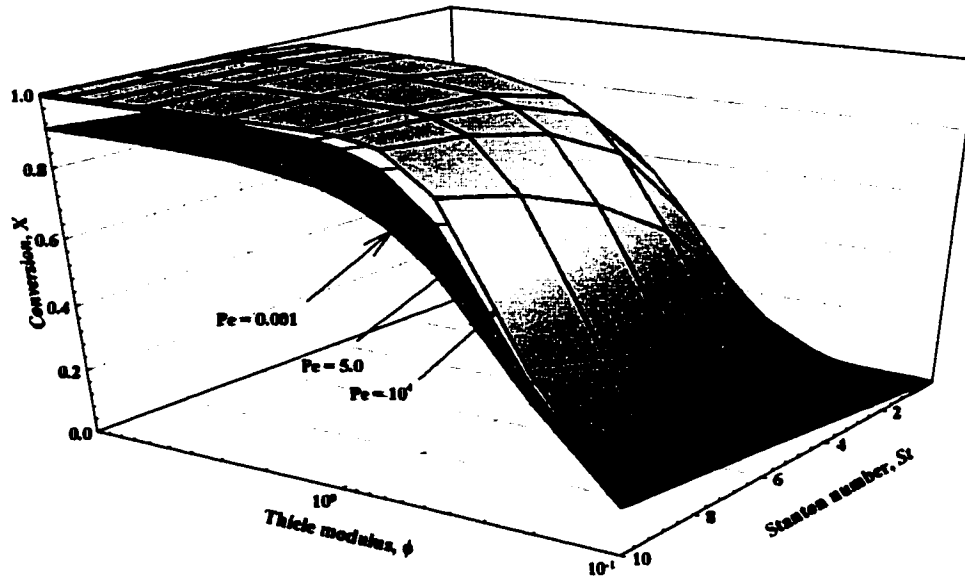


**Figure 5.32:** Effects of Peclet number on reactor conversion for varying Thiele modulus and Stanton number with  $\gamma = 1$ ,  $\theta = 1$  and  $Bi = 0.1$

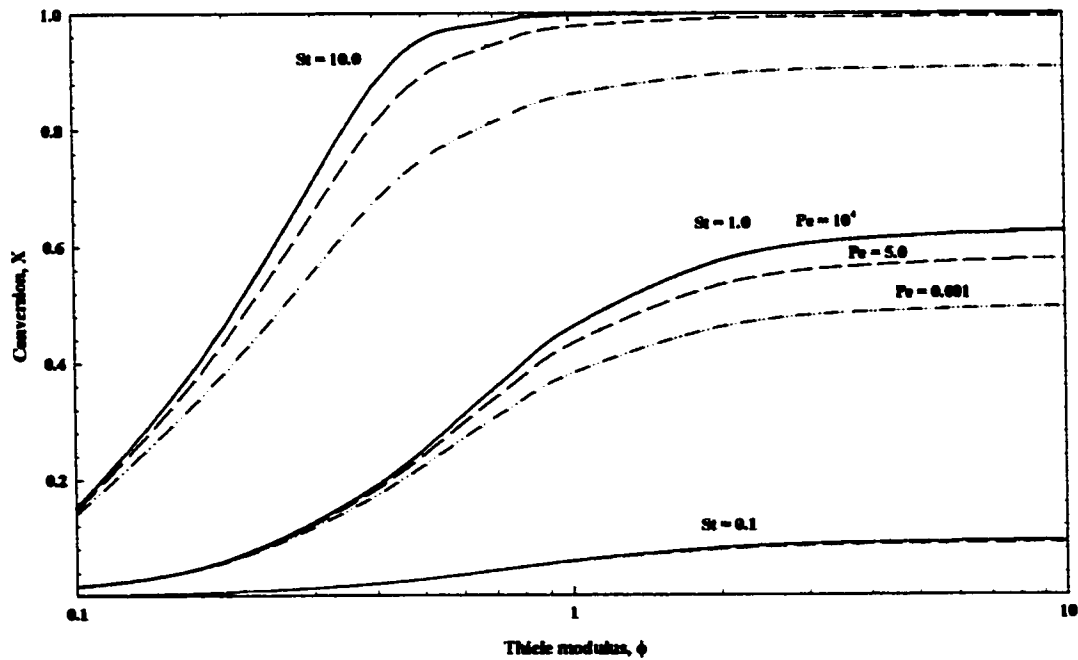


**Figure 5.33:** Effects of Stanton number on reactor conversion as a function of Thiele modulus for  $Pe = 0.001, 5, 10^4$ ;  $\gamma = 1$ ,  $\theta = 1$  and  $Bi = 0.1$

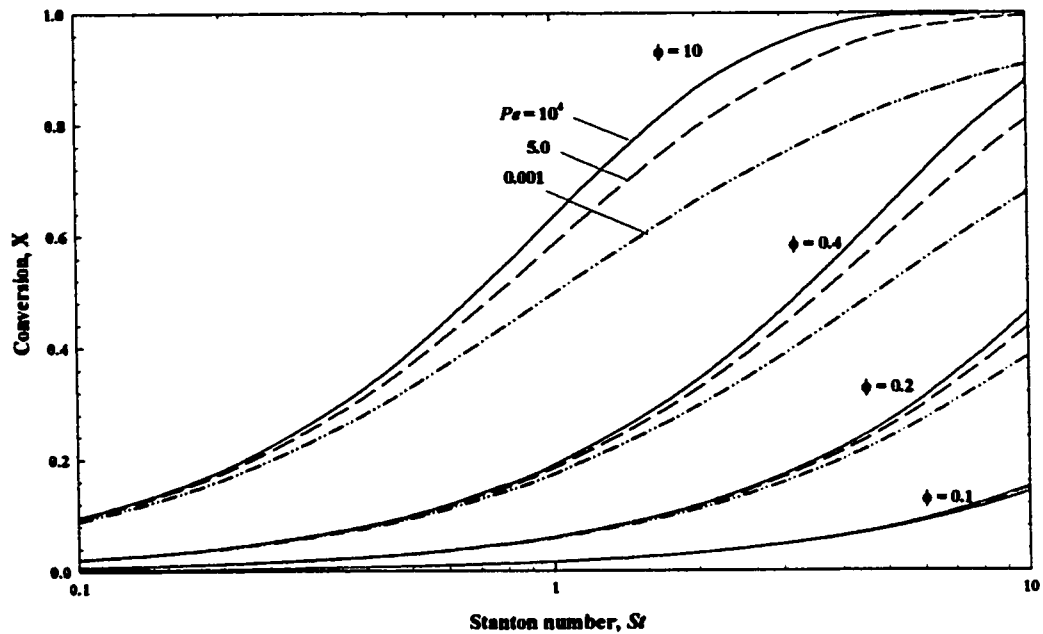


**Figure 5.34:** Effects of Thiele modulus on reactor conversion as a function of Stanton number for  $Pe = 0.001, 5, 10^4$ ;  $\gamma = 1, \theta = 1$  and  $Bi = 0.1$

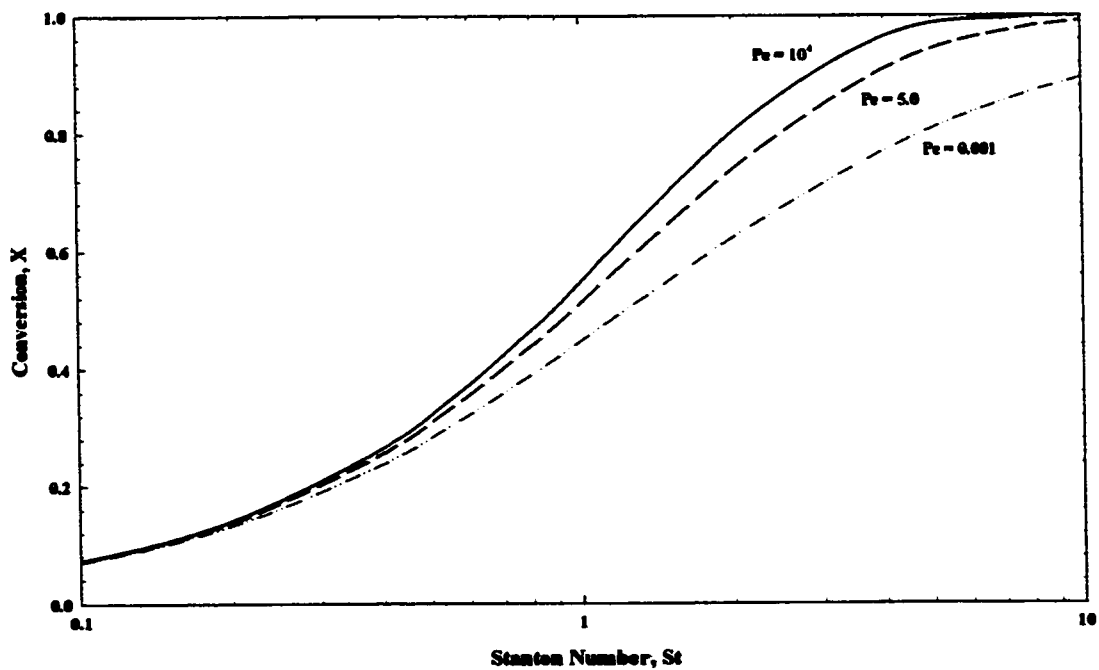


**Figure 5.35:** Effects of Peclet number on reactor conversion as a function of Stanton number with  $\theta = 1, \gamma = 1, \phi = 2$  and  $Bi = 0.1$

### 5.4.2 Effects of $Pe$ , $\theta$ , $\gamma$ and $St$

Figure 5.36 shows the effects of  $Pe$  and  $\theta$  on the effectiveness factor as a function of  $St$  with various values of Michaelis modulus for  $Pe = 0.001, 5.0, 10^4$ ,  $\gamma = 1.0$ ,  $\phi = 2.0$  and  $Bi = 0.1$ . At extremely low  $St$  and when  $\beta_s \leq \beta_{x_0}$ , the internal effectiveness factor asymptotically approaches constant value regardless of  $St$  and is independent of  $Pe$ . At this regime, when the process is kinetically controlled, the effectiveness factor is only a function of  $\theta$ . However, it also shows that when  $\beta_s \leq \beta_{x_0}$  the internal effectiveness factor is independent of  $Pe$  and  $St$  at  $\theta \gamma = 1$ . In spite of that, internal effectiveness factor increases with decreasing  $\theta$  and decreasing  $St$  when  $\theta \gamma < 1$ . Whereas, the effectiveness factor increases with increasing both  $St$  and  $Pe$  when  $\theta \gamma < 1$ . Therefore, PFR showed the highest effectiveness factor  $\theta \gamma < 1$ .

On the other hand, at very high  $St$  when the process is mass transfer controlled it is shown that the effectiveness factor approaching asymptotically the curve of  $\eta$  of  $\theta = 1.0$ . As  $St$  increases further, no change in effectiveness factor was detected. Therefore, the internal effectiveness is independent of  $Pe$ ,  $St$  and  $\theta$ . This is shown in Figure 5.37, where the effectiveness factor is constant regardless of  $\theta$  at  $St = 10.0$ . The effects of  $Pe$  as a function of  $St$  for different product inhibition,  $\gamma$ , was studied and the simulation result is shown in Figure 5.38. A similar conclusion can be drawn from this figure on the effects of  $Pe$  on the effectiveness factor with various values of  $St$  and  $\theta \gamma$ . The crossover point was found



at  $St_{x0} = 0.15$ . Above it, the product inhibition favors the effectiveness factor where it increases as a result of increasing  $St$  and  $Pe$  when  $\theta \gamma > 1$ . The effectiveness factor, however, shows a decreasing function with  $St$  and  $Pe$  when  $\theta \gamma < 1$ . Furthermore, when  $\beta_s < \beta_{x0}$ , the product inhibition reduces the effectiveness factor and it is independent of  $Pe$  at this regime. No further change in effectiveness factor is shown with decreasing  $St$  much below the  $St_{x0}$  (i.e.  $\beta_s \ll \beta_{x0}$ ). Thus, the internal effectiveness factor is independent of both  $St$  and  $Pe$  in this regime.

At the given parameters, the conversion for  $Pe = 5.0$  (DPFR) is always lower than PFR ( $Pe = 10^4$ ) and higher than for CSTR ( $Pe = 0.001$ ). The difference in conversion between the three reactor models is higher in the case of high Stanton number as clearly shown in Figure 5.38. Also, the axial dispersion has no effects on reactor conversion at small degree of conversion and for lower Michaelis modulus,  $\theta$  (i.e. approaches zero order kinetics). Practically, CSTR is favored for lower values of desired conversion and for lower  $\theta$  or zero order kinetics. PFR is however, is more favored over CSTR as conversion increases particularly at high  $\theta$ . On the other hand, PFR gives higher effectiveness factor for  $\gamma > 1$ , which means less resistance to mass transfer. However, for  $\gamma < 1$ , CSTR shows better performance over PFR and is suitable for Michaelis Menten kinetics, i.e.  $\gamma = 0$ .

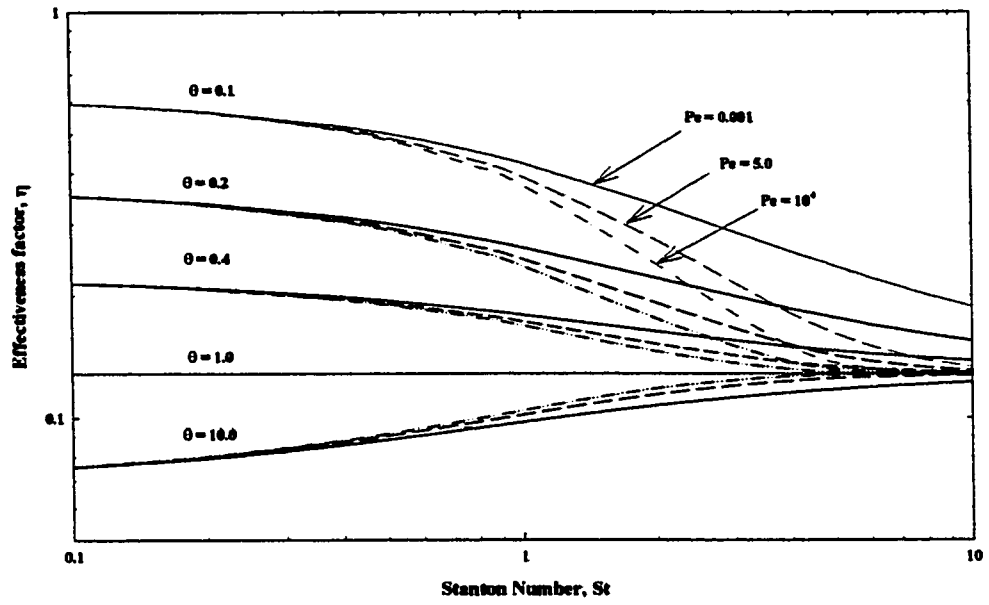


**Figure 5.36: Effects of Michaelis modulus on internal effectiveness factor as a function of Stanton number for  $Pe = 0.001, 5, 10^4$ ;  $\gamma = 1, \phi = 2$  and  $Bi = 0.1$**

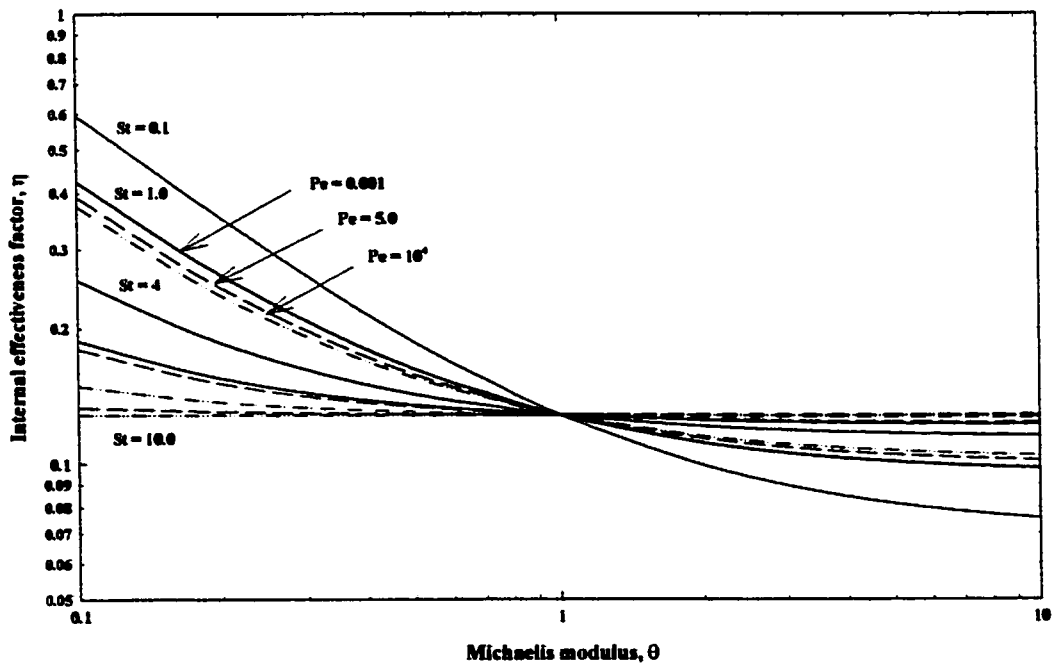


**Figure 5.37: Effects of  $St$  number on internal effectiveness factor as a function of Michaelis modulus for  $Pe = 0.001, 5, 10^4$ ;  $\theta = 1, \phi = 2$  and  $Bi = 0.1$**

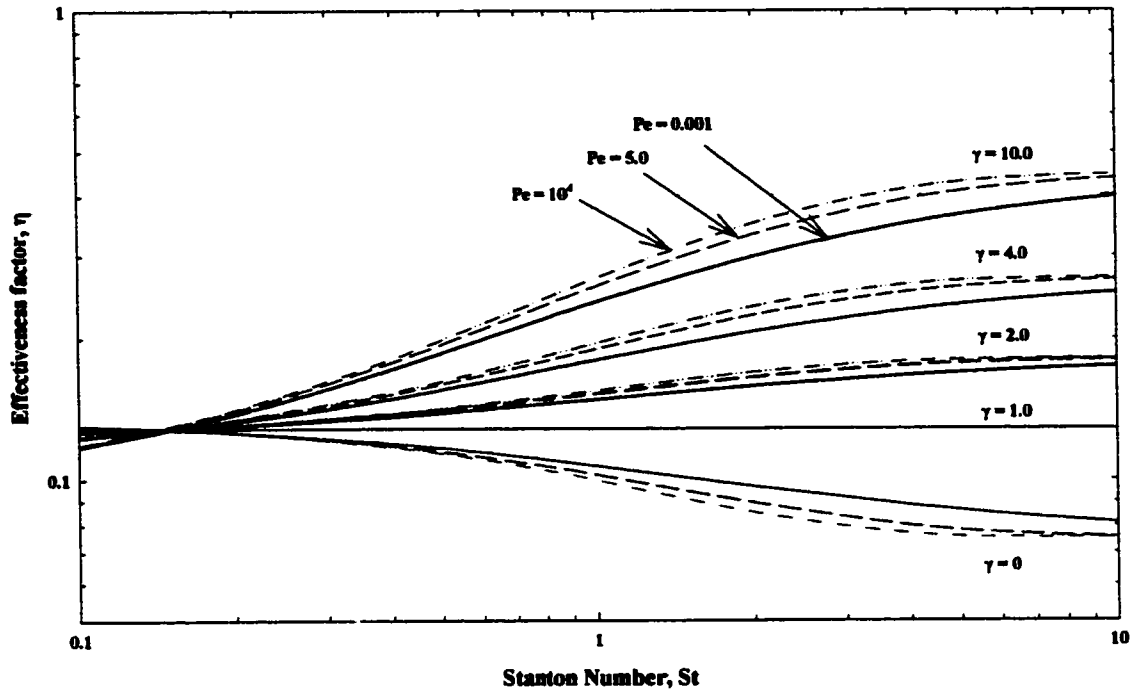


**Figure 5.38: Effects of product inhibition on internal effectiveness factor as a function of  $St$  for  $Pe = 0.001, 5, 10^4$ ;  $\gamma = 1, \phi = 2$  and  $Bi = 0.1$**

## 5.5 Unsteady State Behavior

### 5.5.1 Unsteady State Effects of Michealis Modulus, $\theta$

The dependence of the substrate conversion on the dimensionless time,  $\tau$ , was studied for initial condition at  $\tau = 0$ ,  $S_{bi} = 0$ . Figure 5.39 presents time course of substrate conversion for different Michaelis modulus at  $\gamma = 1.0$ ,  $\phi = 2.0$ ,  $Bi = 0.1$  and  $St = 1.0$ . As evident from Figure 5.39, the whole time course of the substrate conversion can be illustratively divided into three parts: (i) the transient period, (ii) the pseudo – steady state period and (iii) the final steady state period. At the transient period, initially the substrate conversion is independent of  $\theta$  because at extremely low  $\tau$  the process is controlled by the substrate mass transfer to the enzyme supported particle. In the transient period, as a result of increasing  $\tau$  the substrate conversion increases and then it reaches a maximum value below which the substrate conversion slightly decreases to ultimately reach final steady state. The maximum values at which  $\frac{\partial S_b}{\partial \tau} = 0$ , is the region of a pseudo steady state. In the transient period, the bulk substrate rate change is positive where the substrate conversion increases with time, however,  $\frac{\partial S_b}{\partial \tau}$  is negative in the pseudo steady state period. The substrate conversion decreases from the maximum value to reach finally the steady state conversion. In the transient period, the substrate conversion inside enzyme supported on a porous spherical particle decreases with time because the final radial profile of substrate concentration has not yet been reached and definitely the bulk substrate concentration,  $S_b$ , has not reached final steady state. Once the substrate

concentration inside enzyme particle has reached steady state, the maximum concentration will reach a maximum value at which pseudo-steady state characterizes the process.

The effects of increase in Michaelis modulus on the transient substrate conversion were shown to reduce the final steady state time. Also, it is evident from Figure 5.39 that for the smallest  $\theta$  the response is faster where the pseudo-steady state period becomes shorter compared to the kinetic with higher  $\theta$ . On the other hand, the effectiveness factor versus dimensionless time for different Michaelis modulus is shown in Figure 5.40. As can be seen, the effectiveness factor increases with decreasing  $\theta$  for the entire dimensionless time. The trend may be divided into three periods as illustrated in conversion. Initially in the transient period, the effectiveness factor increases with time courses reaching a maximum effectiveness factor. As a result of product inhibition, the effectiveness increases when the process is mass transfer controlled i.e. when  $\beta_s > \beta_{x_0}$  and the effectiveness decreases otherwise. As can be seen from Figure 5.40, the effectiveness factor at pseudo – steady state is greater than the final steady state effectiveness factor when  $\beta_s < \beta_{x_0}$  (i.e. when  $\theta < \theta_{x_0} = 0.53$ ). However, when the  $\beta_s > \beta_{x_0}$  (i.e.  $\theta > \theta_{x_0} = 0.53$ ), the effectiveness factor at pseudo – steady state is lower than that of the final steady state effectiveness factor.

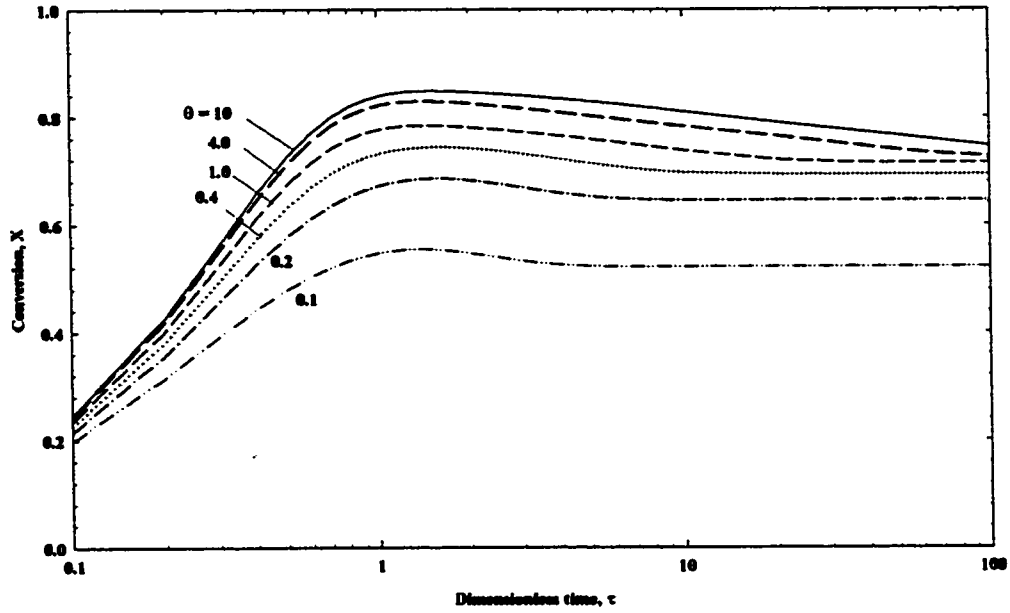


Figure 5.39: Effects of Michaelis modulus on unsteady state reactor conversion with  $\gamma = 1$ ,  $\phi = 2.0$ ,  $Bi = 0.1$ ,  $St = 1.0$

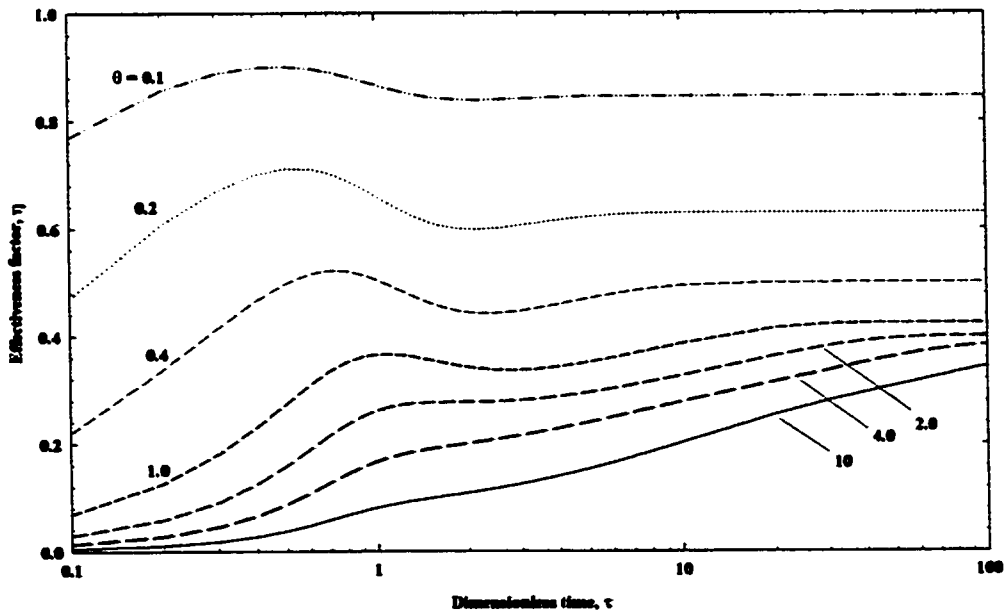
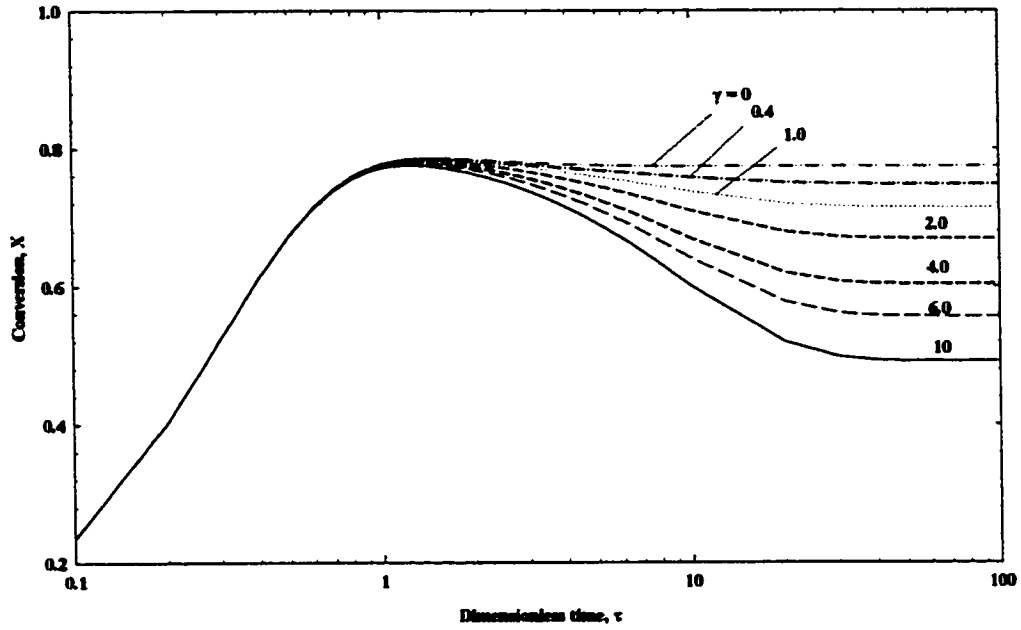


Figure 5.40: Effects of Michaelis modulus on unsteady state effectiveness factor with  $\gamma = 1$ ,  $\phi = 2.0$ ,  $Bi = 0.1$ ,  $St = 1.0$

## **5.5.2 Unsteady State Effects of Product Inhibition, $\gamma$**

A similar study was carried out for different product inhibition  $\gamma$  and the simulation results are expressed in Figure 5.41 and 5.42. Figure 5.41 shows the unsteady state substrate conversions at different product inhibition modulus,  $\gamma$ , at  $\theta = 1.0$ ,  $\phi = 2.0$ ,  $Bi = 0.1$  and  $St = 1.0$ . It is found that the effect of  $\gamma$  is more significant after the pseudo steady state is reached. Also, it can be noted that the product inhibition reduces the substrate conversion and increases the time to reach the final steady state.

Figure 5.42 shows the effects of  $\gamma$  on the unsteady state effectiveness factor with  $\theta = 1$ ,  $\phi = 2.0$ ,  $Bi = 0.1$  and  $St = 1.0$ . Initially in the transient period; the product inhibition reduces the effectiveness factor as a result of kinetic effects. At extremely very low  $\tau$ , the effectiveness factor is independent of  $\gamma$  since the process is mass transfer controlled. Again, it is important to notice that there exists a crossover point in unsteady state at which effectiveness factor is independent of product inhibition modulus. In pseudo – steady state, the effectiveness factor increases upon increasing  $\gamma$ . Furthermore, it is found that when  $\beta_s > \beta_{x_0}$ , the final steady state effectiveness factor increases above the pseudo – steady state effectiveness factor, however, the final effectiveness factor decreases below pseudo – steady state otherwise.



**Figure 5.41: Effects of product inhibition modulus on unsteady state conversion with  $\theta = 1$ ,  $\phi = 2.0$ ,  $Bi = 0.1$ ,  $St = 1.0$**

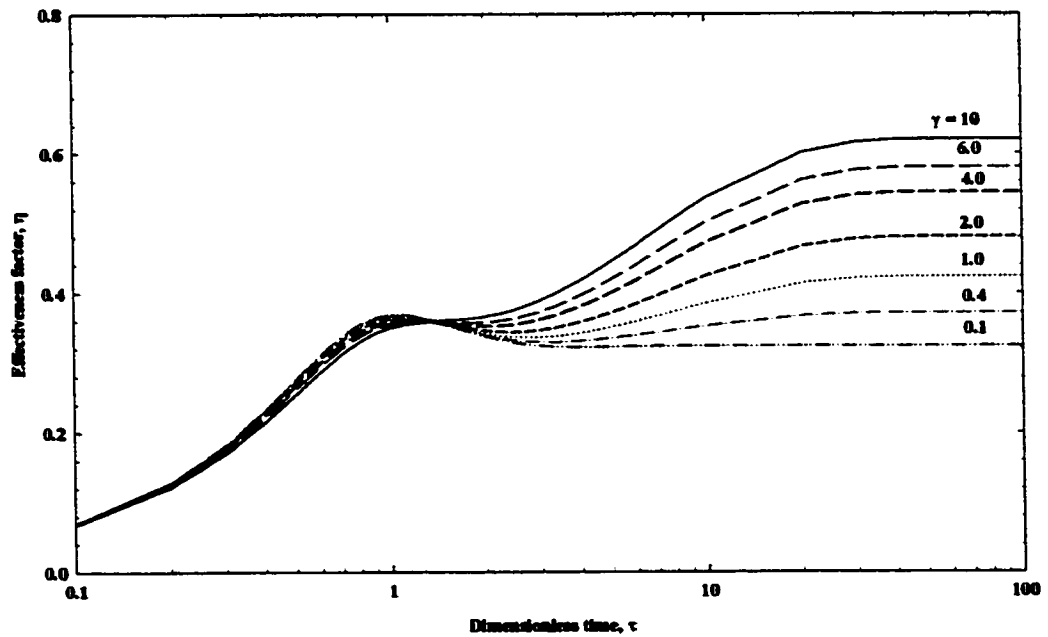


**Figure 5.42: Effects of product inhibition modulus on unsteady state effectiveness factor with  $\theta = 1$ ,  $\phi = 2.0$ ,  $Bi = 0.1$ ,  $St = 1.0$**



### 5.5.3 Unsteady State Effect of $St$ and $\theta$

Figure 5.43 shows the effects of  $St$  on the unsteady state substrate conversion at  $\theta = 0.1, 1, 10$  with  $\gamma = 1.0, \phi = 2.0$  and  $Bi = 0.1$ . The transient substrate conversion increases with the Stanton number. For extremely low  $St$ , the substrate conversion is small compared to those curves of  $St = 1$  and  $10$ . The trend is a function of Michaelis modulus where the substrate conversion varies with  $\theta$  over the entire time courses in transient, pseudo – steady state and final steady state conditions. From Figure 5.43, the time required to reach final steady state depends not only on the external mass transfer but also on the kinetic and intraparticle diffusion. The effectiveness factor is shown in Figures 5.44, 5.45 and 5.46 for Michaelis modulus  $\theta = 0.1, 1,$  and  $10$  respectively.

Figure 5.44 shows the effects of  $St$  on unsteady effectiveness factor at  $\theta = 0.1, \gamma = 1.0, \phi = 2.0$  and  $Bi = 0.1$ . It shows that the effectiveness factor decreases as  $St$  increases for the entire range of dimensionless time,  $\tau$ . This agree with the effect of  $St$  on steady state effectiveness factor when  $\theta \gamma < 1$ . In the transient period it is shown that the effectiveness factor is extremely low as a result of mass transfer limitations in the initial time course. As the time progresses, the substrate penetrates the enzyme particle in which enzymatic reaction takes place implying an increase in effectiveness factor. The trend of effectiveness factor exhibits a maximum value at pseudo-steady state above which the mass transfer limitations and the effects of product inhibition have reduced the effectiveness factor below the pseudo-steady state maximum value.

Although a similar trend was found when  $\theta \gamma = 1$ , the final steady state is found to be

independent of  $St$  as illustrated in Figure 5.45. However, when  $\theta \gamma = 10 > 1$ , Figure 5.46 shows the same trend, but the final steady state is higher than the pseudo-steady state effectiveness factor. This increase in effectiveness factor is due to the effect of product inhibition. As can be seen from Figures 5.44, 5.45 and 5.46, the time required to reach final steady state increases with Michaelis modulus and  $St$ . The trend in Figure 5.45 reaches the final steady state faster for the case of  $St = 0.1$  compared to that one corresponding to  $St = 10$  in which the final steady state was reached at around  $\tau = 1000$ .

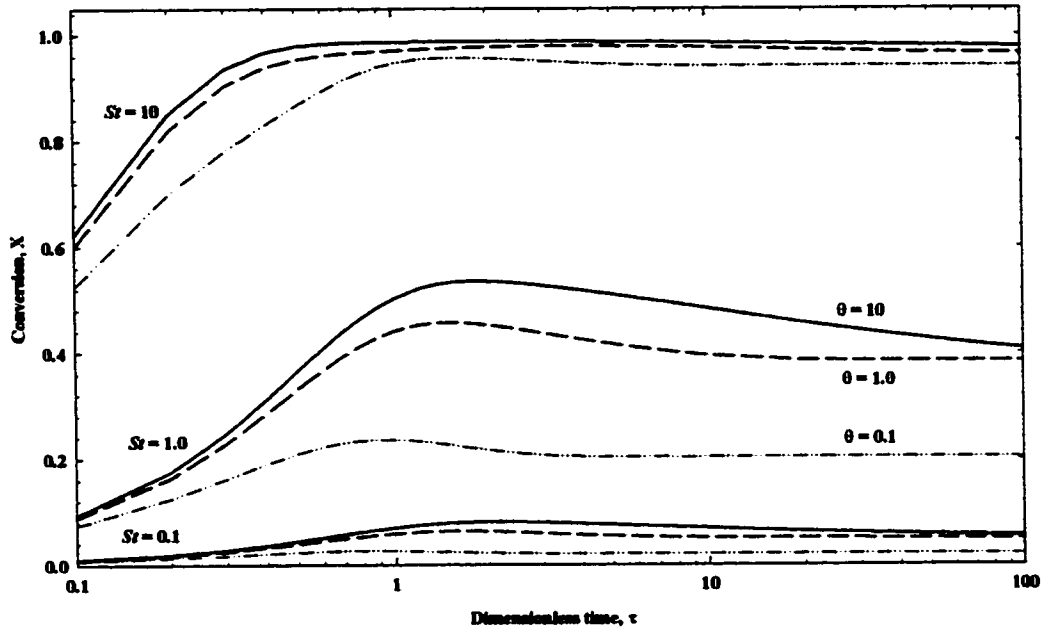


Figure 5.43: Effects of Stanton number on unsteady state conversion with  $\theta = 0.1, 1, 10, \gamma = 1.0, \phi = 2.0, Bi = 0.1$

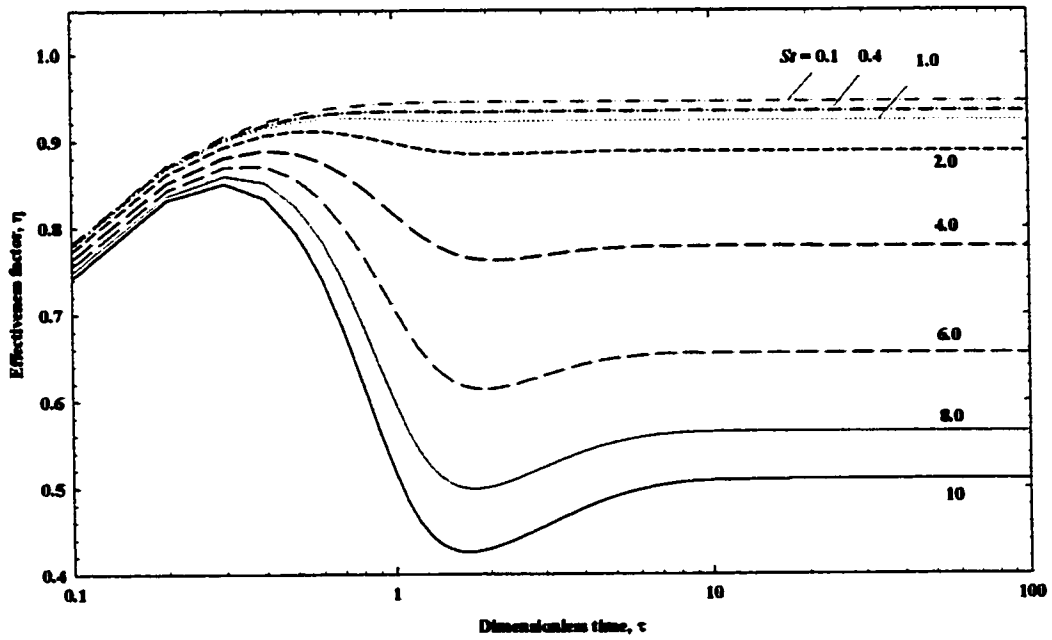
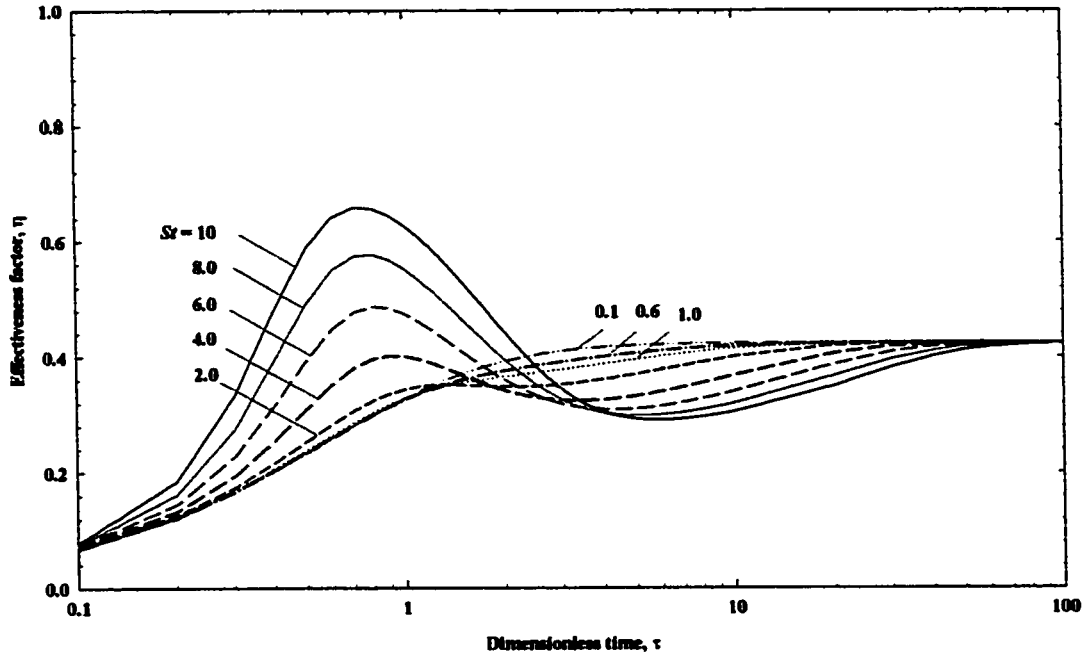
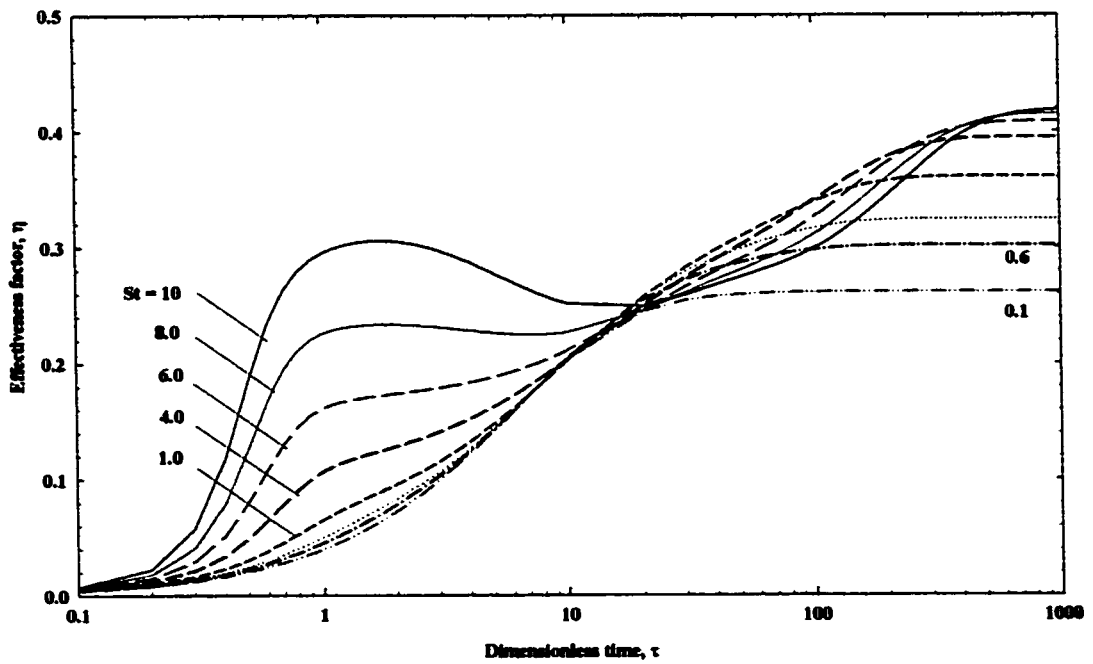


Figure 5.44: Effects of Stanton number on unsteady state effectiveness factor at  $\theta = 0.1, \gamma = 1.0, \phi = 2.0, Bi = 0.1$



**Figure 5.45: Effects of Stanton number on unsteady state effectiveness factor at  $\theta = 1.0$ ,  $\gamma = 1.0$ ,  $\phi = 2.0$ ,  $Bi = 0.1$**



**Figure 5.46: Effects of Stanton number on unsteady state effectiveness factor at  $\theta = 10.0$ ,  $\gamma = 1.0$ ,  $\phi = 2.0$ ,  $Bi = 0.1$**

#### **5.5.4 Unsteady State Effect of $St$ and $\gamma$**

Effects of  $St$  with product inhibition on unsteady state conversion were studied as shown in Figure 5.47. The trend clearly shows the effect of product inhibition for three different external mass transfer  $St = 0.1, 1$  and  $10$ . Initially the conversion increases with time in the transient period where the trend shows that the substrate conversion is independent of  $\gamma$ . Once the pseudo-steady state is reached, the effect of product inhibition reduces the substrate conversion. The higher the product inhibition the larger the difference in conversion as shown for  $\gamma = 10$ . It is found that the time to reach final steady state is longer for higher  $St$  and higher  $\gamma$ . Also, it can be seen from Figure 5.47 that the substrate conversion for Michaelis modulus kinetic (i.e.  $\gamma = 0$ ) does not include a pseudo-steady state and the final steady state is reached immediately after the transient period.

Figures 5.48 illustrates the effects of product inhibition,  $\gamma$ , on unsteady state effectiveness factor as a function of  $St$ . Figures 5.49, 5.45 and 5.50 show the effects of  $St$  on unsteady state effectiveness factor at  $\gamma = 0, 1$  and  $10$  respectively. It is shown that the transient period has similar trend regardless of product inhibition. In this period, the effectiveness factor increases with  $St$  as a result of kinetic effects. As a result of the effects of mass transfer limitations including axial dispersion, the effectiveness factor drops below the maximum effectiveness factor when the process is extremely reaction rate controlled. Pseudo-steady state exhibits an inflection point at which the effectiveness factor trend changes due to the effect of product inhibition. Figure 5.48 shows that the effectiveness factor for  $St > 4.0$  reduces after reaching pseudo-steady state period for the case of  $\theta < \gamma <$

1.0. The effectiveness factor also decreases in the initial interval of pseudo-steady state period and as time course increases. The effectiveness factor increases later in this period as a result of product inhibition.

Therefore, the effect of  $S\tau$ ,  $\theta$  and  $\gamma$  can be summarized as the following:

- The unsteady state substrate conversion trend is divided into three time periods, (i) transient, (ii) pseudo-steady state and (iii) final steady state period. In the transient period, the substrate conversion increases with time. It is found that the substrate conversion increases with  $\theta$  and  $S\tau$  regardless of  $\gamma$ .
- The pseudo-steady state starts when the substrate conversion reaches the maximum conversion at which the substrate concentration profile reach steady state inside enzyme particles. As time progress the substrate conversion decreases slightly below the maximum as a result of product inhibition,  $\theta$  and  $\gamma$ . Also, it can be seen that the product inhibition reduces the substrate conversion and its effects started in this period. Finally the conversion reaches final steady state value, increases with  $\theta$  and  $S\tau$  and decreases with increasing  $\gamma$ .
- The effectiveness factor trend in the transient period can be characterized by three processes in sequence. The process is initially substrate mass transfer controlled, enzymatic reaction and substrate and product mass transfer from microenvironment to bulk phase before pseudo-steady state is reached. Therefore in the transient period, the effectiveness factor trend depends on the Michaelis modulus only. As can be seen from Figures 5.44, 5.45, 5.46, 5.49 and 5.50, the effectiveness factor increases with  $\tau$

and it reaches a maximum where the substrate mass transfer from microenvironment to bulk phase is dominant which reduces the effectiveness factor. The entire transient period is concave downward which gives an indication to favor the effectiveness factor.

- The effectiveness factor shows an inflection point when the pseudo-steady state is reached. At this point, the effectiveness factor changes its slope due to the effects of product inhibition. The product inhibition favors the effectiveness factor and  $\gamma$  effects start when pseudo-steady state (PSS) is reached. The  $\eta$  trend is shown to have similar behavior and it depends on  $\theta$  and  $\gamma$  beside the global parameters such as  $St$ . In PSS period, initially the effectiveness factor decreases with time as a result of product mass transfer limitations from enzyme particle to bulk phase. Then, the  $\eta$  reaches a minimum value above which  $\eta$  starts to increase due to the effects of product inhibition.

Finally, the effectiveness factor increases with  $St$  as time progresses in PSS period when  $\theta \gamma > 1$  and  $\eta$  decreases with increasing  $St$  when  $\theta \gamma < 1$ .

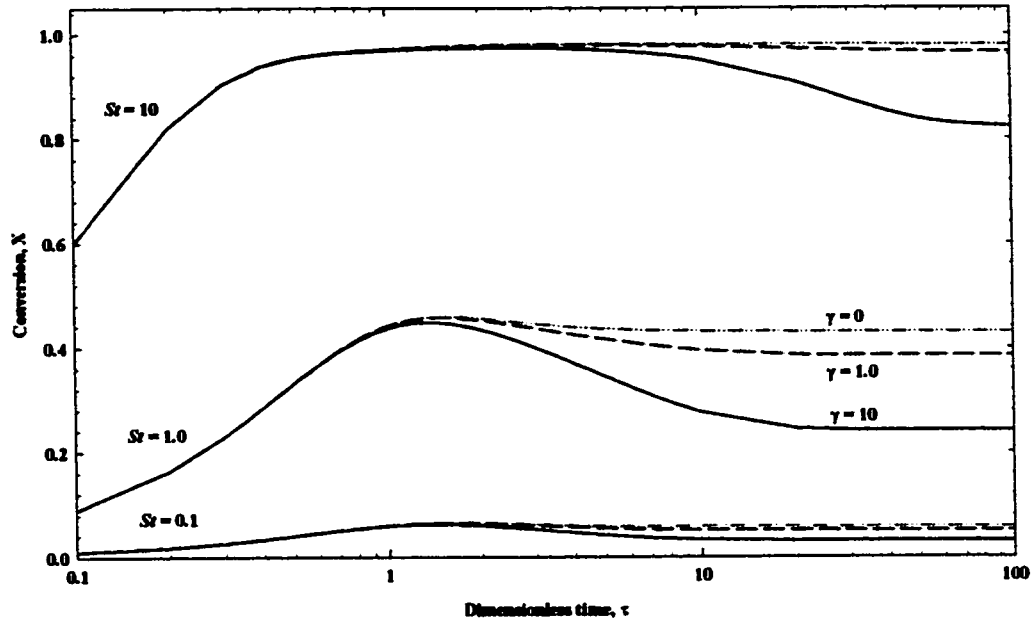


**Figure 5.47: Effects of Stanton number on unsteady substrate conversion at  $\gamma = 0.1, 1, 10, \theta = 1.0, \phi = 2.0, Bi = 0.1$**

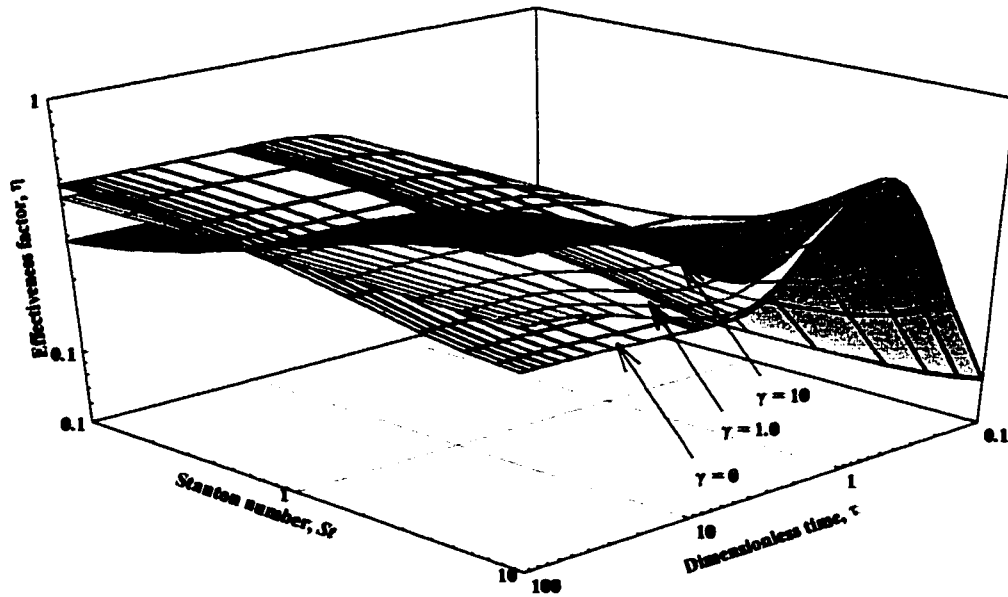


**Figure 5.48: Unsteady state effectiveness factor as a function of Stanton number for different product inhibition  $\gamma = 0, 1, 10, \theta = 1, \phi = 2.0, Bi = 0.1$**



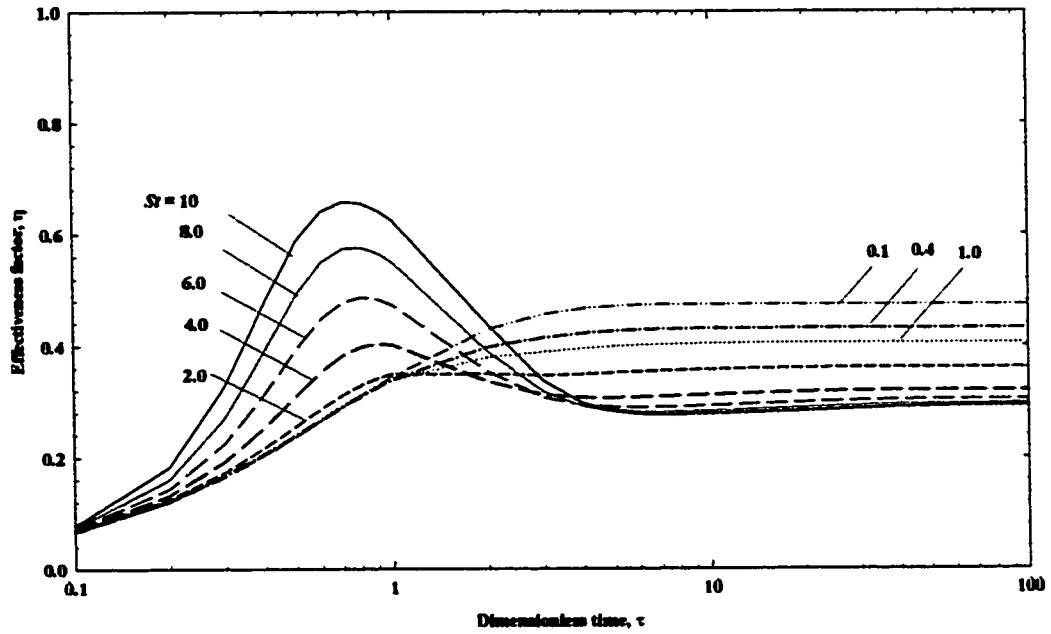


**Figure 5.49: Effects of Stanton number on unsteady state effectiveness factor at  $\gamma = 0$ ,  $\theta = 1.0$ ,  $\phi = 2.0$ ,  $Bi = 0.1$**

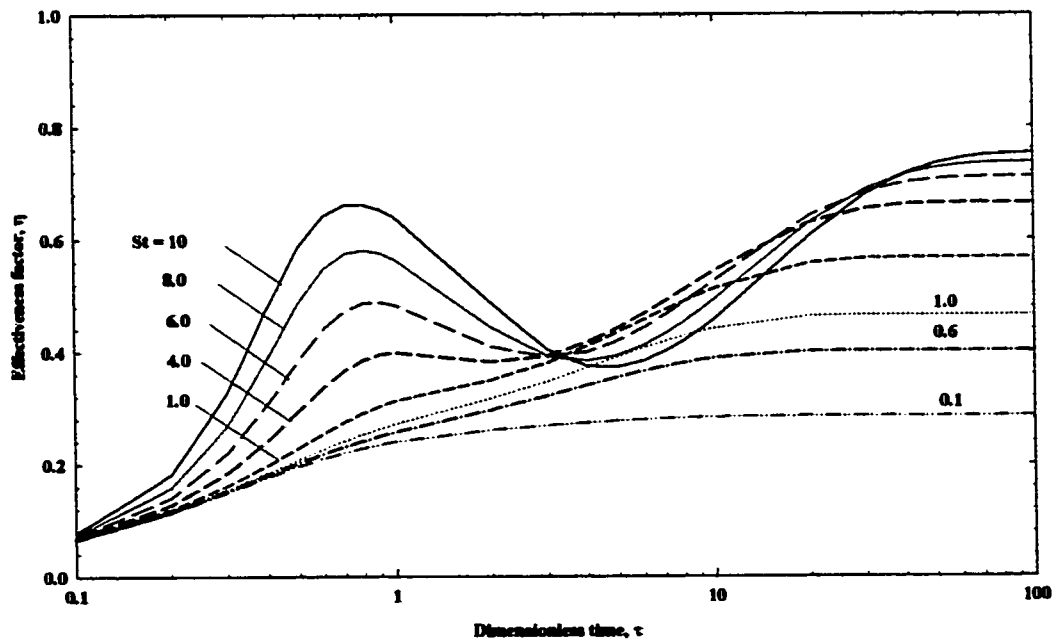


**Figure 5.50: Effects of Stanton number on unsteady state effectiveness factor at  $\gamma = 10$ ,  $\theta = 1.0$ ,  $\phi = 2.0$ ,  $Bi = 0.1$**

### 5.5.5 Unsteady State Effect of Biot number

Figure 5.51 shows the effects of  $Bi$  on unsteady state conversion at  $\theta = 1.0$ ,  $\gamma = 1.0$ ,  $\phi = 2.0$  and  $St = 1.0$ . It is shown when the process lies in the transient period, the substrate conversion increases with time courses as a result of kinetic effect. The effect of increasing  $Bi$  reduces the substrate conversion. The trend shows a maximum substrate conversion when the pseudo-steady state was reached. In PSS period the conversion decreases to reach finally the steady state conversion. From Figure 5.51 the following conclusions can be drawn:

- The PSS period is shorter when the external mass transfer is negligible (i.e.  $Bi = 10$ ). Furthermore, the PSS is propagating as the Biot number decreases when both internal and external limitations have significant effects on determination of conversion. This delay in time is due to effects of mass transfer limitations. Similarly, the PSS reaches earlier for the case of higher  $Bi$  ( $Bi = 10$ ) compared to  $Bi = 0.1$ .
- At extremely high and low  $Bi$ , the difference between substrate conversion at PSS to the conversion at final SS is small (i.e. the PSS period disappear). In mixed regime, however, appreciable difference in substrate conversion was found to be due to the effect of product inhibition.

On the other hand, the effect of  $Bi$  on unsteady state effectiveness factor was studied in Figure 5.52. It is shown that the effectiveness factor increases with  $Bi$  over the entire range of dimensionless time.

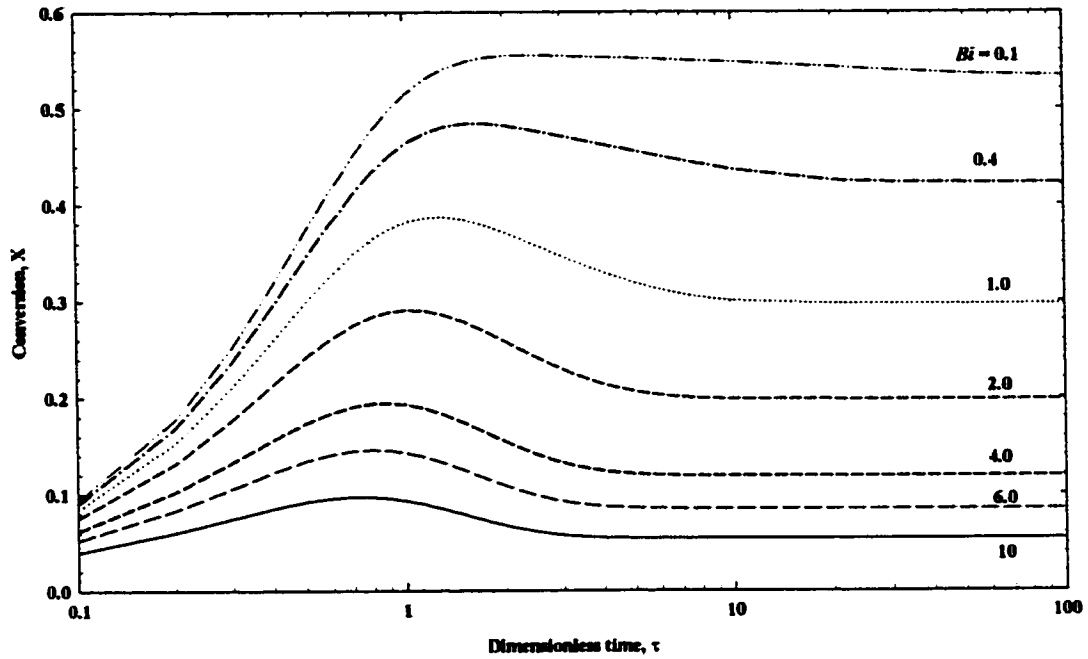


**Figure 5.51: Effects of Biot number on unsteady state reactor conversion at  $\theta = 1$ ,  $\gamma = 1.0$ ,  $\phi = 2.0$ ,  $St = 1.0$**

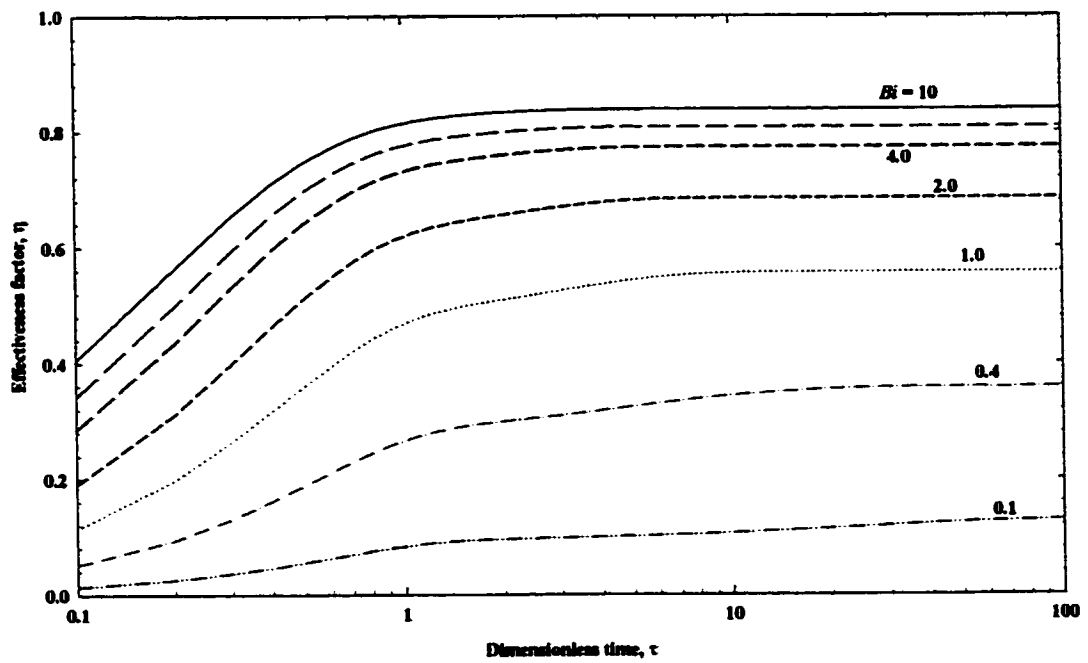
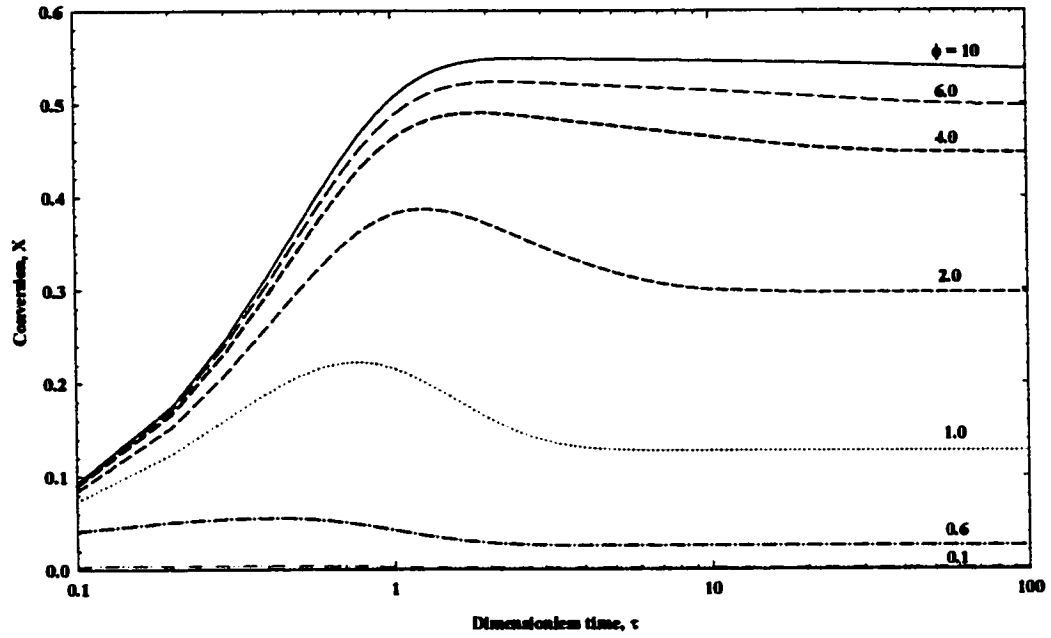


**Figure 5.52: Effects of Biot number on unsteady state effectiveness factor at  $\theta = 1$ ,  $\gamma = 1.0$ ,  $\phi = 2.0$ ,  $St = 1.0$**

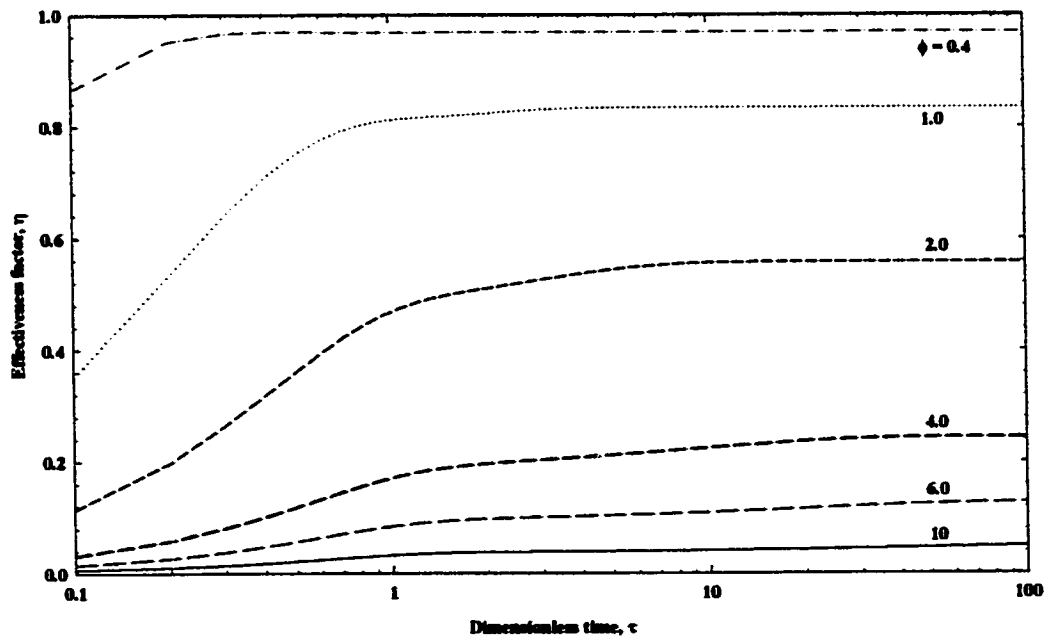
### 5.5.6 Unsteady State Effect of Thiele Modulus

Figure 5.53 presents the effects of Thiele modulus on the unsteady state conversion at  $\theta = 1$ ,  $\gamma = 1.0$ ,  $Bi = 0.1$  and  $St = 1.0$ . It can be seen that the substrate conversion increases rapidly as a result of increasing Thiele modulus in the transient period. However in the pseudo-steady state period, the substrate conversion reaches a maximum conversion. Also, increasing  $\tau$  decreases the conversion slightly to reach final steady state. When the intraparticle diffusion and reaction rate processes have significant contribution in the mixed regime, the substrate conversion will have an appreciable reduction. However, the conversion reaches final steady state faster without the PSS period when the process is either mass transfer or reaction rate controlled regime. Such as for  $\phi = 10$  and  $\phi = 0.1$  show faster response compared to  $\phi$  which lies in mixed regime.

Figure 5.54 presents the effects of Thiele modulus on unsteady state effectiveness factor at  $\theta = 1$ ,  $\gamma = 1.0$ ,  $Bi = 0.1$  and  $St = 1.0$ . The effectiveness factor increases with time in the transient and PSS periods. Also, the time to reach final steady state is longer for the mixed regime in which kinetic and mass transfer processes are dominating. However, the effectiveness factor reaches final steady state faster when the process is either kinetic or mass transfer controlled.



**Figure 5.53: Effects of Thiele modulus on unsteady state conversion at  $\theta = 1$ ,  $\gamma = 1.0$ ,  $Bi = 0.1$ ,  $St = 1.0$**



**Figure 5.54: Effects of Thiele modulus on unsteady state effectiveness factor at  $\theta = 1$ ,  $\gamma = 1.0$ ,  $Bi = 0.1$ ,  $St = 1.0$**

### 5.5.7 Unsteady State Effect of $Pe$

Figure 5.55 shows the effects of  $Pe$  on the unsteady state conversion at  $\theta = 1.0$ ,  $\gamma = 1.0$ ,  $\phi = 2.0$  and  $St = 1.0$ . The effect of axial dispersion reduces the final substrate conversion. Also, a similar effects was observed for the entire range of  $\tau$ . In the transient period, the conversion increases with time and becomes flatter as the  $Pe$  decreases. Once the PSS period has been reached, a maximum conversion was observed below which the conversion slightly decreases with time to reach ultimately the final SS. It can be noted that the PSS conversion is much higher than the final SS conversion for higher  $Pe$  (i.e.  $Pe = 100$ ). Therefore, the effect of  $Pe$  is to increase the PSS conversion at which a concentration profile has just reached the steady state inside enzyme particle.

Moreover the effects of  $Pe$  on unsteady state conversion for  $St = 0.1, 1$  and  $10$  are shown in Figure 5.57. The effect of  $Pe$  is similar to the effect of  $St$  on the effectiveness factor. Figure 5.56 shows that the increase in  $Pe$  favors the effectiveness factor in the transient period, but  $\eta$  decreases in the initial interval of PSS period. As the time progresses above the minimum  $\eta$ , the  $\eta$  shows increasing function with  $Pe$  when  $\theta \gamma > 1$ , while it shows a decreasing function with  $Pe$  when  $\theta \gamma < 1$ . However, in Figure 5.56 the final steady state effectiveness factor is independent of  $Pe$  when  $\theta \gamma = 1$ . Figures 5.58 and 5.59 show the effects of  $St$  on  $\eta$  at  $Pe = 0.01$  and  $Pe = 100$  respectively. It is shown that  $\eta$  shows increasing function with  $St$  in the transient period compared to decreasing function in PSS period. The effect of increasing  $Pe$  further increases the  $\eta$  when PSS period is

reached. Although the final steady state effectiveness factor is one for both cases, it is found that higher  $St$  and  $Pe$  show higher effectiveness factor in the PSS period.

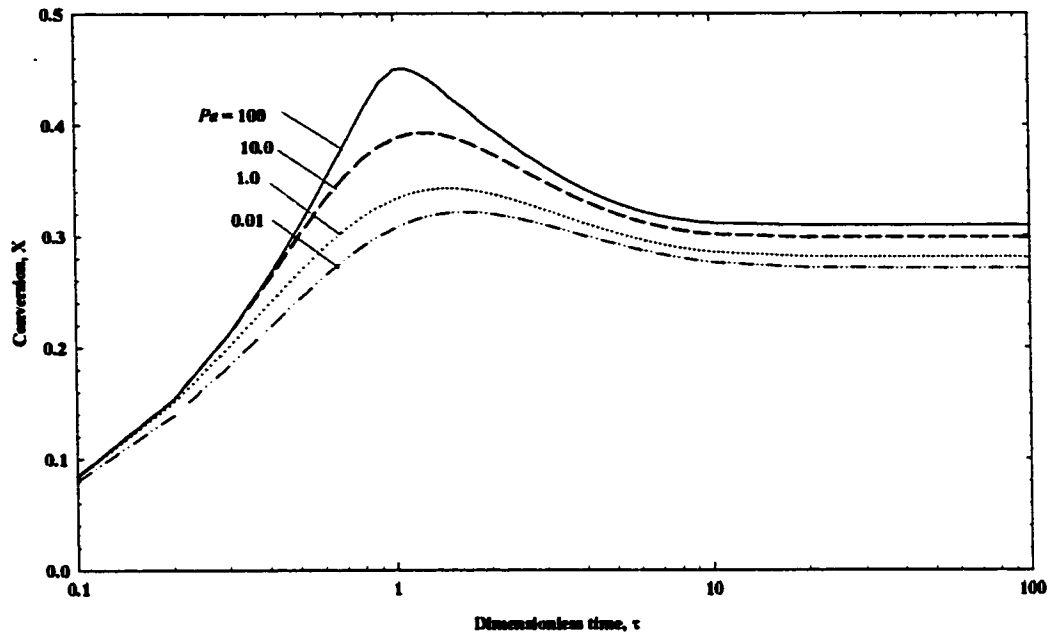


**Figure 5.55: Effects of Peclet number on unsteady state conversion at  $\theta = 1$ ,  $\gamma = 1.0$ ,  $Bi = 0.1$ ,  $\phi = 2.0$ ,  $St = 1.0$**

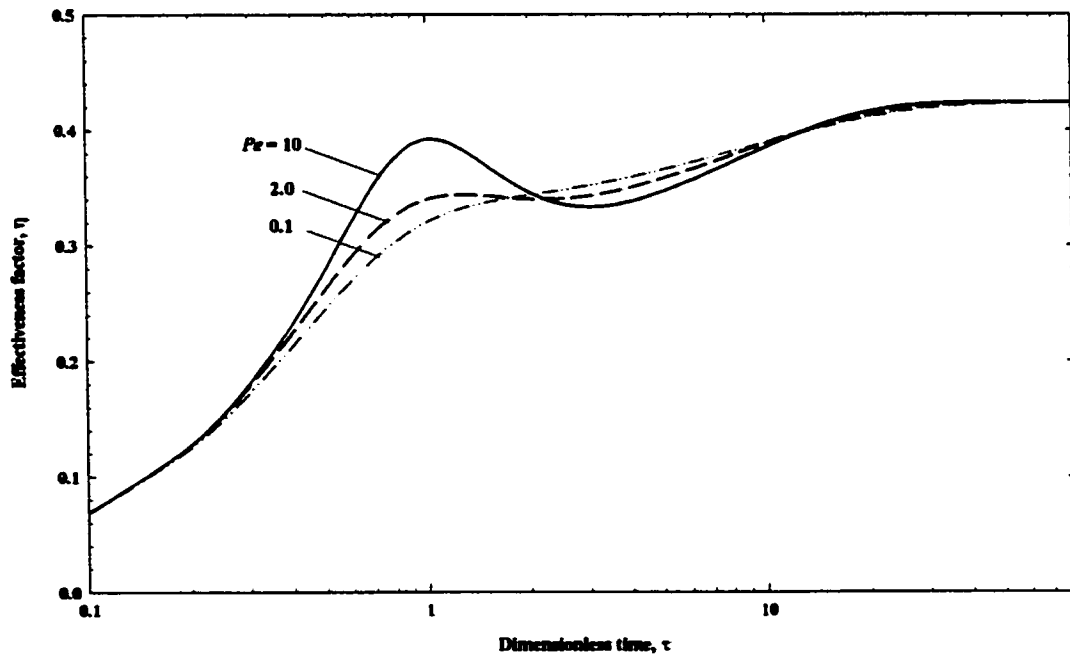


**Figure 5.56: Effects of Peclet number on unsteady state effectiveness factor at  $\theta = 1$ ,  $\gamma = 1.0$ ,  $Bi = 0.1$ ,  $\phi = 2.0$ ,  $St = 1.0$**



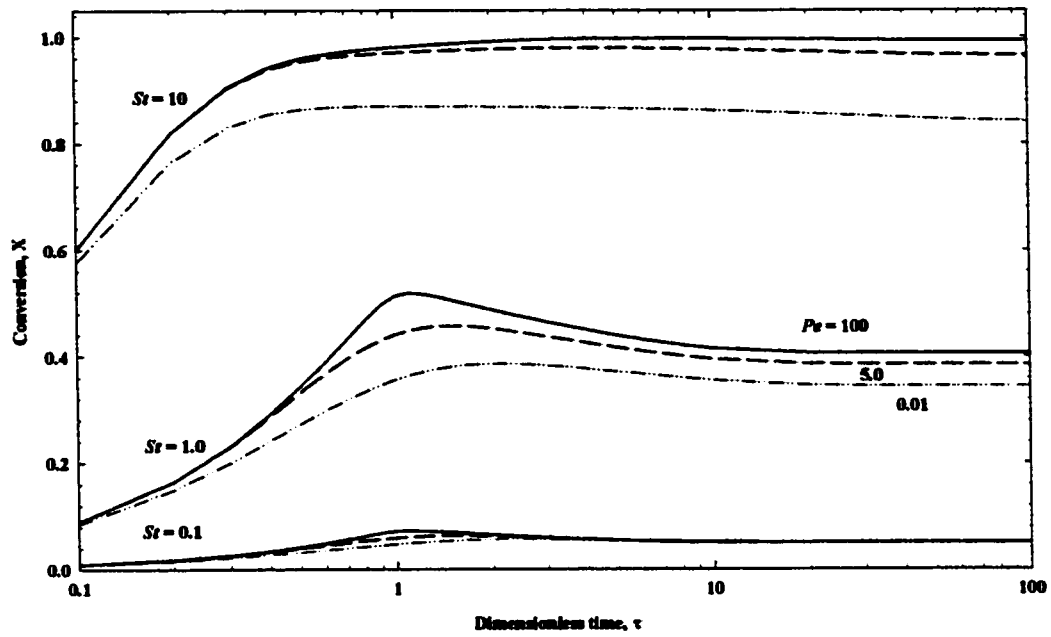


**Figure 5.57: Effects of Peclet number on unsteady substrate conversion for  $St = 0.1, 1, 10; \gamma = 1, \theta = 1.0, \phi = 2.0, Bi = 0.1$**

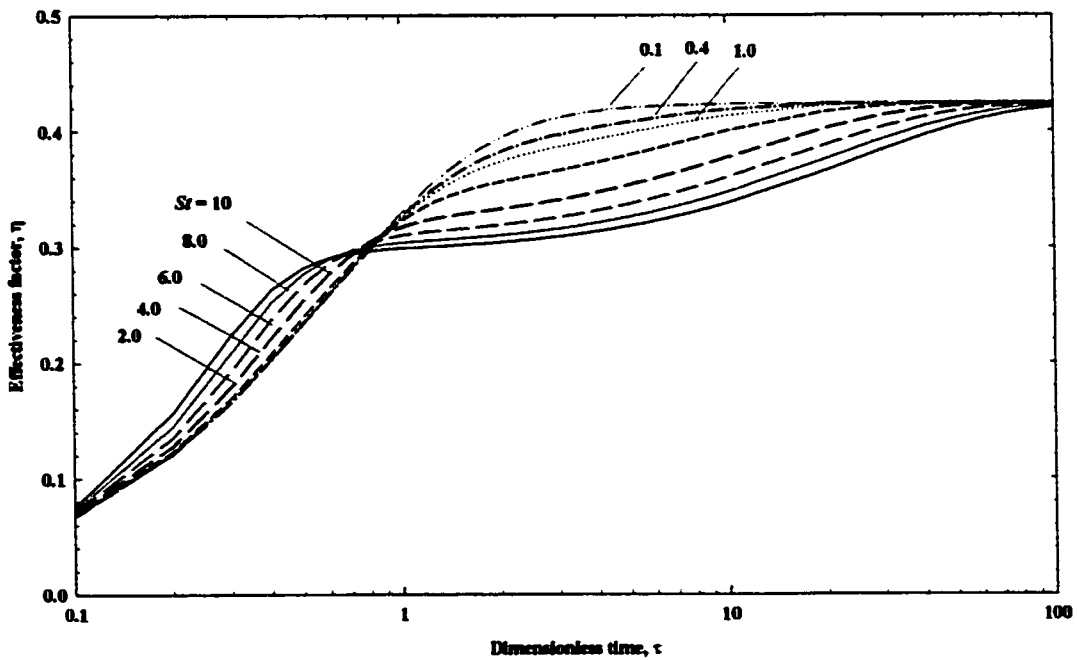


**Figure 5.58: Effects of Stanton number on unsteady state effectiveness factor at  $\theta = 1.0, \gamma = 1.0, \phi = 2.0, Bi = 0.1, Pe = 0.01$**

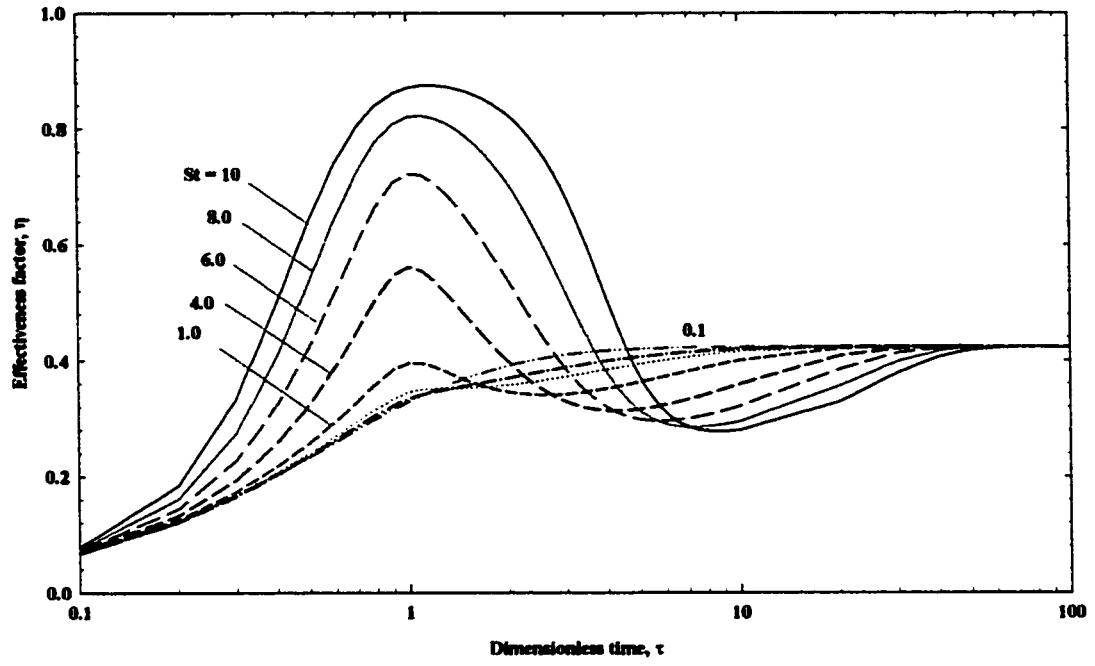


**Figure 5.59: Effects of Stanton number on unsteady state effectiveness factor at  $\theta = 1.0, \gamma = 1.0, \phi = 2.0, Bi = 0.1, Pe = 100$**

# 6

---

## CONCLUSIONS AND RECOMMENDATIONS

### 6.1 Conclusions

A mathematical model for a packed bed immobilized enzyme reactor has been developed considering Michaelis – Menten kinetics with competitive product inhibition. The effects of intraparticle diffusion, external mass transfer, axial dispersion and kinetic parameters have been taken into consideration in the model. The relevant equations were solved by the method of orthogonal collocation on finite elements (OCFE) and Galerkin's method. The performance of packed bed immobilized enzyme reactor has been investigated parametrically for various operational parameters. The effects of  $\theta$ ,  $\gamma$ ,  $\phi$ ,  $St$ ,  $Bi$  and  $Pe$  have been identified quantitatively on the substrate conversion and internal effectiveness factor.

The following results were drawn from simulation results:

1. Intraparticle diffusion resistance, external mass transfer resistances and axial dispersion were shown to reduce internal effectiveness factor.
2. Product inhibition was shown to reduce substrate conversion, and to decrease effectiveness factor when  $\beta_s > \beta_{x_0}$ , however, it increases effectiveness factor when  $\beta_s < \beta_{x_0}$ . The effectiveness factor is found to be independent of product inhibition at cross – over point at which  $\beta_{x_0}$  is defined, where  $\beta_{x_0}$  is a function of  $St$ ,  $Bi$ ,  $\theta$  and  $\phi$ .
3. Effect of Stanton number was shown to reduce the internal effectiveness factor when  $\theta \gamma < 1$  (i.e.  $K_m < K_p$ ), but it favors the effectiveness factor when  $\theta \gamma > 1$ . Due to these opposite trends, the effectiveness factor has been found to be independent of  $St$  at  $\theta \gamma = 1$ .
4. Similarly, the effectiveness factor shows increasing function with  $Pe$  when  $\theta \gamma < 1$  otherwise it shows a decreasing function. This takes place when  $\beta_s > \beta_{x_0}$ . However, the effectiveness factor is independent of  $Pe$  when  $\theta \gamma = 1$  and  $\beta_s \leq \beta_{x_0}$ . On other hand, the substrate conversion increases with  $Pe$  when  $\beta_s > \beta_{x_0}$ , yet, it is independent of  $Pe$  otherwise.
5. The intraparticle diffusion resistances, external mass transfer and axial dispersion were shown to reduce time passage to reach final steady state when the process is in the mixed kinetic regime by exhibiting an intermediate pseudo-steady state period (PSS) between transient and final steady state periods. The PSS period diminishes when the process is either kinetic or mass transfer controlled regime.

## **6.2 Recommendations**

The following recommendations are suggested for future studies and continuation to this work,

- (1) It is recommended to explore further the unsteady state behavior with different initial conditions and with different reactor models.
- (2) Study the effects of enzyme deactivation with practical case study to determine optimal temperature.
- (3) The kinetics of enzymatic reaction should to be generalized to include substrate inhibited reaction. Also to explore the existence of multiple steady state and to study unsteady state for such conditions.
- (4) Setup experimental procedure on continuous or batch immobilized enzyme reactor used to validate the simulation results and to match the predicted transient and / or steady state conversion for various operating conditions. Also, this experimental setup can be used to obtain uncertain parameters (i.e., parameters that are difficult to measure or to estimate such as kinetic and transport parameters) by minimizing the difference between observed and simulated conversion.

## **NOMENCLATURE**

$a$	External surface of support per unit volume of reactor
$A, B$	The first and second derivative matrices of Semi-Legendre polynomial in radial coordinate of immobilized enzyme particle.
$A_z, B_z$	The first and second derivative matrices of Semi-Legendre polynomial in axial coordinate of the reactor.
$C_P$	Product concentration in an immobilized enzyme support particle
$\langle C_P \rangle$	Average product concentration in an immobilized enzyme support particle
$C_{Pb}$	Product concentration in the bulk liquid (reactor phase)
$C_{Pb0}, C_{P0}$	Product concentration at reactor inlet
$C_S$	Substrate concentration in an immobilized enzyme support particle
$\langle C_S \rangle$	Average substrate concentration in an immobilized enzyme support particle
$C_{Sb}$	Substrate concentration in the bulk liquid
$C_{Sb0}, C_{S0}$	Substrate concentration at reactor inlet
$D_{Sp}, D_{Pp}$	Effective substrate and product diffusivity in an immobilized enzyme support particle
$D_{Sz}, D_{Pz}$	Effective substrate and product axial dispersion coefficient
$E_0$	Initial $\beta$ -galactosidase (lactase) concentration (g/l)
$K_e$	Reaction equilibrium constant
$K_L$	Mass transfer coefficient

$K_{La}$	Volumetric mass transfer coefficient
$K_{LS}, K_{LP}$	Mass transfer coefficient in substrate and product side respectively.
$K_m$	Intrinsic Michaelis – Menten constant
$K_P$	Product inhibition constant
$L$	Length of the reactor
$M$	Number of internal collocation points in radial coordinate within an element
$N$	Number of internal collocation points in axial coordinate
$NE$	Number of elements in the radial coordinate of an immobilized enzyme particle
$r$	Radial coordinate of distance in an immobilized enzyme support particle
$\tilde{R}_b$	Dimensionless reaction rate at the surface of the spherical particles
$R_P$	Local product production rate per unit of catalytic particle volume
$\langle R_P \rangle$	Average product production rate
$R_S$	Local substrate consumption rate per unit of catalytic particle volume
$\langle R_S \rangle$	Average substrate consumption rate
$t$	Time inside reactor
$u$	Superfacial fluid phase velocity inside the reactor
$v_{max}$	Maximum reaction rate per unit of catalytic particle volume
$x_1, x_2$	Collocation points in radial and axial coordinates respectively
$x, z$	Reactor radial and axial coordinate
$W$	Quadrature weight matrix of semi-Legendre polynomial

### **Dimensionless variables**

$Bi$	Biot number
$Da$	Damkohler number
$K_E$	Inverse of the equilibrium constant
$P$	Dimensionless product concentration in an immobilized enzyme support particle
$\langle P \rangle$	Dimensionless average product concentration in an immobilized enzyme support particle
$P_b$	Dimensionless product concentration in the bulk liquid
$P_{b0}$	Dimensionless product concentration at the reactor inlet
$Pe$	Peclet number
$\tilde{R}$	Dimensionless reaction rate in an immobilized enzyme support particle
$S$	Dimensionless substrate concentration in an immobilized enzyme support particle
$\langle S \rangle$	Dimensionless average substrate concentration in an immobilized enzyme support particle
$S_b$	Dimensionless substrate concentration in bulk liquid
$S_{b0}$	Dimensionless substrate concentration at reactor inlet
$St$	Stanton number
$X$	Fractional substrate conversion
$Y$	Reactor yield



### **Creek Symbols**

$\alpha_s, \alpha_p$	Effective diffusivity ratio of substrate and product in axial and interparticle respectively
$\beta_s$	Dimensionless residence modulus
$\varepsilon$	Reactor voidage
$\phi$	Thiele modulus
$\theta$	Dimensionless Michaelis – Menten constant
$\gamma$	Dimensionless inhibition modulus
$\eta$	Internal effectiveness factor
$\eta_E$	External effectiveness factor
$\tau$	Dimensionless time
$\xi$	Dimensionless radial coordinate
$\zeta$	Dimensionless axial coordinate
$\Delta$	Defined by equation (3.31c)

## **REFERENCES**

---

1. Abu-Reesh, I. M., "Predicting the performance of immobilized enzyme reactors using reversible Michaelis—Menten kinetics ", *Bioprocess Eng.*, **17**, 1997, 131 – 137
2. Adomaitis, R. A. & Lin, Y.-h., "A technique for accurate collocation residual calculations ", *Chem. Eng. J.*, **71**, 1998, 127 – 134.
3. Adomaitis, R. A. "Objects for MWR ", *Computers & Chem. Eng.*, **26** (in press), 2002, 981-998.
4. Adomaitis, R. A., "Spectral Filtering for Improved Performance of Collocation Discretization Methods ", *Computers & Chem. Eng.*, **25**, 2001, 1621 – 1632.
5. Adomaitis, R. A. and Y. -h. Lin, "A Collocation / Quadrature-Based Sturm-Liouville Problem Solver ", *Applied Math. and Computation*, **110**, 2000, 205 – 223.
6. Adomaitis, R. A. and Y. -h. Lin, "A Technique for Accurate Collocation Residual Calculations ", *Chem. Eng. J.*, **71**, 1998, 127 – 134.
7. Bailey, J. E. and Ollis, D. E., *Biochemical engineering fundamentals*, 2<sup>nd</sup> ed., New York, McGraw-Hill.
8. Bakken, A. P., Hill, C. G., Jr. and Amundson, C. H., " Hydrolysis of Lactose in Skim Milk by Immobilized  $\beta$ -Galactosidase in a spiral flow reactor ", *Biotechnol. Bioeng.*, **33**, 1984, 1249 – 1257.

9. Baratti, R., Gavrilids, A., Morbidelli, M. and Varma, A., "Optimization of a nonisothermal nonadiabatic fixed bed reactor using direc-type silver catalysts for ethylene epoxidation", *Chem. Eng. Sci.*, **49**, 1994, 1936 – 48.
10. Belfort, G., "Membranes and Bioreactors: A Technical Challenge in Biotechnology", *Biotechnol. Bioeng.*, **33**, 1989, 1047 – 1066.
11. Blanch, H. W., Clark, D. S., *Biochemical Engineering*, Marcel Dekker, Inc., New York, 1997
12. Bódalo, A., Gómez, E., Gomez, J. L., Bastida, J. and Maximo, M. F., "Fluidized bed reactors operating with immobilized enzyme systems: Design model and its experimental verification", *Enzyme Microb. Technol.*, **17**, 1995, 915 – 922.
13. Bódalo, A., Gómez, E., Gomez, J. L., Bastida , J., Maximo, M. F. and Dia, F. "A Comparison of Different Methods of  $\beta$ -galactosidase Immobilization", *Process Biochem.*, **26**, 1991, 349 – 353.
14. Bódalo, A., Gomez, J. L., Gómez, E., Bastida , J., Iborra, J. L. and Manjon, A., "Analysis of Diffusion Effects of Immobilized Enzymes on Porous supports with Reversible Michaelis – Menten Kinetics", *Enzyme Microb. Technol.*, **8**, 1986, 433 – 438.
15. Bódalo, A., Gomez, J. L., Gómez, E., Bastida, J. and Martinez, E., "Transient Stirred-Tank Reactors Operating with Immobilized Enzyme Systems: Analysis and Simulation Models and Their Experimental Checking", *Biotechnol. Prog.*, **9**, 1993, 166 – 173.
16. Bury, D. and Jelen, P., "Lactose hydrolysis using a disrupted dairy culture: evaluation of technical and economical feasibility ", *Canadian Agricultural Engineering*, **42** (2), 2000, 75 – 80.
17. Carey, G. F. and Finlayson, B. A., "Orthogonal collocation on finite elements", *Chem. Eng. Sci.*, **30**, 1975, 587–596.

18. Carrara, C. R., Mammarella, E. J. and Rubiolo, A. C.; "Prediction of the fixed – bed reactor behavior using dispersion and plug flow models with different kinetics for immobilized enzyme", *Chem. Eng. J.*, **4096** (in press), 2002, 1-7.
19. Carrara, C. R., and Rubiolo, A. C., "A method for evaluating lactose hydrolysis in a fixed bed reactor with  $\beta$ -Galactosidase immobilized on chitson", *Chem. Eng. J.*, **65**, 1997, 93 – 98.
20. Carrara, C. R. and Rubiolo, A. C., "Determination of kinetics parameters for Free and immobilized  $\beta$ -galactosidase", *Process Biochemistry*, **31**, 1995, 243 – 248.
21. Chang, H. -Y. and R. A. Adomaitis, "Analysis of Heat Transfer in a Chemical Vapor Deposition Reactor: An Eigenfunction Expansion Solution Approach," *Int. J. Heat Fluid Flow*, **20**, 1999, 74-83.
22. Ching, C.B. and Chu, K.H., "Modeling of a fixed bed and a fluidized bed immobilized enzyme reactor" , *Appl. Microbiol. Biotechnol.*, **29**, 1988, 316 – 322
23. Ching, C.B. and Ho, Y.Y., "Flow dynamics of immobilized enzyme reactors", *Appl. Microbiol. Biotechnol.*, **20**, 1984, 303 – 309
24. Clark, D. S. and Bailey, J. E., "Deactivation Kinetics of Immobilized  $\alpha$ -Chymotrypsin Subpopulations", *Biotechnol. Bioeng.*, **26**, 1984, 1090.
25. Clark, D. S. and Bailey, J. E., "Structure-Function Relationships in Immobilized Chymotrypsin Catalysis", *Biotechnol. Bioeng.*, **25**, 1983, 1027.
26. Clark, D. S., Bailey, J. E. and Do, D. D., "A Mathematical Model for Restricted Diffusion Effects on Macromolecule Impregnation in Porous Supports", *Biotechnol. Bioeng.*, **27**, 1985, 208
27. Danckwerts, P. V., "Continuous flow systems, Distribution of residence times", *Chem. Eng. Sci.*, **2**, 1953, 1 – 18.

28. Dennis, K.E., Clark, D. S., Bailey, J. E., Cho, Y. K. and Park, Y. H., "Immobilization of Enzymes in Porous Supports: Effects of Support-Enzyme Solution Contacting", *Biotechnol. Bioeng.*, **26**, 1984, 892.
29. Do, D. D., Clark, D. S., and Bailey, J. E., "Modeling Enzyme Immobilization in Porous Solid Supports", *Biotechnol. Bioeng.*, **24**, 1982, 1527.
30. Figueroa, A. R. C., Jose, T. H. and Maritza, C. A., "Flow optimization in a class of enzymatic plug-flow reactor ", *Biotechnol. Prog.*, **13**, 1997, 109-112.
31. Finlayson, B. A., *Nonlinear Analysis in Chemical Engineering*, New York: McGraw – Hill, 1980.
32. Gardini, L., Servida, A., Morbidelli, M and Carra, S., " Use of orthogonal collocation on finite elements with moving boundaries for fixed bed catalytic reactor simulation", *Computers & Chem. Eng.*, **9**, 1985,1 – 17.
33. Guertin, E. W., Sorensen, J. P. and Stewart, W. E., "Exponential collocation of stiff reactor model", *Computers & Chem. Eng.*, **1**, 1977, 197 – 203.
34. Hassan, M. M. and Beg, S. A., "Theoretical analysis of a packed bed biological reactor for various reaction kinetics", *Chem. Eng. J.*, **36**, 1987, 15 – 27.
35. Hassan, M. M., Atiqullah, M., Beg, S. A. and Chowdhury, M. H. M., "Analysis of nonisothermal tubular reactor packed with immobilized enzyme systems", *Biochem. Eng. J.*, **58**, 1995, 275 – 283.
36. Hassan, M. M., Atiqullah, M., Beg, S. A. and Chowdhury, M. H. M., "Effects of Enzyme Microcapsule Shape on the Performance of a Nonisothermal Packed-Bed Tubular Reactor ", *J. Chem. Technol.*, **66**, 1996, 41 – 55.
37. Illanes, A., Altamirano, C., Aillapan, A., Tomasello, G. and Zuniga, M.E., "Packed-bed reactor performance with immobilized lactose under thermal inactivation", *Enzyme Microb. Technol.*, **23**, 1998, 3 – 9.

38. Jayaraman, V. K., "The solution of Hollow Fiber Bioreactor Design Equations", *Biotechnol. Prog.*, **8**, 1992, 462 – 464.
39. Jayaraman, V. K., "Solution of hollow fiber bioreactor design equations: the case of power – low fluids", *Chem. Eng. J.*, **55**, 1994, B73 – B75.
40. Jayaraman, V. K. and Kulkarni, B.D., " An Efficient Algorithm for Solving Hollow Fiber Bioreactor Design Equations", *Chem. Eng. J.*, **65**, 1997, 77 – 80.
41. Jung, H. J. and Bauer, W., "Determination of process parameters and modeling of lipase – catalyzed transesterification in a fixed bed reactor ", *Chem. Eng. Technol.*, **15**, 1992, 341 – 348.
42. Kaczmarski, K., "Use of orthogonal collocation on finite elements with moving boundaries in the simulation of non-linear multicomponent chromatography: Influence of fluid velocity variation on retention time in LL and HLPC", *Computers & Chem. Eng.*, **20**, 1997, 49 – 64.
43. Kaczmarski, K., Mazzotti, M., Storti, G., and Morbidelli, M., "Modeling fixed-bed adsorption columns through orthogonal collocations on moving finite elements", *Computers Chem. Eng.*, **21**, 1997, 641 – 660.
44. Kelsey, J., Pillarella, M. R. and Zydney, A. L., " Theoretical Analysis of Convective Flow Profile in a Hollow fiber Membrane Bioreactor", *Chem. Eng. Sci.*, **45**, 1990, 3211 – 3220
45. Kill, S., Bhatia, S. K. and Dam-Johanson, K., "Solution of transient problems with steep gradients: Novel front-tracking strategy", *Chem. Eng. Sci.*, **50**, 1995, 2793 – 9799.
46. Kim, S. S. and Cooney, D. O., "An improved Theoretical Model for Hollow fiber Enzymatic Reactor", *Chem. Eng. Sci.*, **31**, 1976, 289 – 294.
47. Kissler, T., Oertzen, G. A. and Bauer, W., "Modeling of a fluidized bed bioreactor for immobilized enzyme (part 1)", *Chem. Eng. Technol.*, **13**, 1990, 20 – 6.

48. Kleinstreuer, C. and Agarwal, S. S., "Analysis and Simulation of Hollow fiber Bioreactor Dynamics", *Biotechnol. Bioeng.*, **3**, 1987, 80 – 89.
49. Kobayashi, T. and Moo-Young, M., "Backmixing and mass transfer in the design of immobilized -enzyme reactors", *Biotechnol. Bioeng.*, **13**, 1971, 893 – 910.
50. Kumar, R. A. and Modak, J. M., "Transient analysis of mammalian cell growth in hollow fiber bioreactor", *Chem. Eng. Sci.*, **52**, 1997, 1845 – 186.
51. Lee, T. T., Newell, R. B. and Wang, F. Y., "Dynamic modeling and simulation of activated sludge process using orthogonal collocation approach ", *Water Research*, **33**, 1999, 73 – 86.
52. Lee, T. T., Wang, F. Y. and Newell, R. B., "Dynamic simulation of bioreactor systems using orthogonal collocation on finite elements", *Computers & Chem. Eng.*, **23**, 1999, 1247 – 1262.
53. Lin, S. H., "Optimal feed temperature for immobilized enzyme packed bed reactor ", *J. Chem. Tech. Biotechnol.*, **50**, 1991, 17 – 26.
54. Lin, S. H., "The effects of mass transfer resistances on encapsulated enzymatic reaction systems ", *Chem. Eng. J.*, **17**, 1979, 55 – 61.
55. Lin, Yi-hung, Chang, H.-Y. and Adomaitis, R. A., " MWRtools: a library for weighted residual method calculations", *Computers & Chem. Eng.*, **23**, 1999, 1041 – 1061.
56. Lortie, R. and Thomas, D., "Heterogeneous One- Dimensional Model for Fixed Bed Enzyme Reactors ", *Biotechnol. Bioeng.*, 1986, 1256 – 1260.
57. Lortie, R., "Evaluation of the performance of immobilized enzyme reactors with Michaelis-Menten kinetics ", *J. Chem. Technol. Biotechnol.*, **60**, 1994, 189 – 193.
58. Lortie, R. and Pelletier, D., "Comparison between dispersion and plug flow models for fixed-bed enzyme reactors ", *AIChE J.*, **38**, 1992, 1477 – 80.

59. Ma, Z. and Guiochon, G., "Application of orthogonal collocation on finite element in the simulation of non-linear chromatography", *Computers & Chem. Eng.*, **15**, 1991, 415 – 426.
60. Manjon, A., Iborra, J. L., Gomez, J. L., Gómez, E., Bastida, J. and Bódalo, A., "Evaluation of Effectiveness factor Along Immobilized Enzyme Fixed-Bed Reactors: Design of a Reactor with Naringinase Covalently Immobilized into Glycophase Coated Porous Glass", *Biotechnol. Bioeng.*, **30**, 1987, 491 – 497.
61. Marrazzo, W. N. and McCoy, B. J., "Enzyme immobilized in a packed bed reactor: kinetic parameters and mass transfer effects", *Biotechnol. Bioeng.*, **23**, 1981, 1237 – 1254.
62. Miyakawa, H., Nagasue, H. and Shiraishi, F., "A highly accurate numerical method for calculating apparent kinetics parameters of immobilized enzyme reactions: 1. Theory" *Biochem. Eng. J.*, **3**, 1999, 91 – 101.
63. Miyakawa, H., Nagasue, H. and Shiraishi, F., "A highly accurate numerical method for calculating apparent kinetics parameters of immobilized enzyme reactions: 2. Accuracies of calculated values", *Biochem. Eng. J.*, **3**, 1999, 103 – 111.
64. Papayannakos, N., Markas, G. and Kekos, D., "Studies on modeling and simulation of lactose hydrolysis by free and immobilized  $\beta$ -galactosidase from *Aspergillus niger*", *Chem. Eng. J.*, **52**, 1993, B1-B12.
65. Park, Y.H., Han, M.H. and Rhee, H.K., "Effect of external mass transfer in a packed bed reactor system for a reversible enzyme reaction", *J. Chem. Technol. Biotechnol.*, **34 B**, 1984, 57 – 69.
66. Paunovic, R. N., Zavargo, Z. Z. and Tekic, M. N., "Analysis of a model of Hollow – Fiber Bioreactor Wastewater Treatment", *Chem. Eng. Sci.*, **48**, 1993, 1069 – 1075.
67. Petzelbauer, I., Nidetzky, B., Haltrich, D. and Kulbe, K., "Development of an Ultra-High-Temperature process for the Enzymatic hydrolysis of lactose. I. The properties of two thermostable  $\beta$ -galactosidase", *Biotechnol. Bioeng.*, **64 (3)**, 1999, 322 – 332.



68. Rice, R. G. and Do, D. D., *Applied Mathematics and Modeling for Chemical Engineers*, John Wiley & Sons, 1995.
69. Santos, A., Ladero, M. and Garcia-Ochoa, F., "Kinetic modeling of lactose hydrolysis by a  $\beta$ -galactosidase from *Kluyveromyces fragilis*", *Enzyme Microb. Technol.*, **22**, 1998, 558 – 567.
70. Shiraishi, F. and Fujiwara, S., "An efficient Method for solving Two – point Boundary Value Problems with extremely high accuracy", *J. Chem. Eng. Japan*, **29**, 1996, 88 – 94.
71. Shiraishi, F., Hasegawa, T. and Nagasue, H., "Numerical Solution of Two-Point Boundary Value Problem by combined Taylor Series Method with a Technique for Rapidly Selecting Suitable Step Sizes", *J. Chem. Eng. Japan*, **28**, 1995, 306 – 315.
72. Shiraishi, F., Hasegawa, T., Kasai, S., Makishita, N. and Miyakawa, H., "Characteristic of Apparent Kinetics parameters in a Packed Bed Immobilized Enzyme Reactor ", *Chem. Eng. Sci.*, **51**, 1996, 2847 – 2852.
73. Shiraishi, F., Miyakawa, H., Hasegawa, T. and Kasai, S., " A computational Method for Determination of the mass transfer coefficient in Packed Bed Immobilized Enzyme Reactors ", *J. Chem. Technol.*, **66**, 1996, 405 – 413.
74. Shyan, R., Davidsson, B. and Vieth, W. R., "Mass Transfer and Biochemical Reaction in Enzyme Membrane Reactor System 2 Expanded Analysis for single Enzyme System", *Chem. Eng. Sci.*, **30**, 1975, 669 – 678
75. Sorensen, J. P., Guertin, E. W. and Stewart, W. E., "Computational models for cylindrical catalyst particles", *AICHE J.*, **19**, 1973, 969 – 975.
76. Suwondo, E., Pibouleau, L., Domenech, S. and Riba, J. P., "Simulation via orthogonal collocation on finite element of a chromatographic column with nonlinear isotherm", *Chem. Eng. Comm.*, **102**, 1991, 161–188.

77. Tomaska, M., Stredansky, M., Tomaskova, A. and Sturdik, E., "Lactose hydrolysis in aqueous two-phase system by whole cell  $\beta$ -galactosidase of *Kluyveromyces marxianus*", *Bioprocess Eng.*, **12**, 1995, 17 – 20
78. Vasic-Racki, D., Pavlovic, N., Cizmek, S., Drazic, M. and Husadzic, B., "Development of reactor model for glucose isomerization catalyzed by whole-cell immobilized glucose isomerase", *Bioprocess Eng.*, **7**, 1991, 183 – 187
79. Villadsen, J. and Michelsen, M. L., *Solution of differential equation by polynomial approximation*, International Series in physical and Chemical Engineering Series, Englewood Cliffs, NJ: Prentice – Hall, 1978.
80. Villadsen, J. V. and Stewart, W. E., "Solution of boundary-value problems by orthogonal collocation", *Chem. Eng. Sci.*, **22**, 1967, 1483 – 1501.
81. Waterland, L. R., Michaels, A. S., Roberson, C. R., "A Theoretical Model for Enzymatic Catalysis using Asymmetric Hollow Fiber Membrane", *AIChE J.*, **20**, 1974, 50 – 60.
82. Willaert, R., An Smerts and De Vuyest, Luc, "Mass transfer limitation in diffusion – limited isotropic Hollow fiber bioreactors", *Biotech. Techn.*, **13**, 1999, 317 – 328.
83. Xiu, G.-H., Jiang, L. and Ping, Li, "Mass – transfer limitations for immobilized enzyme-catalyzed kinetic resolution of Racemate in a fixed-bed reactor", *Biotech. Bioeng.*, **74**, 2001, 29-39.
84. Yang, S. T. and Okos, M. R., "A new graphical method for determining parameters in Michaelis – Menten – type kinetics for enzymatic lactose hydrolysis ", *Biotechnol. Bioeng.*, **34**, 1989, 763 - 773.

## **VITA**

---

<b>Name</b>	Ali Ebrahim AL-Muftah
<b>Nationality</b>	Bahraini
<b>Marital Status</b>	Single
<b>Date &amp; Place of Birth</b>	20 June 1976, Muharraq (Bahrain)
<b>Education and Qualifications</b>	B. Sc. in Chemical Engineering from University of Bahrain, Isa Town, Bahrain (1994-1999).  M. Sc. in Chemical Engineering from King Fahd University of Petroleum & Minerals, Dhahran, King Saudi Arabia (2000-todate)